Asymptotic Limits of Negative Group Delay Phenomenon in Linear Causal Media

by

Miodrag Kandic

A Thesis Submitted to the Faculty of Graduate Studies of

The University of Manitoba

in Partial Fulfillment of the Requirements for the Degree of

Doctor of Philosophy

Department of Electrical & Computer Engineering

University of Manitoba

Winnipeg, Canada

September 2011

UNIVERSITY OF MANITOBA | Faculty of Graduate Studies

Final Oral Examination of the Ph.D. Thesis

The undersigned certify that they have read, and recommended to the Faculty of Graduate Studies for acceptance, a Ph.D. thesis entitled

Asymptotic Limits of Negative Group Delay Phenomenon in Linear Causal Media

by

Miodrag Kandic

In Partial fulfillment of the requirements for the degree: Doctor of Philosophy

Advisor:

Dr. G. Bridges, Dept. of Elec. & Comp. Eng., University of Manitoba

Committee:

Dr. D. Oliver, Dept. of Elec. & Comp. Eng., University of Manitoba
Dr. J. Page, Dept. of Physics & Astronomy, University of Manitoba

External Examiner:

Dr. B. Frank, Dept. of Elec. & Comp. Eng., Queen's University

Date of Oral Examination: Tuesday, 30 August 2011

The Student has satisfactorily completed and passed the Ph.D. Oral Examination.

Chair of Ph.D. Oral:

Dr. M. Lawall, Faculty of Graduate Studies, University of Manitoba

Advisor:

Dr. G. Bridges, Dept. of Elec. & Comp. Eng., University of Manitoba

Committee:

Dr. D. Oliver, Dept. of Elec. & Comp. Eng., University of Manitoba
Dr. J. Page, Dept. of Physics & Astronomy, University of Manitoba

External Examiner:

Dr. B. Frank, Dept. of Elec. & Comp. Eng., Queen's University

The Faculty of Graduate Studies is in receipt of this form: June 14, 2011

Abstract

Abnormal electromagnetic wave propagation characterized by negative group velocity and consequently negative group delay (NGD) has been observed in certain materials as well as in artificially built structures. Within finite frequency intervals where an NGD phenomenon is observed, higher frequency components of the applied waveform are propagated with phase advancement, not delay, relative to the lower frequency components. These media have found use in many applications that require positive delay compensation and an engineered phase characteristic, such as eliminating phase variation with frequency in phase shifters, beam-squint minimization in phased array antenna systems, size reduction of feed-forward amplifiers and others.

The three principal questions this thesis addresses are: can a generic formulation for artificial NGD structures based on electric circuit resonators be developed; is it possible to derive a quantitative functional relationship (asymptotic limit) between the maximum achievable NGD and the identified trade-off quantity (out-of-band gain); and, can a microwave circuit exhibiting a fully loss-compensated NGD propagation in both directions be designed and implemented? A generic frequency-domain formulation of artificial NGD structures based on electric circuit resonators is developed and characterized by three parameters, namely center frequency, bandwidth and the out-of-band gain. The developed formulation is validated through several topologies reported in the literature. The trade-off relationship between the achievable NGD on one hand, and the out-of-band gain on the other, is identified. The out-of-band gain is shown to be proportional to transient amplitudes when waveforms with defined “turn on/off” times are propagated through an NGD medium. An asymptotic limit for achievable NGD as a function of the out-of-band gain is derived for multi-stage resonator-based NGD circuits as well as for an optimally engineered linear causal NGD medium.

Passive NGD media exhibit loss which can be compensated for via active elements. However, active elements are unilateral in nature and therefore do not allow propagation in both directions. A bilateral gain-compensated circuit is designed and implemented, which overcomes this problem by employing a dual-amplifier configuration while preserving the overall circuit stability.

Acknowledgments

I would like to extend my sincere appreciation towards my advisor Dr. Greg Bridges, for his continued guidance and plethora of support. I would also like to recognize the attention to detail and express gratitude to my examination committee: Dr. Brian Frank, Dr. John Page, and Dr. Derek Oliver. Thank you for taking the time to read and evaluate this thesis.

Thanks to Alan McKay and Brad Tabachnick for assisting in obtaining the necessary components used in several fabricated devices, and Sinisa Janjic and Zoran Trajkoski for assisting with the fabrication process.

I wish to acknowledge the funding I have received from the Natural Sciences and Engineering Research Council of Canada, the University of Manitoba Graduate Fellowship, the University of Manitoba Students Union, and the Faculty of Engineering.

I would like to thank James Dietrich for his help in testing the fabricated devices in the RF laboratory, and Prof. Ernest Bridges for his input on various subjects pertinent to my research.

Finally, I wish to express my gratitude to my friends and family, whose support over the years has made the completion of this thesis possible.

To the memory of my parents

Contents

List of Figures

1. Introduction

Electromagnetic wave propagation in any medium obeys fundamental physical laws describing electromagnetic phenomena, which can be formulated by Maxwell's equations. Maxwell's equations relate electromagnetic fields (which are vector quantities and functions of both space and time in general) and the medium properties such as electric permittivity, conductivity, charge density and magnetic permeability. Depending on the considered problem, either differential (point) form or the integral form of Maxwell's equations may be preferred. Furthermore, when only the time-harmonic (sinusoidal) electromagnetic fields are considered, Maxwell's equations reduce to a simplified form. For a linear medium, this simplification does not limit the application of the obtained solution since any time-varying waveform can be expressed through the Fourier transform as an integral (or a sum, for periodic waveforms) of time-harmonic components with their respective frequencies, amplitudes and phases. Therefore, if a medium response is known for all individual time-harmonic components that a given arbitrary waveform is comprised of, the overall response for that same waveform can be determined by applying the inverse Fourier transform on the time-harmonic components at the medium output.

The medium's response to a time-harmonic excitation is commonly broken down into magnitude (amplitude) and phase characteristics, which are functions of frequency. The magnitude characteristic represents frequency-dependent factors that time-harmonic waveforms are scaled by as they are propagated through the medium, while the phase characteristic represents frequency-dependent phase shifts (in radians, or degrees) that

time-harmonic waveforms undergo. Consequently, phase delay, t_{ph}, can be obtained as a ratio of the time-harmonic waveform phase shift and its frequency. Further, the speed of propagation for time-harmonic components at each frequency (phase velocity, v_{ph}) can be obtained by dividing the medium's length with corresponding phase delay, t_{ph}. For an undistorted propagation, the magnitude characteristic should ideally be constant within the frequency band of interest, ensuring that all time-harmonic components of the applied waveform are attenuated or amplified by the same factor. At the same time, the phase characteristic for undistorted propagation needs to be a linear function of frequency, ensuring that all time-harmonic components propagate at the same phase velocity, v_{ph} (dispersionless propagation), and are therefore delayed by the same amount of time, t_{ph}.

In practical applications, close to ideal transmission is limited to a certain frequency band, within which the amplitude characteristic does not deviate from the ideally constant value by more than a pre-defined factor, and simultaneously the phase characteristic is close to being a linear function of frequency. Conversely, large amplitude and/or phase characteristic deviations from their respective ideal shapes result in distortion (the output waveform shape deviating from the input one).

Regardless of how much distortion they introduce, most media exhibit "normal" propagation characteristics, where the speed of propagation of individual time-harmonic components stays subluminal (slower than the speed of light in vacuum, $v_{ph} \leq c$), at all frequencies. Intuitively, all physically realizable media are expected to exhibit subluminal characteristics in order to comply with the special theory of relativity.

However, certain media exhibit "abnormal wave propagation" characteristics within limited frequency bands, where time-harmonic components can seemingly propagate at

superluminal ($v_{ph}>c$), or even negative phase velocities ($v_{ph}<0$). The latter case indicates that the output time-harmonic waveform is advanced in phase and therefore in time, relative to the input one. These media are known to have a "Negative Phase Velocity" or "Negative Phase Delay" property, which in turn yields a "Negative Refractive Index" or NRI ($n=c/v_{ph}<0$).

When a "carrier" time-harmonic waveform of frequency ω is modulated (such as amplitude or frequency modulated) by another waveform, the modulated waveform is comprised of time-harmonic components of different frequencies. The frequencies of the most dominant time-harmonic components in this case are within an interval centered at the carrier frequency. Group delay of a medium, τ_g, is characterized by the phase characteristic slope at a given frequency. As it will be shown in Chapter 2, for an amplitude modulated carrier case where the most dominant frequency components are within a narrow band relative to the carrier frequency, the medium's group delay characteristic value at the carrier frequency represents the time delay of the "envelope" (modulation part) of the waveform, whereas the time-harmonic carrier is delayed by the phase delay. For an undistorted propagation of the modulation part of the waveform, the phase characteristic slope (group delay) needs to be constant within the waveform's frequency band. Group velocity, v_g, can be obtained by dividing the medium's length with by the group delay, τ_g.

Superluminal group velocity has been observed in some media within limited frequency bands, where a group velocity faster than the speed of light in vacuum, c, is exhibited. Further, within limited frequency bands certain media exhibit a Negative Group Velocity (NGV), and consequently Negative Group Delay (NGD), which is

another example of “abnormal wave propagation”. The NGD phenomenon is the central scope of this thesis. In this case, the slope of the phase characteristic is negative over a limited frequency bandwidth, compared to the “normal” wave propagation case. This property indicates that the envelope of the aforementioned amplitude modulated example waveform will be advanced in time at the medium’s output relative to the input waveform envelope, given that the waveform frequency spectrum lies within the region exhibiting the NGD phenomenon.

Since the NGD phenomenon is exhibited within limited frequency bands only, it does not violate any fundamental physical laws, such as relativistic causality. Waveforms comprised of time-harmonic frequency components which are entirely band-limited are infinitely extended in time. Therefore, observing a time-advancement of the envelope of such a waveform does not violate causality, since the waveform has no beginning and no end in time. When a band-limited waveform is truncated (i.e. defined “turn on/off” times are introduced), its frequency spectrum extends outside of the original frequency band. As it will be addressed in greater detail in Chapter 2, the truncated waveform frequency components which fall outside of the NGD region affect the propagation of the waveform part located in the immediate vicinity of the “turn on/off” times. Therefore, the “turn on/off” parts of the waveform are positively delayed and do not violate causality. The same is true for any points of non-analyticity in the waveforms, when either the waveform itself as a function of time or any of its derivatives are discontinuous. If the part of the truncated waveform between (and excluding) the “turn on/off” points in time is an analytic (smooth) function of time, this part will be advanced in time (negatively delayed). Since the values of an analytic function over the entire domain can be predicted

from any given part of the function, the entire smooth part of the applied truncated waveform can theoretically be determined from its early part immediately following the "turn on" time. Therefore, the smooth part of the truncated waveform carries no new information compared to the early part following the "turn on" time, and time-advancement of this part does not violate causality.

1.1 Literature Overview

Early research on abnormal electromagnetic wave propagation was conducted by Sommerfeld and Brillouin in the 1910s, and it was comprehensively summarized in a Brillouin's book [1] published in 1960. This book studies wave propagation through abnormal dispersion media described by a Lorentzian dielectric model (such as plasma), and it is frequently referenced in pertinent publications to this day. In order to facilitate mathematical analysis, the propagation of a simple semi-infinite (step-modulated) sinusoidal waveform with a defined "turn on" time (before which there was no signal applied, and the medium itself was "at rest") was studied. The medium response to a step-modulated sinusoidal waveform is indicative of the medium transient response to any waveform with a defined "turn on" (and/or "turn off") point in time, since that arbitrary step-modulated waveform can be broken down into step-modulated sinusoidal components through the Fourier analysis.

Furthermore, important distinctions between "front", signal, group and energy velocities are summarized in this book [1]. It was shown that the initial signal "turn on" disturbance (or "front") travels through a dispersive medium (exhibiting a frequency

dependent electric permittivity, and therefore frequency dependent phase and group velocities) at exactly the speed of light in vacuum, *c*, and therefore does not violate causality. The reason for the luminal propagation of the "front" is that this part of the waveform is associated with high-frequency electric field components which are oscillating too fast for the medium charges to respond. Therefore, the medium has a perceived permittivity of vacuum at these frequencies. This is true for any dispersive medium, not just the particular Lorentzian medium studied in [1].

The "front" propagation through a Lorentzian medium is followed by the Sommerfeld (or 1^{st}) precursor (forerunner), which is a very low energy transient waveform with an infinitely small initial amplitude and period which both progressively increase with time. The initial period of the 1^{st} forerunner is independent of both the input semi-infinite sinusoidal waveform period, and of the resonant frequency of the medium. The physical explanation of this phenomenon is that the charges in a dispersive medium need to be set in motion first, before they can oscillate at either the resonant frequency of the medium (free oscillations) or at the frequency of the applied waveform (forced oscillations). The 2^{nd} (Brillouin) precursor initially has a small frequency (a large period), which then rapidly increases to reach the resonant frequency of the medium, and finally the applied step-modulated sinusoidal waveform frequency.

The "signal arrival time" is somewhat arbitrarily defined [1] as the point in time at which the output waveform amplitude following the forerunners' evolution is on the same order of magnitude as the steady-state part of the output waveform. The "signal velocity" is then easily related to the "signal arrival time", through the medium physical length.

Finally, the "energy velocity" is given by the energy passing per second through a surface of unit area perpendicular to the direction of wave propagation [1]. "Energy velocity" is always defined unlike group velocity, which loses interpretation in highly dispersive media (output pulse is too distorted in shape to compare with the input pulse). Only under the assumption of slowly varying dispersion characteristic, is the energy velocity equal to the group velocity [1].

A series of publications in the 1970s and 1980s followed this fundamental work, mostly dealing with propagation of more complex waveforms, such as a Gaussian pulse modulated carrier waveform, through abnormally dispersive media [2,3]. Furthermore, a useful analogy between wave propagation in abnormal media and particle tunneling was studied in several publications in the early 1990s [4,5]. In their frequently cited work from 1993 [6], Bolda, Chiao and Garrison presented a mathematical proof that anomalous dispersion phenomena not only do not violate the relativistic causality requirements, but they must exist within some frequency bands for all dispersive media. This is a consequence of Kramers-Kronig relations which are applicable to all physically realizable, causal linear media. Kramers-Kronig relations provide a link between the attenuation (amplitude) and dispersion (phase) characteristics in linear causal media, as presented in a classic book by Jackson [7], and discussed by Waters *et al*. [8]. The superluminal group velocity in a distributed Bragg reflector was demonstrated in both frequency and time domain by Mojahedi *et al*. [9,10]. The distinction between the "front" (information) velocity and group velocity was demonstrated in a medium with a slow group velocity by Stenner *et al*. [11].

Extensive analytical precursor (forerunner) evolution calculations in different types of dispersive media were studied by Oughstun *et al*. [12-14]. His more recent publications deal with Brillouin precursor evolution in a specific type of media (Rocard-Powles-Debye model dielectrics), and the possibility for considerably deeper penetration into this absorbing medium for specific signal shapes [15]. A joint time-frequency analysis technique for precursor fields in passive media was presented by Safian *et al*. [16].

The negative phase velocity and consequently negative refractive index (NRI) concept was introduced by Veselago in 1968 [17]. He presented a theoretical possibility of having simultaneously negative electric permittivity, ε, and magnetic permeability, μ, in which case there is a valid solution to Maxwell's equations and electromagnetic propagation is possible. The NRI concept regained its popularity at the beginning of this century. Pendry revisited this concept in 2000 [18], suggesting that NRI phenomenon could be used to make a planar interface point-to-point focusing lens, capable of sub-wavelength resolution. The first NRI medium consisting of split-ring resonators was designed by Smith *et al*. in 2000 [19] and experimentally verified in 2001 [20]. This design was fairly bulky, and it achieved an NRI effect over a very narrow bandwidth.

Caloz and Itoh reported synthesizing an NRI medium over a relatively wide bandwidth at microwave frequencies in 2002 [21], by periodically loading a transmission line with lumped series capacitors and shunt inductors. Around the same time a group from University of Toronto led by Eleftheriades and Iyer synthesized a periodically loaded transmission line circuit type [22]. The NRI materials, also known as Left-Handed-Materials (LHM) or Metamaterials, soon became a widely popular research area

resulting in numerous publications to date. Based on their property of progressively advancing (instead of lagging) the phase along the physical length of an LHM, applications in physically short phase shifters and delay lines were exploited, including the design of a broadband Wilkinson balun [23] and broadband power divider [24], both by Eleftheriades *et al*. Furthermore, physically short phase shifters based on combined phase-advancing LHM, and phase-delaying Right-Handed-Materials (RHM), can be applied in the design of phased array antenna systems. Phased array designs require a connection of the individual antenna array elements via delay lines, where the phase shift of the lines determines the radiation angle of the overall array. Physically short phase shifters operate on the principle of combining the positive and negative phase shifts, to add up to a desired overall phase shift value. For example, if a 0° phase shift is needed between two series-fed phased array elements which are spaced apart at a distance corresponding to a 180° phase shift at the design frequency, the traditional approach requires connecting them through a 360° delay line, thus taking additional space. With a combined LHM/RHM approach, the physical 180° separation can be bridged through a traditional delay line with a -90° phase shift, cascaded with an LHM +90° phase shift line, thus making the overall phase shift zero as required, but with an equivalent physical length of only 180°. LHM theory and numerous applications were summarized in Eleftheriades' book [25].

The common NRI (LHM) materials exhibit a negative phase delay (or negative phase velocity – backward wave propagation) but their group velocity is still positive, as it was experimentally confirmed by Wang *et al*. [26]. Certain applications, such as phased array antenna systems, can benefit from a simultaneous NRI and NGD phenomenon. As

explained previously, NRI in this application ensures shortening of the delay lines connecting the elements in a series-fed array configuration, but the group delay between the elements is still positive. This causes the "beam-squint" effect, where different frequency components are radiated at different angles (radiation angle is frequency dependent). The NGD effect can be used to cancel the slope of (or flatten out) the positively delayed phase characteristic within the design bandwidth, thus ensuring that all frequency components within the signal bandwidth are radiated (or received) at the same angle, resulting in a reduced "beam-squint".

A negative group delay synthesizer operating at microwave frequencies was first proposed by Lucyszyn *et al*. [27] in 1993. This device operates in reflection mode, using a Lange coupler. It is built with lumped components, varactors and field effect transistors operating as variable resistors. The achieved NGD is tunable and relatively high over a narrow-band centered at 1 GHz, but accompanied with high losses. The same reflection topology was used to build a controllable phase shifter, a delay line, and an attenuator in addition to the group delay synthesizer [28].

Group delay circuits have proved useful in many applications, such as the one reported by Noto *et al*. who proposed a passive resonator-based NGD circuit for reducing the physical length of delay lines in feed-forward amplifiers [29]. Traditional feed-forward amplifier designs are commonly used for cancelling inherent distortion in amplifiers, by comparing the distorted waveform at the amplifier output to the delayed original input waveform. The input waveform needs to be delayed in time by the same amount as the delay introduced by the amplifier, for a correct identification of the amplifier distortion. Hence, a delay line needs to be employed, which can have a

considerable physical length relative to the amplifier circuit dimensions. By cascading an NGD circuit with the amplifier, the overall group delay can be reduced and thus the length of the required delay lines gets reduced as well.

As previously mentioned, applications such as phased array antenna systems can benefit from a simultaneous NRI and NGD effect. The first such design was synthesized by Siddiqui *et al*., consisting of a transmission line circuit periodically loaded with *RLC* resonators (responsible for NGD) and series capacitors and shunt inductors (responsible for NRI) [30,31]. The circuit is lossy as a consequence of the resistive element introduced by the resonators. The loading reactive elements responsible for NRI also serve the impedance matching purpose, at the design frequency. Simultaneous NRI and NGD effect in a coplanar waveguide design was reported by Ibreaheem *et al*. [32]. Characteristics of abnormal wave propagation in passive media were comprehensively discussed and demonstrated on a superluminal group delay experiment and an experiment involving combined NGD/NRI effect, by Mojahedi *et al*. [33].

In order to compensate for loss associated with NGD circuits, active components can be employed. A very low frequency bandpass amplifier exhibiting NGD was proposed by Mitchell *et al*. [34,35]. The causal effects of this circuit were studied by abrupt changes in the testing pulses. Solli *et al*. have also demonstrated causal effects in electronic circuits exhibiting NGD [36]. Kitano *et al*. synthesized a baseband active NGD circuit [37,38], using the circuit approach to derive equations describing the NGD phenomenon. Another low frequency design [39] uses the phase behavior of an active Friend filter in the region beyond the amplifier roll-off frequency.

Ravelo *et al*. proposed the first active gain-compensated NGD circuit operating at microwave frequencies. This design consists of a FET based amplifier with a shunt RLC resonator at the amplifier output [40]. A broadband version of this circuit was proposed, synthesized by cascading several stages of the original circuit, each tuned at different frequencies [41]. Ravelo *et al*. also proposed several applications for their active circuit such as a broadband balun [42] and a broadband and constant phase shifter [43]. This group also proposed a baseband version of their active NGD circuit [44], where the RLC resonators are replaced by *RL* elements, acting as high-pass filters. Applications of the baseband active NGD circuit on the equalization of the interconnect propagation delay [45,46], and on the reduction of propagation delay of the *RC*-line model [47] were reported. An overview of different gain-compensated active NGD applications reported by Ravelo *et al*. is given in [48]. A gain-compensated microwave design exhibiting simultaneous NRI and NGD effect was reported by Shafai and Oh [49,50], and its application to beam-squint minimization.

Distortion due to medium dispersion can be reduced in numerous telecommunication applications by maintaining the group delay constant and positive, not necessarily negative or fully compensated for (zero group delay). Lowering the group delay variation over a bandwidth (group delay equalization) can be achieved by adding frequency response masking filters [51-53], parameter-varying filters [54], or multistage circuits incorporating inductive-series peaking [55]. A group delay equalized monolithic integrated circuit amplifier operating at microwave frequencies was reported by Murase *et al*. [56]. Kyoung-Pyo *et al*. reported a group delay equalization technique in low noise amplifiers [57]. Choi *et al*. recently reported another NGD circuit application in feed-

forward amplifiers [58]. Podilchak *et al*. reported a fully integrated CMOS circuit exhibiting a tunable NGD within 13-26 GHz, applicable to GD equalization [59].

1.2 Motivation and Contribution

The motivation for the research presented in this thesis arose from the fact that the field of applicable NGD microwave devices is relatively new, leaving room for further analysis and improvements. The major drawback of the early NGD circuits was their inherent loss, which is resolved by active compensation reported in more recent work at the expense of the achieved NGD magnitude (active elements introduce a positive delay), signal distortion due to out-of-band gain, and other trade-offs.

One of the points that seems to be lacking from current publications is a quantified relationship between the maximum achievable NGD in physically realizable (causal) media, and its trade-off quantities such as attenuation (for passive media), out-of-band gain (for active NGD circuits), bandwidth, transient response amplitude and transient settling time. As a part of the contribution work, a generic formulation applicable to various passive or active resonator-based NGD circuit topologies is presented in this thesis [60]. The generic formulation is derived based on observed similarities of propagation characteristics of many different NGD circuit topologies, and it is successfully verified against several NGD designs, including the design reported in [61]. NGD asymptotic limits for the proposed generic formulation are derived as a function of the number of impedance-matched resonator-based stages, and as a function of the out-of-band gain [60].

Furthermore, the subject of NGD asymptotic limits as a function of the undesirable out-of-band gain is extended to any physically realizable (causal) and linear medium. These generic limits are derived under certain approximations and they apply to media which support a causal propagation of optical electromagnetic waves, sound waves, or voltage and current waveforms propagated in electric circuits of any topology. These asymptotic NGD limits are derived from Kramers-Kronig relations, which relate the amplitude and phase responses for all linear, causal media. This is the reason for the wide applicability of the derived limits.

As another contribution of this thesis, a transient analysis is performed for multi-stage resonator-based circuits, and their baseband equivalents. The out-of-band gain is a frequency domain trade-off quantity observed in the propagation characteristic of an NGD medium. Infinitely extended-in-time smooth waveforms are only affected by the in-band frequency characteristic of an NGD medium, which introduces only minimal distortion if most of the waveform's frequency power spectrum is within the NGD bandwidth (usually a 3 dB maximum amplitude characteristic variation is prescribed). However, waveforms with defined turn-on and/or turn-off points in time (or finite-duration waveforms) have their frequency spectrum affected by the out-of-band gain effect inherent to NGD media, which results in increased transient amplitudes following the waveform discontinuities. Several time-domain examples demonstrating a direct link between the frequency-domain out-of-band gain and the transient amplitudes associated with finite-duration waveform propagation through an NGD medium are also presented [60,62]. For practically applicable NGD devices the transients need to stay below a pre-defined magnitude, and they need to decay sufficiently within a given time frame.

Transient effects in resonator-based NGD circuits are explored for different applied finite-duration waveforms. Cascading bandpass filters with resonator-based circuits is also explored, and its effect on the achieved NGD and the effect on the transients magnitude.

Finally, a novel bilateral gain-compensated NGD circuit is introduced, which allows a bidirectional operation exhibiting NGD [63]. Potential application to bidirectional transmit/receive configuration of constant phase shifters such as those used in phased array antenna systems, is also demonstrated.

1.3 Thesis Outline

The thesis is organized as follows:

In Chapter 2, elements of NGD theory are presented providing the necessary background for the subsequent chapters. The compliance of this phenomenon with causality is investigated, and demonstrated on an example. NGD application in microwave engineering is demonstrated on the distortion-reduction examples in a phased array antenna configuration, and in an error-cancelling feed-forward amplifier.

In Chapter 3, a comparison of several resonator-based NGD circuit configurations is compared in terms of their relevant parameters, and a generic formulation is derived and proposed. Design and fabrication of an active gain-compensated NGD circuit is also presented. This circuit's frequency-domain parameters are expressed by relatively simple explicit formulae, with a good agreement with measured characteristics within the

frequency band of interest. The proposed circuit was fabricated and tested in the frequency and steady-state time domain, showing a good agreement with expected characteristics. NGD asymptotic limits are also derived in this chapter based on the generic formulation of multi-stage resonator-based circuits. The derived NGD limits were successfully compared against several NGD circuits reported in publications. The derived asymptotic NGD limits are given as a function of the out-of-band gain and the number of cascaded and impedance-matched resonator-based stages. It is shown that for a given out-of-band gain and fixed bandwidth, distributed designs with larger number of stages yield larger NGD values. Consequently, for a given NGD value, distributed designs yield smaller out-of-band gain. The effects of adding a bandpass filter to the generic model is explored as well, which can be used to model practical NGD designs. It is shown that the addition of a bandpass filter lowers both the achieved NGD and the out-of-band gain proportionally, so the overall derived limits remain almost unchanged. The limits are verified for baseband frequency designs as well.

In Chapter 4, an asymptotic NGD limit as a function of out-of-band gain is presented, regardless of the circuit topology used. The analysis is based on magnitude and phase characteristic dependence in physically realizable, causal systems, defined by Kramers-Kronig relations. The derived asymptotic limit is successfully verified against the resonator-based circuits presented in Chapter 3.

In Chapter 5, a time-domain transient analysis is also conducted, investigating the propagation of a semi-infinite sinusoidal waveform as one of the simplest waveforms with a well defined “turn on” time. A direct relationship between the out-of-band gain and the transient magnitude is confirmed. Therefore, the frequency-domain asymptotic

limits from Chapter 4 are adapted to express the relationship between the achieved NGD and the transient magnitude. Further, several transient experiments are conducted on a fabricated gain-compensated circuit.

In Chapter 6, a novel bilateral gain-compensated NGD circuit is presented. Gain compensated NGD circuits proposed in literature thus far are all single-directional, due to the unilateral nature of employed amplifiers. In the novel design, high-isolation splitters are used to allow a bidirectional operation, while preserving the stability of the circuit. An application to bidirectional transmit/receive configuration of a constant phase shifter is demonstrated.

Finally, Chapter 7 summarizes the presented material, and outlines the proposed future work. The thesis is concluded by the list of references.

2. Negative Group Delay (NGD)

Background Theory

In the first chapter, the literature on abnormal wave propagation was briefly reviewed, including negative group velocity and consequently negative group delay as one of them. In this chapter, negative group delay theory and its physical interpretation in terms of signal propagation is covered in more detail, which is a necessary background for subsequent chapters. NGD application to several engineering examples is also demonstrated.

2.1 Frequency and Time-Domain Interpretation of NGD

The propagation characteristic of a medium is commonly presented through a dispersion diagram, such as the one shown in Fig. 2-1. The function in this figure represents the difference in phase per unit length of a distributed medium (horizontal axis), between an assumed steady-state sinusoidal excitation of a given frequency (vertical axis) applied at the input of the medium, and its response at the output. It is assumed that the sinusoidal waveform applied at the input of the medium will retain its form at the output, and it can only undergo a change in amplitude and/or phase, not in frequency. For a medium with a finite length, these requirements are summarized as

$$u_{IN}(t) = U_{IN}\sin(\omega t), \tag{2.1a}$$

$$u_{OUT}(t) = U_{IN} A(\omega) \sin(\omega t - \phi(\omega)), \tag{2.1b}$$

where $\phi(\omega)=\beta(\omega)z$ represents an overall phase shift from input to output of the entire medium of length z, and similarly $A(\omega)$ represents the amplification factor across the medium for a steady state sinusoidal component of frequency ω.

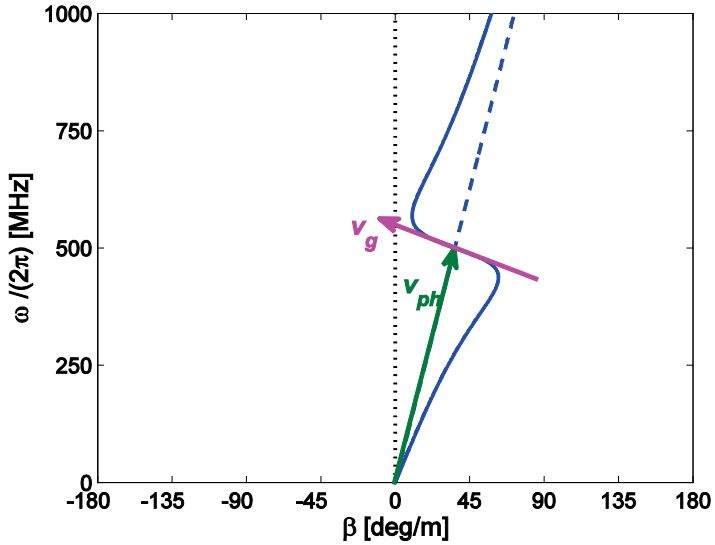

Figure 2-1: A dispersion characteristic of a medium (ω-β diagram).

Expressed in the phasor form, commonly used to represent time-harmonic waveforms as complex numbers, expression (2.1) can be re-stated as

$$U_{OUT}(\omega) = U_{IN} A(\omega) e^{j\phi(\omega)}. \tag{2.2}$$

The waveform at the output of a medium of length z, can alternatively be expressed in terms of the medium propagation constant $\gamma(\omega)$, as

$$U_{OUT}(\omega) = U_{IN} e^{-[\alpha(\omega)+j\beta(\omega)]z} = U_{IN} e^{-\gamma(\omega)z}. \quad (2.3)$$

The propagation constant notation shown in (2.3), where a positive real part of $\gamma(\omega)$, labeled as $\alpha(\omega)$ represents attenuation per unit length, and a positive imaginary part $\beta(\omega)$ represents phase delay per unit length, is commonly used in the engineering communities, and will be used throughout this thesis. In the commonly used alternate notation however, the propagation constant is usually characterized by notation exp[$jk(\omega)$], so the attenuation and the phase delay are represented by the imaginary, and real part of $k(\omega)$, respectively.

Even though the propagation characteristic discussed above characterizes the medium with respect to time-harmonic waveforms, it can be applied to any waveform given that the medium is linear (an input waveform expressed as a sum of two or more components yields an output response that can be obtained by superposing the output responses corresponding to the individual input components). The arbitrary waveform needs to be represented first by its frequency spectrum, obtained through the Fourier transform given by (2.4a). Each of the frequency spectrum components is time-harmonic, and therefore in a general case undergoes a specific change in both magnitude and phase as it appears at the medium output, according to the medium propagation characteristic. Finally, an inverse Fourier transform (2.4b) needs to be applied to the spectrum components at the output, to obtain the time-form of the output waveform. The described Fourier transform pair is given by

$$U_{IN}(\omega) = \int_{-\infty}^{\infty} u_{IN}(t) e^{-j\omega \cdot t} dt \,, \tag{2.4a}$$

$$u_{OUT}(t) = \frac{1}{2\pi} \int_{-\infty}^{\infty} U_{IN}(\omega) e^{-\gamma\omega \cdot z} e^{j\omega \cdot t} d\omega \,. \tag{2.4b}$$

For the aforementioned alternate notation, in addition to the propagation constant difference the complex time-harmonic factors $\exp(\pm j\omega \cdot t)$ need to be swapped in expressions (2.4).

Propagation without distortion occurs in media affecting the amplitude and/or time delay of the original waveform only, while retaining its shape. This requirement can be written as

$$u_{OUT}(t) = A \cdot u_{IN}(t - t_0), \tag{2.5}$$

where A is the amplitude scaling constant and t_0 is the waveform delay. The distortionless propagation occurs in media exhibiting a propagation characteristic given by

$$\gamma(\omega) = \alpha(\omega) + j\beta(\omega) = \alpha + j\omega t_0 / z \,. \tag{2.6}$$

The condition (2.6) can be easily derived through Fourier analysis. In a perfect distortionless medium, all frequency components of the waveform undergo a constant magnitude attenuation or amplification. Furthermore, all frequency components are delayed by the same amount of time, which means that the speed of propagation is

independent of frequency, hence the medium is dispersionless. Therefore, this case corresponds to a constant magnitude characteristic versus frequency, and a linear relationship between the phase and frequency, where the slope of the phase line is determined by the constant time delay t_0. For waveforms whose frequency spectrum components are confined within a specific frequency band, it is enough to have these ideal propagation criteria met in that same frequency band only.

Some of the most commonly used properties in describing waveform propagation through a medium, are phase and group velocity (and consequently phase and group delay when the medium length is taken into account). In order to demonstrate these quantities, an input excitation in the form of a time-harmonic carrier (with a frequency ω_0 and a phase shift θ_0) is considered, which is amplitude-modulated by a slow varying (relative to the carrier) arbitrary waveform $U_{env}(t)$. By employing (2.4a), the frequency spectrum of such a waveform can be shown to be identical in form to the "baseband" spectrum of the modulating waveform $U_{env}(t)$, except that it is shifted by the carrier frequency ω_0. Now, the input waveform can be written as

$$u_{IN}(t) = U_{env}(t)\cos(\omega_0 t + \theta_0) = \frac{1}{\pi}\mathrm{Re}\left\{\int_0^\infty U_{env}(\omega - \omega_0)e^{j\theta_0}e^{j\omega\cdot t}d\omega\right\}. \qquad (2.7)$$

Assuming that within the frequency bandwidth of interest the phase characteristic changes approximately linearly with frequency and the amplitude characteristic is close to constant, a 1st order approximation yields

$$\phi(\omega) \approx \phi_0 + (\omega - \omega_0)\frac{d\phi(\omega)}{d\omega}\bigg|_{\omega=\omega_0}, \qquad A(\omega) \approx A(\omega_0) = const. \tag{2.8}$$

The output waveform can now be described by

$$u_{OUT}(t) \approx A(\omega_0)\frac{1}{\pi}\mathrm{Re}\left\{\int_0^\infty \left[U_{env}(\omega-\omega_0)e^{j\theta_0}e^{j\phi_0 - j\omega_0(d\phi/d\omega)|_0}\right]e^{j\omega(d\phi/d\omega)|_0}e^{j\omega\cdot t}d\omega\right\}, \tag{2.9}$$

which yields

$$u_{OUT}(t) \approx A(\omega_0)U_{env}\left(t + \frac{d\phi(\omega)}{d\omega}\bigg|_{\omega=\omega_0}\right)\cos\left(\omega_0\left(t + \frac{\phi_0}{\omega_0}\right) + \theta_0\right). \tag{2.10}$$

Inspecting the expression (2.10) reveals that the output waveform will retain the amplitude-modulated waveform, with its time-harmonic carrier shifted in time by the phase delay (t_{ph}=-ϕ_0/ω_0) and the modulating "envelope" part of the waveform is shifted by the group delay (τ_g=-$d\phi/d\omega$, evaluated at ω_0). These time delay quantities are determined by the medium length and corresponding phase and group velocities, and can be summarized as

$$v_g = \frac{d\omega}{d\beta} \rightarrow \tau_g = \frac{L}{v_g} = -\frac{d\phi}{d\omega}, \qquad v_{ph} = \frac{\omega}{\beta} \rightarrow t_{ph} = \frac{L}{v_{ph}} = -\frac{\phi(\omega)}{\omega}. \tag{2.11}$$

Fitting the expressions above with the dispersion characteristic from Fig. 2-1, the phase velocity can be interpreted as the slope of a line connecting the origin and a point of interest on the ω-β curve. Similarly, group velocity can be interpreted as the slope of the tangent on the dispersion characteristic, at the point of interest. The instance depicted in Fig. 2-1 represents a positive phase velocity and delay, and a negative group velocity and delay, in the region of interest.

Negative group delay phenomenon is demonstrated on an example in the time domain, as shown in Fig. 2-2.

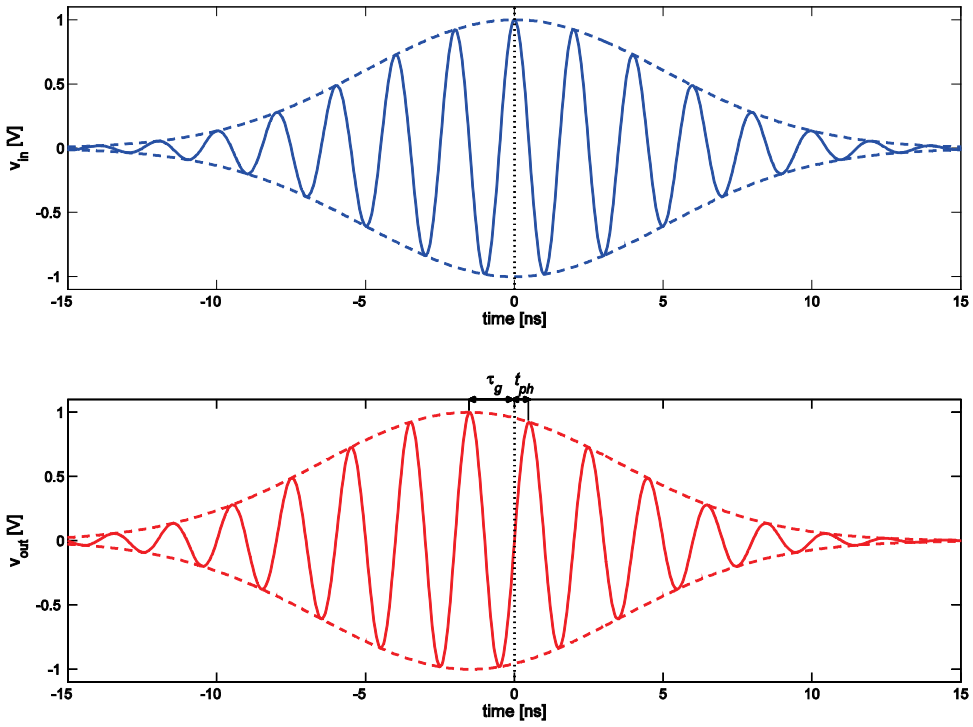

Figure 2-2: A negative group delay example of an amplitude modulated waveform.

The waveform shown in Fig. 2-2 is a Gaussian pulse modulated sinusoidal carrier. The envelope of the output waveform seems to be advanced in time relative to the input

envelope, thus exhibiting a negative group delay. The output sinusoidal carrier on the other hand is positively delayed by value t_{ph}, thus exhibiting a positive phase delay. The Gaussian envelope peak forms at the output even before the input envelope peak enters the medium. This phenomenon seems to be counter-intuitive, and the conditions under which it is possible need to be clarified to make sure fundamental physical laws, such as causality, are not violated.

The waveform depicted in Fig. 2-2 is a steady-state waveform turned on infinitely long back in time theoretically speaking, and it is a smooth function in time with a pre-determined shape. One could argue that the envelope peak of such a waveform does not carry any additional information compared to its initial "tail" part, since once that early part of the waveform is established, the entire waveform is known. Therefore, the fact that the output envelope peak forms before the input one does not necessarily contradict physical laws. Mathematically speaking, this waveform can be completely determined by its "early" part, by finding all its derivatives at an early point in time, and expanding into an infinite Taylor series. Once the entire waveform is predicted, Fourier analysis can be performed to determine all its frequency components. The dispersion characteristic of the medium then simply rearranges the frequency components of the waveform, so the envelope peak at the output appears before the input one.

A more practical case will be examined now, when the waveform starts at a defined point in time. The commonly used waveform for this purpose [1] is a semi-infinite (step-modulated) sinusoid, since it is relatively easy to obtain the analytical solution to the output response of a medium, depending on its propagation characteristic.

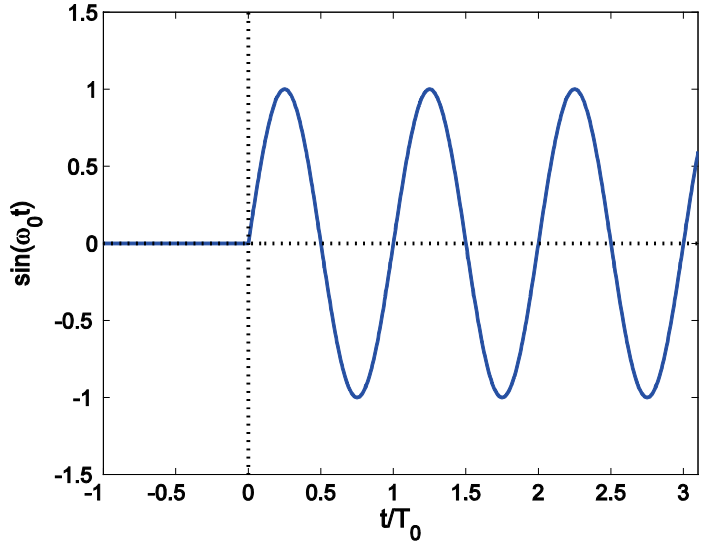

Figure 2-3: A semi-infinite (step-modulated) sinusoidal signal with a period T_0, and a frequency ω_0.

The waveform shown in Fig 2-3 and its frequency spectrum components obtained by the Fourier transform can be written as:

$$u(t)=\begin{cases}0 & ,\ t<0\\ \sin(\omega_0 t), & t\geq 0\end{cases}, \qquad U(\omega)=\int_{-\infty}^{\infty}u(t)e^{-j\omega t}dt\approx\frac{\omega_0}{\omega_0^2-\omega^2}. \tag{2.12}$$

The Fourier transform is only defined for waveforms satisfying the Dirichlet condition (i.e. the integral of the absolute value of the waveform over the entire time domain has to be finite). Since the original semi-infinite sinusoid function does not satisfy this condition, it can first be multiplied by an exponentially decaying factor $e^{(-at)}$, which will make it satisfy the Dirichlet condition. Then, the Fourier transform of this function is found and the decay constant, a, is set to approach zero, which yields expression (2.12). Figure 2-4 shows the magnitude frequency spectrum of a semi-infinite sinusoidal signal, with frequency ω_0.

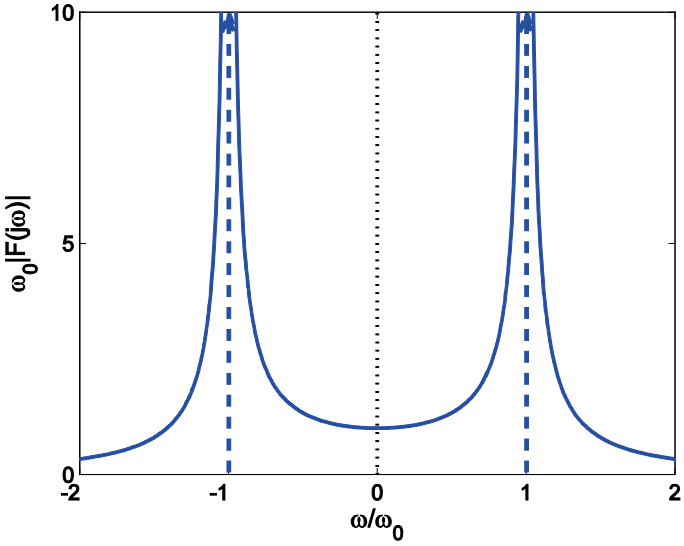

Figure 2-4: Amplitude frequency spectrum of a semi-infinite sinusoidal signal.

As seen from Fig. 2-4, the frequency spectrum of a semi-infinite sinusoid signal is spread around its frequency ω_0, as opposed to having a single component at that frequency, for the infinite sinusoid case. Propagation of this waveform in NGD media will be analyzed in Chapter 5. As a background for that analysis, the inverse Fourier analysis for the signal itself will be conducted here. The inverse Fourier integral in this case is given by

$$u(t) = \frac{1}{2\pi}\int_{-\infty}^{\infty} U(\omega) e^{j\omega\cdot t} d\omega = \frac{\omega_0}{2\pi}\int_{-\infty}^{\infty} \frac{e^{j\omega\cdot t}}{\omega_0^2 - \omega^2} d\omega \,. \tag{2.13}$$

This integral can be evaluated in a complex plane using the integration path deformation, as illustrated in Fig 2-5. The original path is along real-ω axis, and it appears to pass through the frequency-domain integrand function poles at $\pm\omega_0$. However, it needs to be kept in mind that the Fourier transform function in this case was obtained as a limit case of a decaying semi-infinite sinusoidal waveform, in order to satisfy the Dirichlet

condition. This limit case, as the decay constant approaches zero ($a \to 0$), makes the frequency spectrum poles to be placed slightly above the real-ω axis ($\omega_p = \pm\omega_0 + j \cdot a$).

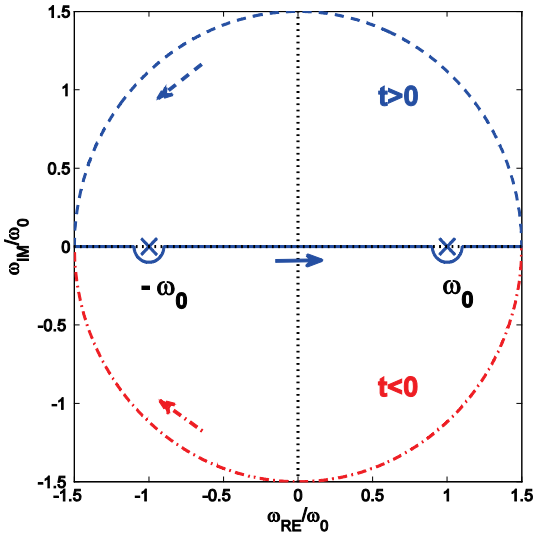

Figure 2-5: Complex plane integration for inverse Fourier transform of a step-modulated sinusoidal waveform.

The path deformation in complex plane integration is allowed as long as the path stays on the same side of poles. Since it has been established that the poles lie just above the real axis, the path can be deformed around the poles, so it goes through the lower half-plane, as shown in Fig. 2-5. The integration path goes from the negative to positive infinity of the real ω-axis, bending through the lower half-plane around poles at $\pm\omega_0$.

For time $t<0$, an infinite radius lower half-plane semi-circle can be added to the integration path, since the exponential term under the integral $e^{(j\omega t)}$ will be negligible. This added path will form a closed loop with the original integration path, which does not encompass any poles so the entire integral will be zero. Therefore, the time-domain function is equal to zero for times $t<0$, as expected. Similarly, for times $t \geq 0$, an infinite

upper half-plane semi-circle can be added to the integration path, which will now complete a closed loop encompassing both poles. Thus, using the Cauchy Residue Theorem, the function can be evaluated as the sum of the residues at the poles, as

$$\oint \frac{f(\omega)}{\omega-\omega_0} d\omega = \mathrm{Re}\, s(f) = j2\pi f(\omega_0), \tag{2.14a}$$

which finally yields

$$u(t) = \begin{cases} 0, & t < 0 \\ \sum \mathrm{Re}\, s(U) = -\dfrac{je^{j\omega_0 t}}{2} + \dfrac{je^{-j\omega_0 t}}{2} = \sin(\omega_0 t), & t \geq 0 \end{cases}. \tag{2.14b}$$

A similar procedure is employed when determining the time-domain signal at the output of a medium. The original Fourier spectrum of the input signal is first multiplied by the complex transfer function of the medium ($H(\omega)=A(\omega)e^{j\phi(\omega)}$), and the inverse Fourier transform of the total expression is evaluated to obtain the output signal. For a step-modulated sinusoidal excitation this procedure yields

$$u_{OUT}(t) = \frac{1}{2\pi}\int_{-\infty}^{\infty} A(\omega)e^{j\phi(\omega)}U_{IN}(\omega)e^{j\omega\cdot t}d\omega = \frac{\omega_0}{2\pi}\int_{-\infty}^{\infty} A(\omega)\frac{e^{j\omega\cdot[t-t_{ph}(\omega)]}}{\omega_0^2-\omega^2}d\omega, \tag{2.15}$$

where the medium phase characteristic is written in terms of the frequency-dependent phase delay time $\phi(\omega)=\omega\cdot t_{ph}(\omega)$. Applying the same path deformation procedure to

expression (2.15), a lower half-plane infinite-radius semi-circle can be added for times $t<t_{ph}(\omega\to\infty)$, which is the phase delay of the medium at high frequencies. The output signal will be zero in this case, meaning that $t_{ph}(\omega\to\infty)$ is the earliest time that the signal onset, or "front", can appear at the output, as given by

$$u_{OUT}(t)=\begin{cases}0, & t<t_{ph}(\omega\to\infty)\\ \sum \mathrm{Re}\,s\left[U(\omega)H(\omega)\right], & t\geq t_{ph}(\omega\to\infty)\end{cases},$$

$$t_{ph}(\omega\to\infty)=-\left.\frac{\phi(\omega)}{\omega}\right|_{\omega\to\infty}=\frac{L}{v_{ph}(\omega\to\infty)}. \tag{2.16}$$

Therefore, regardless of what the dispersion characteristic is in the frequency region where most of the signal spectrum is located, the time delay of the signal "front" at the output is determined by the dispersion characteristic at high frequencies, $\omega\to\infty$. The physical reasoning behind this fact is that the signal onset introduces discontinuities in derivatives. Intuitively, this abrupt change in signal derivatives corresponds to higher frequency components of the signal spectrum. A typical negative group delay medium dispersion characteristic, with a common engineering representation with frequency on the horizontal axis and angular phase delay on vertical axis, looks like the top plot shown in Fig. 2-6. The bottom plot depicts the corresponding group delay, obtained by (2.11). The NGD property is observed around the center frequency of the characteristic shown in Fig. 2-6. However, as frequency is increased, both group and phase delays become

positive and approach a constant value that is always less or equally than the speed of light in vacuum, $c \approx 3 \times 10^8$ *m*/*s*.

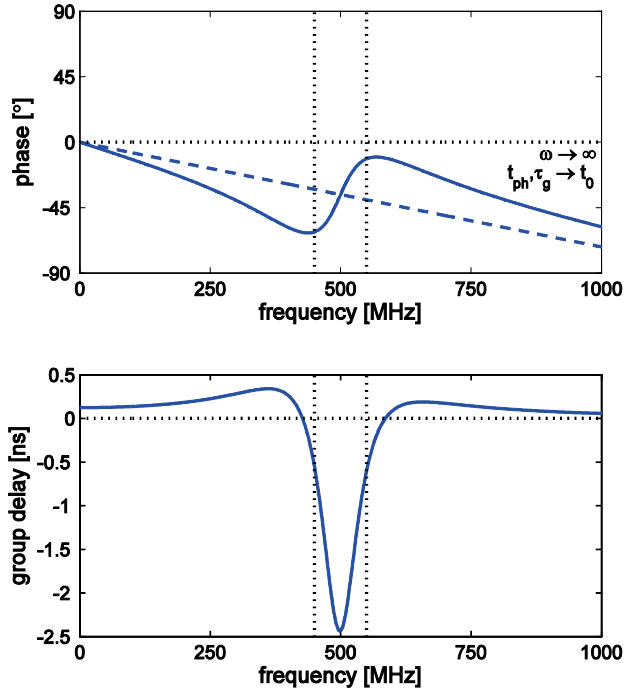

Figure 2-6: Typical dispersion and group delay characteristics of an NGD medium.

Therefore, even though certain parts of the waveform can appear at the output even before they enter the input of the medium (NGD phenomenon), the speed of propagation of the initial onset of the waveform, or the "front", is always positively delayed and slower than the speed of light in vacuum, *c*. This way, the relativistic causality is not violated in this type of a medium. The analysis presented above is not restricted to the simple, semi-infinite sinusoidal waveform. It extends to any waveform with a defined "turn on" point in time, before which the waveform and all of its derivatives are equal to zero. Such a waveform can be represented by step-modulated time-harmonic frequency components, through Fourier analysis.

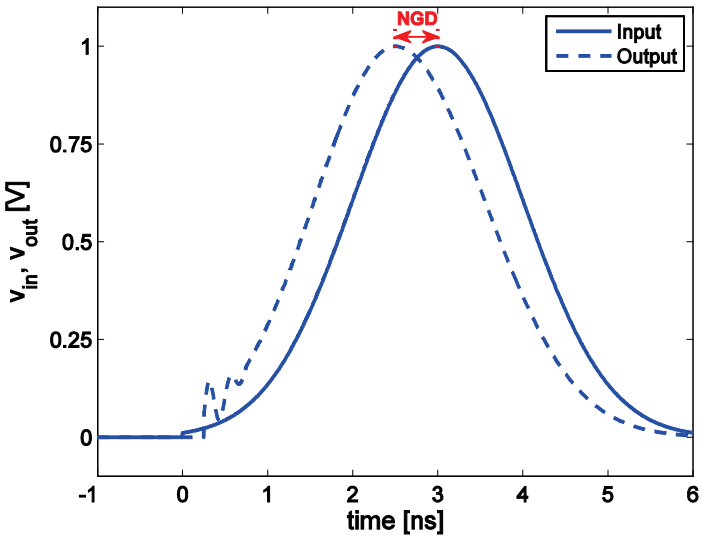

Figure 2-7: An illustration of input and output waveform envelopes in an NGD medium.

Figure 2-7 shows an exaggerated illustration of example baseband waveforms (or waveform envelopes, if modulated waveforms are considered) at the input and output of an NGD medium. The input waveform is a Gaussian pulse, and it has a "turn on" time at t=0. The onset of the illustrated output waveform is positively delayed, and it contains transients. After the transients have decayed, the rest of the output waveform is slightly distorted, or reshaped, and the output peak precedes the input peak (NGD). In general, the output waveform can have different amplitude than the input waveform, depending if the medium introduces loss or gain. The output waveform amplitude also depends on the level of the medium's amplitude characteristic distortion within the NGD bandwidth, which translates into distortion of the steady-state part of the waveform. It is also intuitive that the waveform propagating through an NGD medium needs to be distorted to a degree, if one part of the waveform is shifted in time by one value (onset delayed positively in the example above) and another part of the waveform is delayed by another value (peak delayed in the opposite direction).

2.2 NGD Engineering Application Examples

After covering the NGD phenomenon background in the previous section and its interpretation in both, the frequency and time domains, several selected engineering applications will now be discussed.

The traditional feed-forward amplifier configuration, without the NGD compensation, is shown in Fig. 2-8. This application attempts to cancel some of the signal distortion introduced by a non-ideal amplifier. The non-ideal amplifier with a gain G produces an output signal, $v_{out}(t)$, which can be modeled as the sum of the ideally amplified input signal, $G \cdot v_{in}(t)$, and a fictitious "error" waveform it introduces, $G \cdot e(t)$, both delayed by the amplifier's positive delay, t_{amp}. The error term is then determined by scaling the distorted output signal to the input level via an attenuator, and subtracting it from the original input signal.

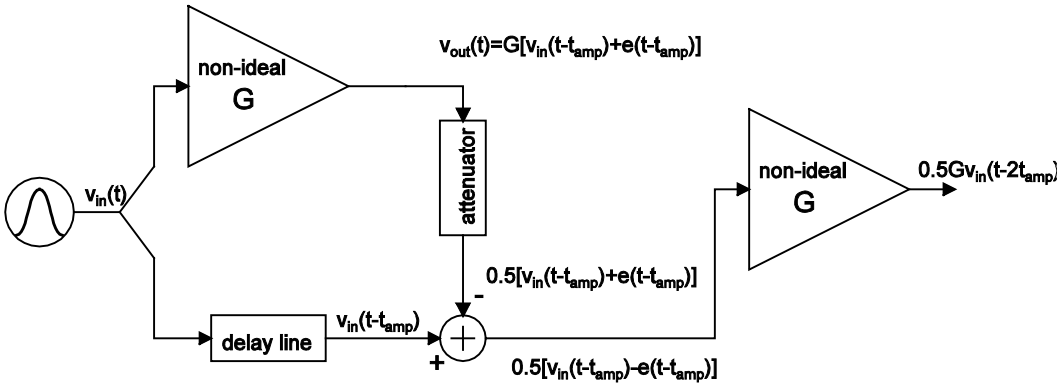

Figure 2-8: Error-cancelling feed-forward amplifier configuration.

For the subtraction of the two quantities to be accurate, the original input signal needs to delayed by the same amount, t_{amp}, which is accomplished through a simple transmission line. Finally, the difference signal is fed to an identical non-ideal amplifier, and the

output of the 2nd stage amplifier is a distortionless amplified and delayed version of the input signal. One drawback of this design is the added delay line needed for the time-alignment of the input signal, which can be physically long relative to circuit dimensions. For example, if the delay of the amplifier, and therefore the needed delay of this line is 90° at 500 MHz, that translates into a 0.5 ns delay of the line, or 15 cm length in air/vacuum. Based on the relative effective permittivity of the substrate the circuit is fabricated on, ε_{reff}, this length is scaled down by a factor of $(\varepsilon_{reff})^{-1/2}$. For some typical permittivity values, this transmission line length is still considerably long compared with the lumped circuit dimensions, and can take up significant additional space. An NGD circuit can be cascaded with the non-ideal amplifier, thus reducing the amplifier delay t_{amp}, which in turn requires a physically shorter delay line leading to reduction in size of the overall design. If the input signal of interest is an amplitude-modulated signal, the NGD circuit will compensate for the delay of the signal envelope only, according to (2.10). In this case, a negative refractive index (NRI) circuit is needed as well, to compensate for the delay of the signal carrier, so the entire waveform delay, t_{amp}, will be reduced.

In another example, NGD can provide delay line compensation in phased array antennas [49,50]. An uncompensated series-fed linear array configuration, radiating in a broadside direction is shown in Fig. 2-9. At the design frequency, the array antenna elements are usually spaced 180° apart for an optimal overall radiation pattern. For a broadside radiation angle the elements need to be in phase, which for a series-fed array is achieved by connecting them with 360° long delay lines, as shown in Fig. 2-9. Therefore, at exactly the design frequency the array achieves a perfect broadside radiation angle.

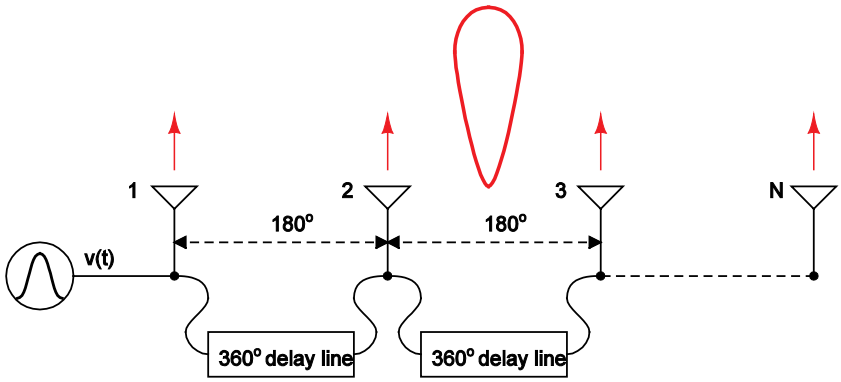

Figure 2-9: Broadside linear *N*-element phased array configuration.

However, signals used in information transfer have a finite non-zero bandwidth around the center frequency. Different frequency components of the signal will experience different angular phase shifts through the connecting delay lines, with only the center frequency experiencing the exact 360° shift, as shown in Fig. 2-10.

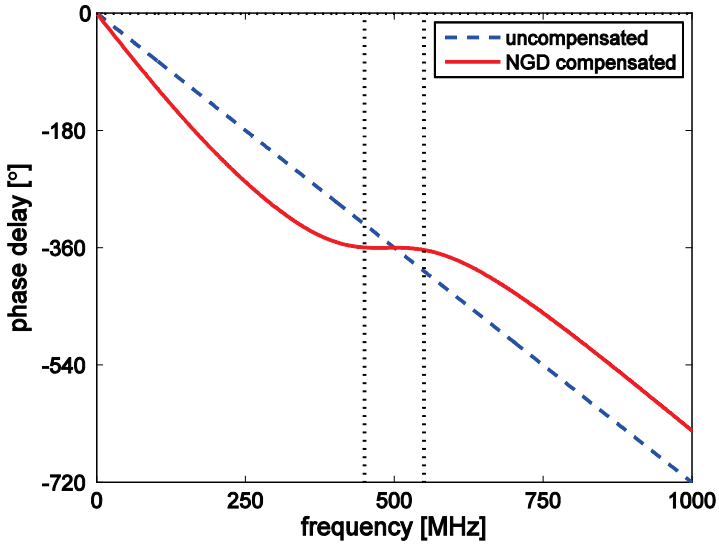

Figure 2-10: Phase characteristic between two adjacent elements in a linear broadside phased array.

This results in frequency components of the signal being radiated at different angles, which is known as "beam-squint" [49]. NGD circuits can be employed to cancel the positive group delay within the entire bandwidth of interest, which in the frequency

domain is manifested in flattening the phase characteristic slope, as shown in Fig. 2-10. Unlike the previous feed-forward amplifier application example, the goal here is to compensate for the group delay only and leave the carrier delay at the original value, since it relates to the desired radiation angle. The desired frequency characteristic in this example is known as a constant phase shifter, where all frequency components within a bandwidth are delayed by the same angular value.

Usefulness of NGD compensation in this phased array application is illustrated on a time-domain example, as shown in Fig. 2-11. This example corresponds to the delay line frequency domain characteristic from Fig. 2-10, with the center frequency of 500 MHz (2 ns period). A sinusoidal carrier of this period is modulated by a Gaussian signal with a standard deviation of 5 ns. For illustration purposes, the input waveform is shown as it appears at the element which is 8 delay lines (with 360° delay each, at 500 MHz) apart from the first element, corresponding to a 16 ns delay.

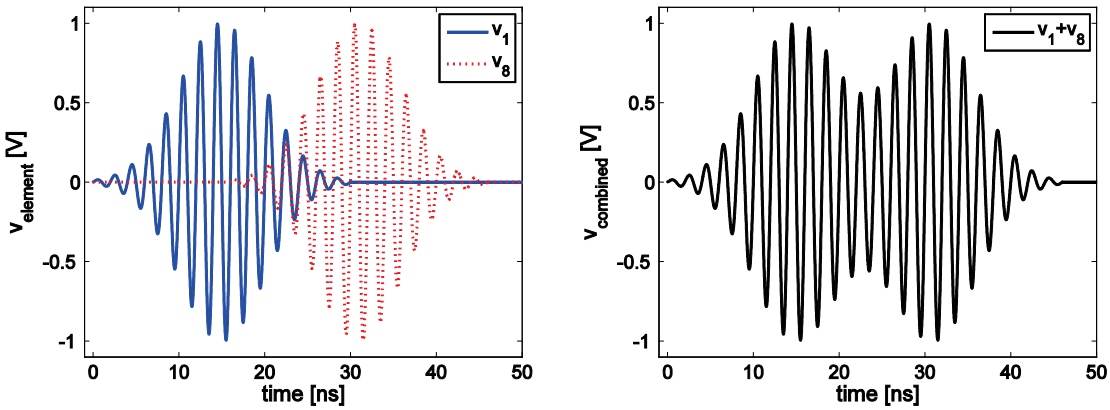

Figure 2-11: An illustration of a time-domain distortion in an uncompensated phased array.

If the waveforms are left group delay uncompensated, as they add up at a far-field point of the broadside array radiation the combined waveform will be distorted, as shown in the

second plot in Fig. 2-11. An ideal NGD compensation would line up the envelope of the delayed waveform with the input one, thus canceling the illustrated distortion.

In phased array applications, only the group delay needs to be compensated for, and the angular phase delay needs to be left at the desired firing angle value. Negative phase delay (LHM) circuits can play an important role in engineering that desired phase delay value. Therefore, combined LHM and NGD circuits are useful in phased array applications [49,50]. For example, instead of the regular 360° delay lines shown in Fig. 2-9, which connect elements which are 180° apart, a 90° positive delay line can be cascaded with a -90° LHM line, thus achieving a desired overall 0° phase shift, but now only with half the physical size. Not only does this save physical space, but it reduces the line's positive group delay slope, thus requiring less NGD in order to compensate for it.

Aside from phased array antennas, constant phase shifters have been used in balun applications where a broadband phase shift of 180° between two ports in needed, to feed a bipole antenna for example [42]. Constant phase shifters have also been used in Wilkinson power dividers [23], where a constant with frequency phase shift is needed for the desirable high isolation between two of the device's three ports.

Having covered the NGD phenomenon background in this chapter, with its frequency and time domain interpretations and some engineering examples, the next chapter will explore commonly used resonator-based NGD circuits. A generic formulation will be derived for this type of circuits, along with their NGD asymptotic limits and trade-offs.

3. NGD Asymptotic Limits in Resonator-Based Media

In this chapter different resonator-based electrical circuits, which act as negative group delay media within a certain frequency bandwidth, will be studied and compared. Further, a generic formulation for these types of circuits will be derived, and NGD asymptotic limits and trade-offs will be explored.

As discussed in the previous chapter, the NGD phenomenon corresponds to the region with a negative tangent slope to the ω-β (frequency vs. propagation constant) dispersion characteristic. This also corresponds to a positive tangent slope of the commonly used phase characteristic shown in Fig. 2-6, with frequency on the horizontal axis and the difference between the output and input harmonic waveform phase on the vertical axis.

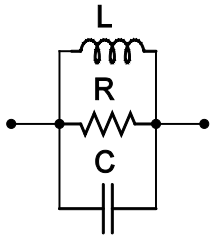

Figure 3-1: A parallel *RLC*-resonator.

One circuit element that can achieve an NGD effect over a finite frequency bandwidth is a parallel *RLC*-resonator, consisting of a resistor *R*, an inductor *L*, and a capacitor *C*, as shown in Fig. 3-1. The impedance of an inductor is directly proportional to the applied

frequency ($Z_L=j\omega L$), where the imaginary unit j depicts a positive 90° difference between the sinusoidal electrical voltage and the corresponding current through the inductor. Similarly, the impedance of a capacitor is inversely proportional to frequency ($Z_C=-j(\omega C)^{-1}$), and there is a -90° difference between the voltage and the current through this element. At the resonance frequency $\omega_0=1/(LC)^{1/2}$, the inductor and capacitor impedances are equal in magnitude but opposite in sign, so they effectively cancel leaving the resistance R as the overall effective impedance of the resonator.

For frequencies below the resonance, the inductor impedance will dominate since it is the smallest impedance in magnitude, out of the 3 parallel elements. Therefore, the overall current through the resonator will lag the applied voltage by an angle between 0° and 90°, depending on the frequency and the element values. At the resonance, the overall impedance will be equal to the resistance R and purely real, meaning that the voltage and current will be in phase. Similarly, for frequencies above the resonance, the capacitor will dominate and the overall current will lead the applied voltage by an angle between 0° and 90° (the overall impedance will be complex, with a negative imaginary part). This shift from a lagging to leading current through the resonator yields an NGD behavior, which will be discussed later. The bandwidth of a resonator $\Delta\omega$ is the difference between the 2 frequencies at which the imaginary part of the impedance is equal in magnitude to the real part. This corresponds to the upper bandwidth point (-45° impedance angle), and the lower bandwidth point (+45°), as shown in Fig 3-2. At the same time, the absolute value of the impedance drops down by a factor of $\sqrt{2}$ at the bandwidth edges, as shown in Fig 3-3.

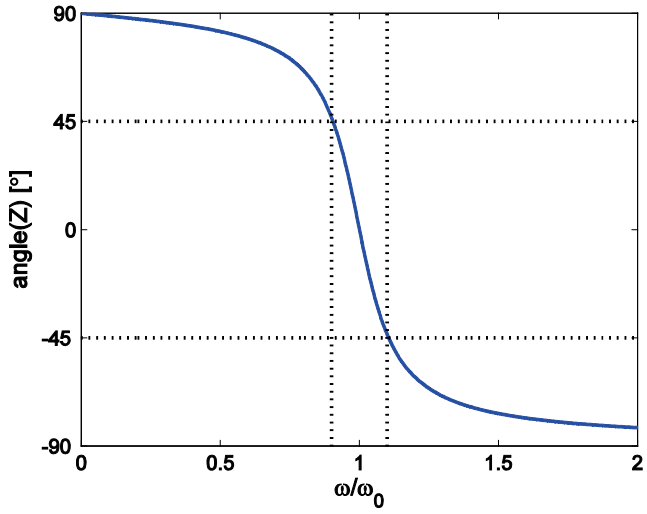

Figure 3-2: Impedance phase characteristic of a parallel *RLC*-resonator.

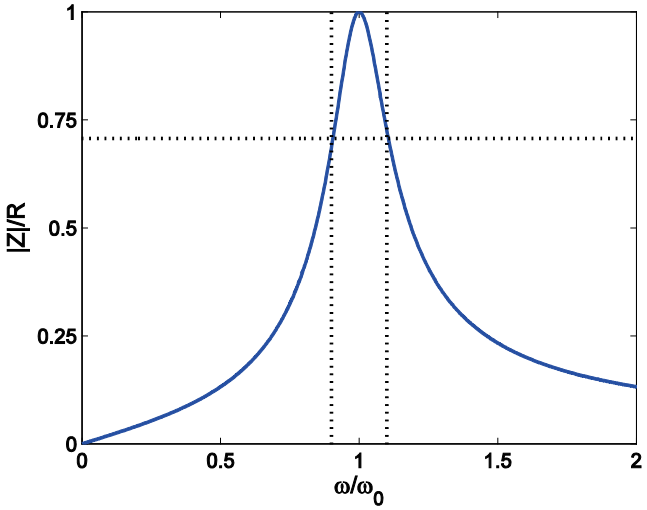

Figure 3-3: Impedance magnitude characteristic of a parallel *RLC*-resonator.

The quality factor of a resonator is defined as the ratio of the resonance frequency, and the above defined bandwidth [64], as $Q=\omega_0/\Delta\omega=f_0/\Delta f$. Furthermore, the overall complex impedance of the parallel resonator can be written as

$$Z(\omega)=\frac{1}{\frac{1}{R}+j\omega C+\frac{1}{j\omega L}}=\frac{R}{1+j\omega CR\left(1-\frac{\omega_0^2}{\omega^2}\right)}, \tag{3.1}$$

where, again, the resonance frequency is given by $\omega_0=1/(LC)^{1/2}$. The difference between the upper and lower bandwidth edge frequency (at each edge the real and imaginary parts of the impedance are equal in magnitude) can be determined from (3.1) as

$$\Delta\omega = \frac{1}{RC} = \frac{\omega_0^2 L}{R}. \tag{3.2}$$

Now, the quality factor, overall impedance, and bandwidth edge frequencies can be written as

$$Q = \frac{\omega_0}{\Delta\omega} = \frac{R}{\sqrt{L/C}}, \tag{3.3a}$$

$$Z(\omega) = \frac{R}{1 + jQ\dfrac{\omega}{\omega_0}\left(1 - \dfrac{\omega_0^2}{\omega^2}\right)}, \tag{3.3b}$$

$$\omega_{up,lo} = \omega_0\sqrt{1 + \frac{1}{4Q^2}} \pm \frac{\Delta\omega}{2}. \tag{3.3c}$$

As it can be seen from (3.3c), the center of the frequency bandwidth does not coincide perfectly with the resonance frequency, due to the non-symmetric impedance characteristic around resonance (imaginary impedance, or reactance of an inductor and a capacitor is a linear, and a reciprocal function of frequency, respectively). In the example depicted in Fig. 3-2 and Fig. 3-3, the value of Q=5 was used, corresponding to the bandwidth center frequency being higher than the resonance frequency by 0.5% only.

In the next section different resonator-based circuit topologies that achieve an NGD by employing parallel or series *RLC* resonators will be examined and their generic formulation will be proposed.

3.1 Generic Formulation of Single-Resonator Based NGD Circuits

During the analysis of different topologies of resonator-based NGD circuits, it was observed that most of them have the same transfer function form in the frequency domain, as reported in contribution [60]. The generic transmission characteristic (frequency-dependent complex ratio of output and input steady-state sinusoidal waveforms) for circuit topologies comprised of a single resonator and arbitrary resistive matching networks, was derived in Appendix A as

$$S_{21}(\omega) = (A_0 G) A \frac{\omega^2 - \omega_0^2 - j\frac{1}{Q}\omega_0\omega}{\omega^2 - \omega_0^2 - j\frac{1}{Q}A\omega_0\omega} e^{-j\beta\cdot l}, \tag{3.4}$$

where βl accounts for the additional phase delay due to finite physical dimensions, A is the ratio of the maximum and minimum values of the transfer function amplitude, which will be called out-of-band gain, A_0=$S_{21}(\omega_0)$ is the transfer function value at the resonance, and G is the gain of an optional amplifier cascaded with the resonator which compensates for the inherent resonator loss. An example of the transfer function magnitude and phase

characteristic is shown in Fig. 3-4 for a resonance frequency f_0=500 MHz, resonator bandwidth Δf=100 MHz (Q=5), neglecting the physical length delay, and for several different values of the out-of-band gain A.

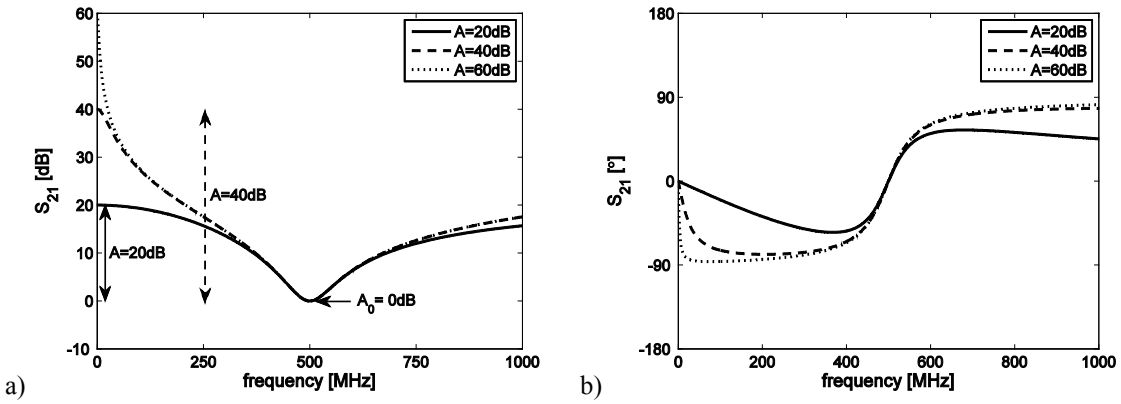

a) b)

Figure 3-4: Amplitude a) and phase b) transfer function characteristics of a single-stage resonator circuit.

The phase characteristic and the corresponding group delay are given by

$$\phi(\omega) = \arctan\left(\frac{\mathrm{Im}(S_{21})}{\mathrm{Re}(S_{21})}\right), \quad \tau_g(\omega) = -\frac{d\phi(\omega)}{d\omega}. \tag{3.5}$$

Applying (3.5) to (3.4) yields the following expression for the group delay as a function of frequency

$$\tau_g(\omega) = -Q\omega_0(\omega^2 + \omega_0^2)\left(\frac{1}{Q^2(\omega^2 - \omega_0^2)^2 + \omega^2\omega_0^2} - \frac{A}{Q^2(\omega^2 - \omega_0^2)^2 + A^2\omega^2\omega_0^2}\right). \tag{3.6}$$

The maximum NGD occurs approximately at the resonance frequency, and it can be evaluated from (3.6) as

$$NGD_{MAX} \approx NGD_0 = -\tau_g\Big|_{\omega=\omega_0} = \frac{2Q}{\omega_0}\left(1-\frac{1}{A}\right). \tag{3.7}$$

Note that the negative of the group delay τ_g is used to define NGD. Therefore, a positive value of NGD corresponds to a negative group delay. From (3.7), it is evident that an upper limit for NGD_{MAX} is achieved when $A\to\infty$, suggesting a trade-off between NGD and out-of-band gain. Therefore, from (3.7) it can be written

$$NGD_{MAX} \le NGD_{MAX}\Big|_{A\to\infty} = \frac{2Q}{\omega_0} = \frac{1}{\pi}\frac{1}{\Delta f}. \tag{3.8}$$

Alternatively, it can be stated that the NGD-bandwidth product of a single-stage resonator circuit has an upper limit of $NGD_{MAX}\cdot\Delta f\le 1/\pi$. It is important to express group delay as a fraction of the reciprocal bandwidth, $1/\Delta f$, which gives us a measure of the transmitted waveform temporal duration in the time domain (pulses with a narrower frequency spectrum are wider in time, and vice versa). For example, a simple pulse waveform such as a half-period sinusoid of frequency f_s, has a temporal width of exactly $1/(2f_s)$, or $1/\Delta f$ if the waveform bandwidth is defined to be $\Delta f=2f_s$. On the other hand, more complex pulse forms, such as an infinite-in-time Gaussian pulse, will have a "Full-Width-Half-Maximum" (FWHM, a temporal width between the points where the pulse value drops to half its peak value) of approximately $2.25/\Delta f$, if Δf is chosen such that it spans over 6 standard deviations of the corresponding frequency spectrum of the pulse, $\Delta f=6\sigma_f$ (over 99.998% of the pulse power is within Δf). Therefore, according to (3.12) this circuit can achieve a maximum NGD of about 32% of a half-period sinusoidal pulse,

or only about 14.2% of a Gaussian pulse FWHM, when the pulse temporal standard deviation is $\sigma_f = \Delta f/6$.

Figure 3-5a shows a group delay as a function of frequency evaluated from (3.6) for f_0=500 MHz, Δf=100 MHz (Q=5), and different values of the out-of-band gain A. Figure 3-5b shows the maximum NGD as a function of A, for this particular case. As expected, the maximum NGD occurs approximately at the resonance frequency and it increases with A, with the NGD upper limit of 3.18 ns as predicted by (3.8).

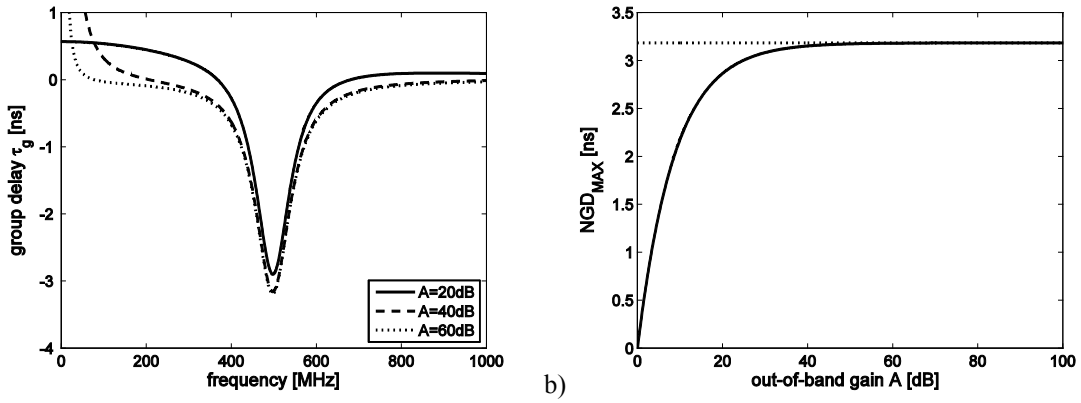

a) b)

Figure 3-5: Single-stage resonator circuit a) group delay as a function of frequency, and b) maximum NGD (at the resonance frequency) as a function of the out-of-band gain, A.

Having explored the NGD characteristics of the generic single-stage resonator-based case described by (3.4), now particular circuit topologies can be examined in terms of how their circuit parameters relate to the generic formulation parameters A, ω_0, Q and A_0.

3.1.1 Unmatched Parallel *RLC* Resonator Circuit

This circuit topology is assembled by simply connecting the studied parallel *RLC* resonator to a voltage source with impedance Z_0 on one end, and to a load on the other, as shown in Fig. 3-6.

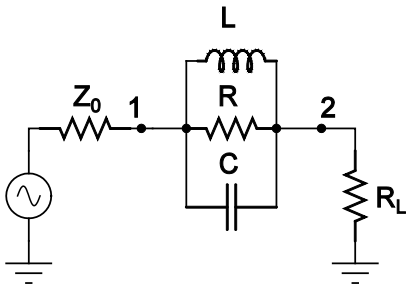

Figure 3-6: An unmatched parallel *RLC*-resonator NGD circuit.

When the load and source impedances are the same (R_L=Z_0), and such matched load is connected directly to the source (without the resonator in between), it can be shown that the maximum available power is transferred from the source to the load [64]. At microwave frequencies, devices are commonly analyzed through scattering parameters (*S*-parameters), which give us a measure of how much of the available source power is transmitted to the load, how much is reflected back to the source, and consequently how much is dissipated within the device.

The transmission coefficient $S_{21}(\omega)$ is a ratio of a sinusoidal waveform voltage, with frequency ω, at the output of a circuit terminated in the load impedance Z_0 (same value as the source impedance), to the corresponding voltage at the source terminals which would be established if the source was directly connected to a matched load (referred to as "incident voltage", as in the maximum power transfer case). Similarly, the reflection coefficient $S_{11}(\omega)$ is defined as a ratio of the reflected voltage at the device input to the

incident voltage, when the output is terminated in an impedance equal to the source impedance. Values of *S*-parameters are complex numbers, capturing both the magnitude and phase of the aforementioned sinusoidal waveform ratios. Since the power delivered to a load is proportional to the square of the voltage, the square values of *S*-parameters magnitudes represent the power delivered to the load ($|S_{21}|^2$), or reflected power ($|S_{11}|^2$), relative to the maximum available power (transferred in the matched source-load case). Here it is assumed that the device/network/system under test is linear, i.e. the output to input voltage ratio does not depend on the magnitude of the applied sinusoidal waveform.

Applying basic circuit theory, the input reflection coefficient for the circuit shown in Fig 3-6 can be expressed as

$$S_{11}(\omega) = \frac{Z(\omega)}{2Z_0 + Z(\omega)}, \tag{3.9}$$

where $Z(\omega)$ is the frequency dependent resonator impedance given by (3.3b). The circuit's transfer function, or transmission coefficient $S_{21}(\omega)$, is given by the derived generic form (3.4), with G=1 (a passive circuit with no gain), and parameters A and A_0 given by

$$A_0 = \frac{2Z_0}{2Z_0 + R}, \quad A = 1 + \frac{R}{2Z_0} = \frac{1}{A_0}. \tag{3.10}$$

The transmission and reflection coefficient magnitude plots for a selected case with Q=5 and R=250 Ω, as well as the transmission phase plot are shown in Fig. 3-7.

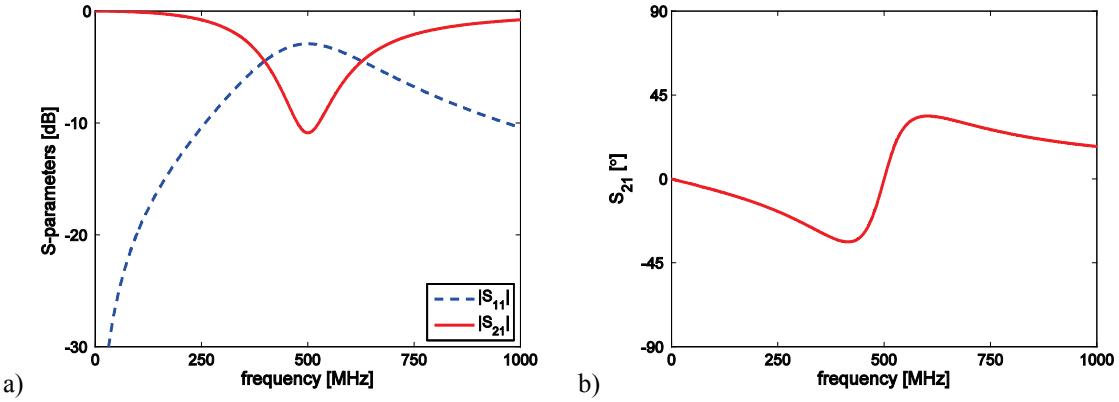

a) b)

Figure 3-7: Unmatched parallel *RLC* circuit a) input reflection and transmission magnitude and b) transmission phase plots for Q=5, R=250 Ω.

The minimum transmission magnitude (maximum loss), A_0, occurs at the resonance frequency, when the resonator has a maximum impedance of R. At the same time, the largest negative group delay (tangent slope on the phase characteristic) occurs approximately at the resonance frequency as well, and can be determined from (3.7) and (3.10) as

$$NGD_{MAX} = \frac{2Q}{\omega_0}(1 - A_0) = \frac{2Q}{\omega_0}\left(1 - \frac{1}{A}\right). \tag{3.11}$$

From the expression (3.11), it is clear that there is a trade-off between the negative group delay, and the power dissipated in the resonator. The closer the transmitted power at resonance, A_0, is to zero (or to negative infinity in decibels), the larger the NGD is. This result is expected since the resonator is connected in series with the source and load impedances, so the higher the resonator impedance is (more loss), the more it will dominate the series connection and consequently yield more NGD.

The output waveform envelope will therefore be attenuated, in addition to being advanced in time. The extent to how much NGD can be achieved, is limited by how much loss can be tolerated (or compensated for through a cascaded amplifier) in a given application. The theoretical NGD limit (allowing infinite loss) for this type of circuit is given by

$$NGD_{MAX} \le \frac{2Q}{\omega_0} = \frac{2}{\Delta\omega} = \frac{1}{\pi}\frac{1}{\Delta f} \approx 0.32\frac{1}{\Delta f}. \tag{3.12}$$

In conclusion of the unmatched parallel *RLC* circuit analysis, it is worth mentioning that an equivalent effect can be achieved using a series *RLC* circuit connected in parallel with the load and the source, as shown in Fig. 3-8. The quality factor of this circuit is reciprocal to the one of the parallel circuit, and also less power is transmitted to the load for smaller values of resonator resistance, as given by

$$Q_{SERIES} = \frac{\omega_0}{\Delta\omega} = \frac{\sqrt{L/C}}{R}, \quad A_0 = S_{21}(\omega_0) = \frac{2R}{2R + Z_0}, \quad A = 1 + \frac{Z_0}{2R}. \tag{3.13}$$

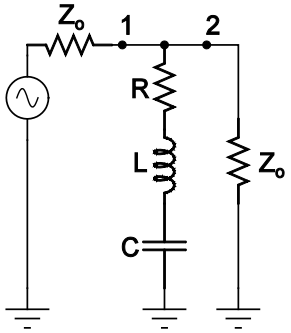

Figure 3-8: An unmatched series *RLC*-resonator NGD circuit.

However, the relationship between the maximum NGD and transmitted power remains the same as for the parallel resonator case, and can be obtained from (3.7) and (3.13) as

$$NGD_{MAX} = \frac{2Q}{\omega_0}(1 - A_0) = \frac{2Q}{\omega_0}\left(1 - \frac{1}{A}\right). \tag{3.14}$$

Therefore, this circuit achieves the same effect as the parallel *RLC* resonator. One type of resonator could be chosen over the other based on the circuit topology that might be more convenient for a particular application, or based on the more reasonable inductor and capacitor values for a given resonance frequency and desired bandwidth (or *Q*-factor).

3.1.2 *R*-matched *RLC* Resonator Circuit

This circuit consists of the same parallel resonator, with the addition of a matching resistor R_m at the input, as shown in Fig 3-9.

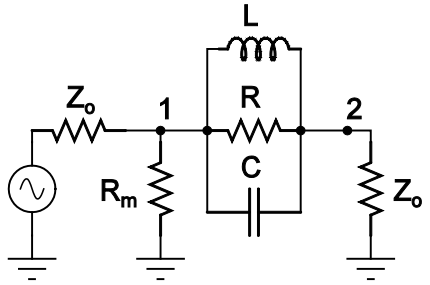

Figure 3-9: An *R*-matched series *RLC*-resonator NGD circuit.

The circuit's transmission characteristic is described by the generic expression (3.4), with the expression parameters related to circuit parameters by

$$A_0 = S_{21}(\omega_0) = \frac{Z_0}{Z_0 + R}, \qquad A = \frac{2}{Z_0}\frac{(R+Z_0)^2}{3R+2}. \tag{3.15}$$

The transmission and reflection coefficient magnitude plots as well as the transmission phase plot are shown in Fig. 3-10, for the same selected case with Q=5 and R=250 Ω, and the required matching resistor $R_m = Z_0(1+ Z_0/R)$=60 Ω.

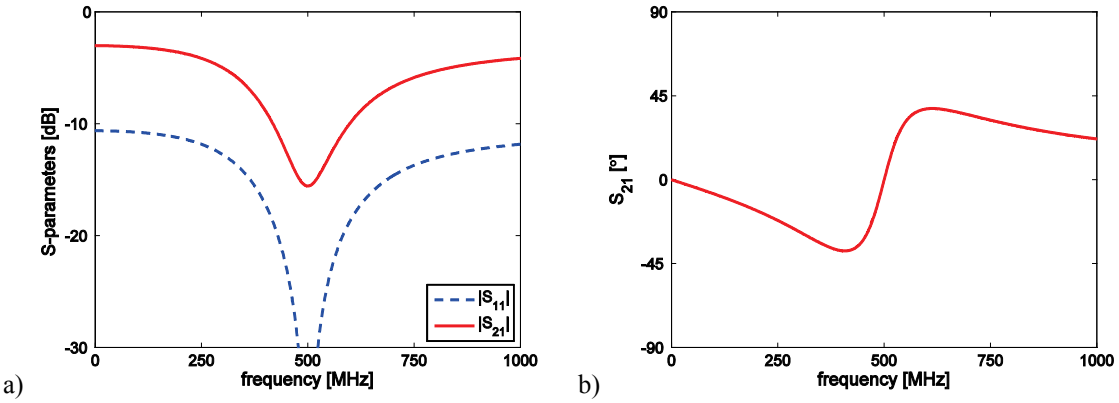

Figure 3-10: R-matched parallel RLC circuit a) input reflection and transmission magnitude and b) transmission phase plots for Q=5, R=250 Ω and R_m=60 Ω.

It can be noted that the transmission coefficient magnitude value at low and high frequencies (when the resonator impedance is essentially zero) is not 100% (or zero dB), as in the previous case, due to the power to ground dissipation through the matching resistor R_m. The limit value of the low and high frequency end transmission coefficient value, for a large out-of-band gain, is given by

$$\lim_{A\to\infty} S_{21}(0) = \lim_{A\to\infty} S_{21}(\infty) = \lim_{A\to\infty}(A_0 A) = \frac{2}{3}. \tag{3.16}$$

Comparing this circuit with the unmatched one, it can be noted that even though the circuit is matched at the input, so no power is reflected back to the source at the resonance frequency, less power is transmitted to the load for the same value of resonator resistance. This is due to more power being lost in the circuit itself, through the matching shunt to ground resistor R_m. At the same time this circuit yields a larger NGD, so the overall performance of different circuits is better compared through their NGD vs. maximum transmission loss, A_0, characteristics, as will be shown later. The NGD vs. out-of-band gain characteristic, however, will be the same for all circuits, as per (3.4). For this circuit in particular, the maximum NGD can be obtained from (3.7) and (3.15) as

$$NGD_{MAX} = \frac{2Q}{\omega_0}\left(1-\frac{A_0}{2}\right)\left(1-A_0\right) = \frac{2Q}{\omega_0}\left(1-\frac{1}{A}\right). \tag{3.17}$$

The maximum achievable NGD value is the same as for the unmatched circuit, $NGD_{MAX}=1/(\pi\cdot\Delta f)$, as expected.

3.1.3 π-matched *RLC* Resonator Circuit

This circuit has a matching resistor R_{sh} at the output as well as input as shown in Fig. 3-11, making the circuit symmetric and two-port matched at the resonance frequency.

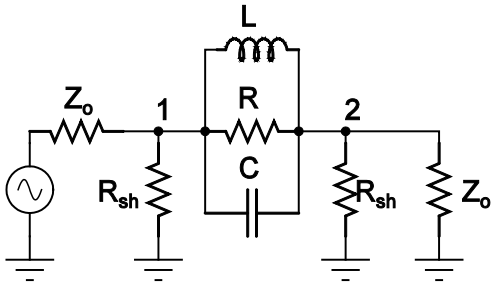

Figure 3-11: A π-matched series *RLC*-resonator NGD circuit.

This circuit's transmission characteristic is described by the generic expression (3.4) again, with the expression parameters related to circuit parameters by

$$A_0 = \frac{R_{sh} - Z_0}{R_{sh} + Z_0}, \qquad A = \frac{R_{sh}}{R_{sh} - Z_0}, \tag{3.18a}$$

where

$$R_{sh} = \frac{Z_0}{R}\left(Z_0 + \sqrt{Z_0^2 + R^2}\right). \tag{3.18b}$$

The limit value of the low and high frequency end transmission coefficient value, for a large out-of-band gain, in this case is given by

$$\lim_{A\to\infty} S_{21}(0) = \lim_{A\to\infty} S_{21}(\infty) = \lim_{A\to\infty}(A_0 A) = \frac{1}{2}. \tag{3.19}$$

The transmission and reflection coefficient magnitude plots, as well as the transmission phase plot are shown in Fig. 3-12. The resonator resistance and *Q*-factor are chosen to be

the same as in previous cases with Q=5 and R=250 Ω, while the matching resistor for this particular circuit is determined from (3.18b) and yields R_{sh}=61 Ω.

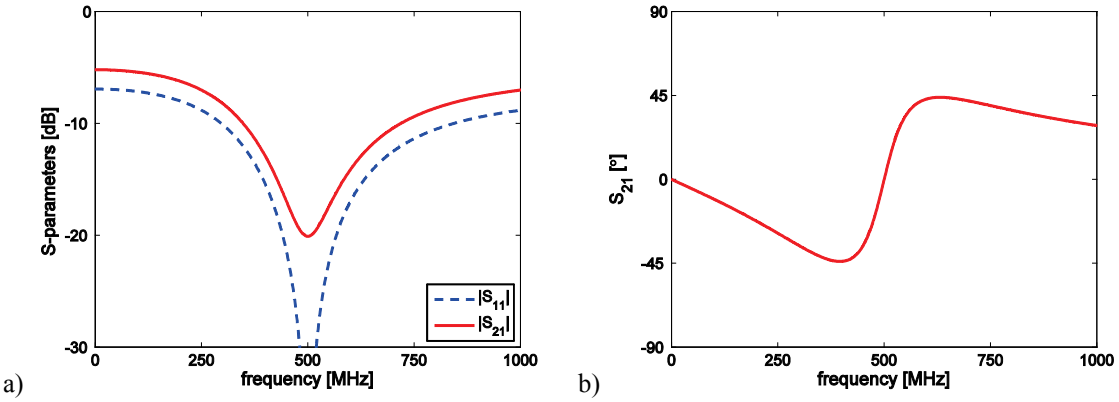

Figure 3-12: R-matched parallel RLC circuit a) input reflection and transmission magnitude and b) transmission phase plots for Q=5, R=250 Ω and R_{sh}=61 Ω.

Comparing this circuit with the previous two, it can be noted that even less power is transmitted to the load for the same value of resonator resistance. This is not surprising, since the additional power is lost through the two matching resistors R_{sh} to ground, as confirmed by (3.19). The maximum phase slope is also steeper in this case, and the NGD vs. maximum transmission loss, A_0, characteristic for this circuit can be obtained from (3.7) and (3.18) as

$$NGD_{MAX} = \frac{2Q}{\omega_0}\left(\frac{1-A_0}{1+A_0}\right) = \frac{2Q}{\omega_0}\left(1-\frac{1}{A}\right). \tag{3.20}$$

The maximum theoretical NGD that can be achieved with this circuit, $NGD_{MAX}=1/(\pi\cdot\Delta f)$, is the same as for the previous two topologies, as expected.

3.1.4 *LC*-matched *RLC* Resonator Circuit

This circuit achieves input impedance matching through a shunt inductor at the load, and a series capacitor at the input end, as shown in Fig 3-13. The matching elements are purely reactive so they do not consume any power, unlike resistors. Furthermore, the circuit topology with a series capacitor and shunt inductor alone (without the resonator), is a building block for Left-Handed Materials (LHM), which exhibit negative phase delay within certain frequency bands [22]. The circuit shown in Fig 3-13 is therefore expected to exhibit a negative phase delay, in addition to negative group delay [30,31].

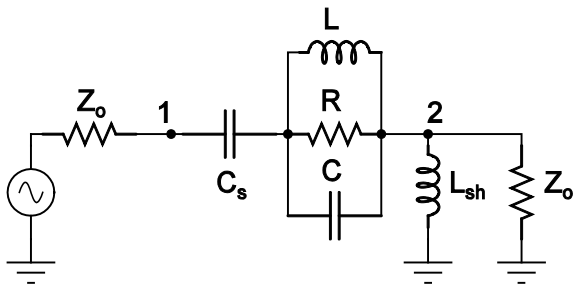

Figure 3-13: An *LC*-matched series *RLC*-resonator NGD circuit.

Certain applications such as series fed networks for phased array antennas [65] require simultaneous engineering of the phase and group delays. In this case it is beneficial to use LHM to achieve physically shorter delay lines between the array elements, which will also result in a smaller group delay that needs to be compensated for via NGD circuits, as discussed in Section 2.2. The configuration in Fig 3-13 is more compact than the one which would have a separate LHM stage cascaded by resistive matched NGD stage, since the reactive LHM elements are used as NGD matching elements. However, the impact of this configuration on the achievable NGD will be examined in more detail and compared to a separate LHM/NGD configuration later.

For a given resonator resistance, R, the reactive elements are designed to provide input impedance matching at the resonance frequency, ω_0, and their values can be determined by basic circuit theory as

$$L_{sh} = \frac{Z_0}{\omega_0}\sqrt{\frac{Z_0 - R}{R}}, \qquad C_s = \frac{1}{\omega_0\sqrt{R(Z_0 - R)}}. \tag{3.21}$$

Furthermore, the value of the resonator resistance has to be smaller than the source impedance ($R<Z_0$), in order to make the input matching possible for this configuration. The shunt inductor value is chosen so that the load impedance Z_0 is transformed to a complex value, with a real part of the overall impedance at the load (point "2" in Fig. 3-13) is $Re\{Z_2\}=(Z_0-R)$, at the resonance frequency. At that same frequency, the resonator impedance is purely resistive, R, yielding a matched overall real part of the input impedance to be matched, under the given restriction $R<Z_0$. The negative reactance of the series capacitor cancels the positive, inductive reactance of the complex load at the resonance frequency $Im\{Z_{\mathrm{LOAD}}\}=-(\omega_0 C_s)^{-1}$, as seen at the input. These conditions yield the derived expressions (3.21). The transmission coefficient in the region of interest (within the resonator bandwidth), has a local minimum which occurs close to the resonance frequency, and it is given by

$$A_0 = S_{21}(\omega_0) = \sqrt{\frac{Z_0 - R}{Z_0}}. \tag{3.22}$$

Unlike the generic expression (3.4) for resistive matched resonators where the transfer function is a rational function of 2nd order polynomials, the *LC*-matched case involves 4th order polynomials, due to four reactive elements. After some algebra it is derived as

$$S_{21}(\omega) = A_0 A \frac{\omega^2\left(\omega^2 - j\frac{1}{Q}\omega_0\omega - \omega_0^2\right)}{\omega^4 - jk_3\omega_0\omega^3 - k_2\omega_0^2\omega^2 + jk_1\omega_0^3\omega + k_0\omega_0^4}, \tag{3.23a}$$

where

$$k_3 = \frac{3A^2-1}{2A^2Q} + \frac{\sqrt{A^2-1}}{2}\frac{A^2+1}{A^2}, \qquad k_2 = \frac{3A^2-1}{2A^2} + \frac{\sqrt{A^2-1}}{Q},$$

$$k_1 = \frac{A^2-1}{2A^2Q} + \frac{\sqrt{A^2-1}}{2}\frac{A^2+1}{A^2}, \qquad k_0 = \frac{A^2-1}{2A^2}, \tag{3.23b}$$

$$A = \frac{1}{A_0} = \sqrt{\frac{Z_0}{Z_0 - R}}. \tag{3.23c}$$

The transmission and reflection coefficient magnitude plots, as well as the transmission phase plot, are shown in Fig. 3-14. The case shown has Q=5 (as for previous topologies), and a resonator resistance of R=49 Ω, which is close to the maximum allowed value of $R<Z_0$=50 Ω. The circuit is matched at the resonance frequency, and the minimum transmission coefficient within the bandwidth of interest (about -17 dB), occurs at a frequency slightly lower than the resonance frequency. The output phase characteristic is entirely positive within the resonator bandwidth, corresponding to the negative phase

delay (output phase is advanced relative to the input), confirming that this circuit also exhibits LHM properties, in addition to NGD.

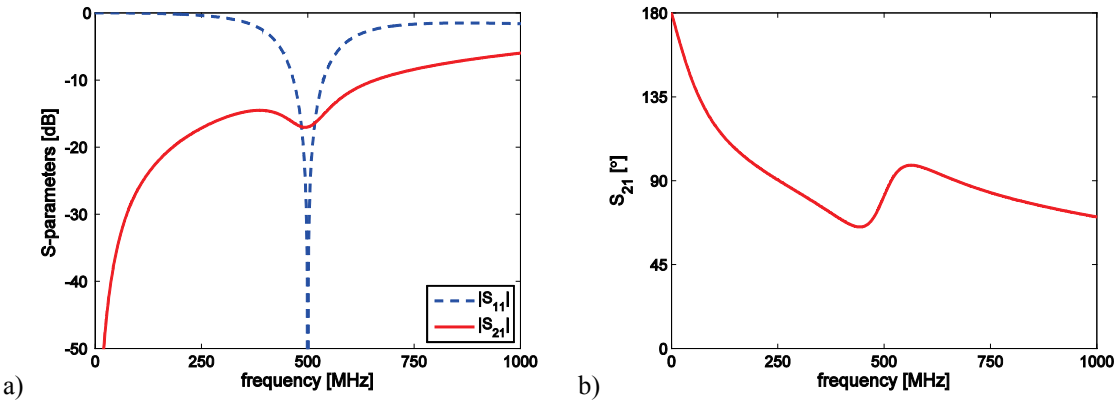

a) b)

Figure 3-14: *LC*-matched parallel *RLC* circuit a) input reflection and transmission magnitude and b) transmission phase plots for Q=5, Z_0=50 Ω, R=49 Ω, L=3.12 nH, C=32.48 pF, L_{sh}=2.27 nH, C_s=45.47 pF.

The transmission coefficient approaches zero (or negative infinity on a decibel scale) for frequencies close to zero (DC), due to the series capacitor at the input. The maximum NGD as a function of the out-of-band gain can be derived by applying (3.5) on (3.23) as

$$NGD_{MAX} \approx -\tau_g(\omega)\Big|_{\omega=\omega_0} = \frac{Q}{\omega_0}\left(1-\frac{1}{A^2}-\left(2-\frac{1}{A^2}\right)\frac{\sqrt{A^2-1}}{A^2Q}\right), \tag{3.24}$$

which is more complex than the generic NGD vs. A expression for resistive-matched resonator topologies given by (3.7). The parameter Q/ω_0 outside of brackets in (3.24) can be written as $1/(2\cdot\Delta f)$, similar to (3.12). Observing the bracketed part of expression (3.24), it can be noted that the circuit will have a better performance (larger NGD relative to $1/\Delta f$, for a given out-of-band gain) for higher values of Q, unlike the resistive-matched cases where NGD values a fraction of $1/\Delta f$ are independent of Q. This effect is caused by

the matching reactive elements, which are frequency dependent. A larger quality factor (smaller frequency bandwidth) yields less variation in these reactance values over the bandwidth, which leads to less "interference" with the resonator phase characteristic. Since A_0A=1 for this circuit (at high frequencies the transmission coefficient is $S_{21}(\infty)$=1), the maximum NGD as a function of transmission loss can be expressed as

$$NGD_{MAX} \approx \frac{Q}{\omega_0}\left(1 - A_0^2 - \frac{2 - A_0^2}{Q} A_0^2 \sqrt{1 - A_0^2}\right). \tag{3.25}$$

The theoretical NGD limit for this circuit is reduced to a half, compared to the resistive-matched cases, and it is given by

$$NGD_{MAX} \leq \frac{Q}{\omega_0} = \frac{1}{2\pi}\frac{1}{\Delta f} \approx 0.16\frac{1}{\Delta f}. \tag{3.26}$$

Therefore, using reactive matching elements in this configuration yields a negative group, as well as a negative phase delay effect, at the expense of a 50% reduction in maximum achievable NGD.

The motive behind the *LC*-matched approach seems intuitive at first. Reactive matching elements do not dissipate any power ideally and also provide a LHM behavior, which is needed in mentioned applications [49,50]. However, the question is if this approach was worth the 50% reduction in the achievable NGD limit, or if a "decoupled" LHM cascaded with a resistive-matched NGD topology would be preferred in achieving a combined LHM/NGD behavior?

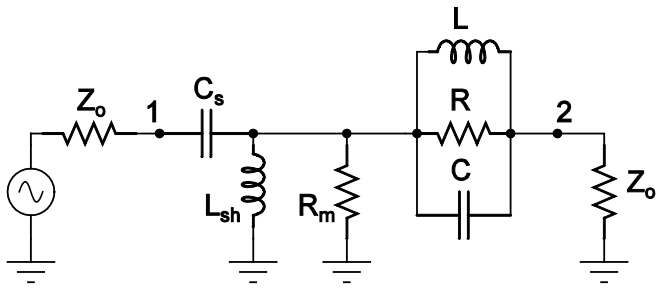

Figure 3-15: Separated *LHM* and *R*-matched series *RLC*-resonator NGD circuit.

To answer this question, the original topology can be compared to the one shown in Fig. 3-15, which consists of a LHM part with a series capacitor, C_s, and a shunt inductor, L_{sh}, cascaded with an *R*-matched NGD circuit. The values of C_s and L_{sh} are different in this topology from those in Fig. 3-13, and are chosen to provide a specified negative phase delay at the resonance frequency, and as close impedance match at the input as possible. The comparison of *S*-parameters and group delay of the two topologies for cases having the same *Q*, the same center frequency attenuation, and the same negative phase delay, is shown in Fig. 3-16. Clearly, the "decoupled" LHM/NGD configuration yields larger NGD than the *LC*-matched configuration in this case. Furthermore, the *LC*-matched configuration does not provide independent designs of NGD and negative phase delay values, since the two reactive elements are designed for matching, which doesn't leave any degrees of freedom for phase delay engineering. The decoupled LHM/NGD configuration on the other hand can provide an independent NGD and phase delay design, especially when the LHM part of the circuit is broken down into cascaded parts with smaller individual phase delays, in which case this part exhibits good wideband matching [22].

In conclusion, the *LC*-matched NGD configuration from Fig. 3-13 does not outperform the decoupled LHM/NGD topology from Fig. 3-15, and it also does not allow

an independent design of NGD and negative phase delay. In addition, the NGD limit is reduced by a half.

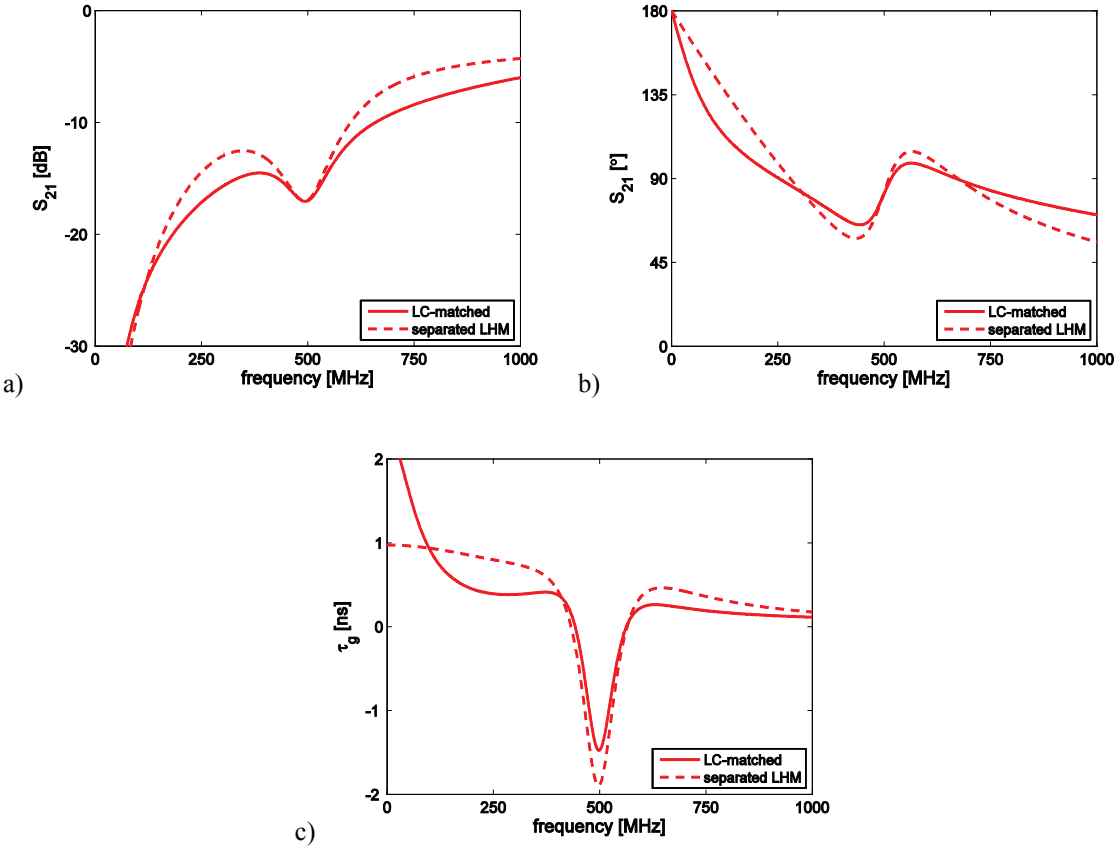

Figure 3-16: Decoupled *LHM* and *R*-matched NGD circuit a) magnitude, b) phase and c) group delay plots for Q=5, Z_0=50 Ω, R=220 Ω, L=14.01 nH, C=7.23 pF, L_{sh}=12.32 nH, C_s=4.93 pF.

3.1.5 Comparison of Different Single-Stage Resonator Circuits

Now that several different passive topologies of *RLC* resonator-based NGD circuits have been analyzed, they can be compared in terms of their maximum NGD vs. the out-of-band gain, A, or vs. loss at the resonance frequency, A_0. The negative group delay is best expressed relatively as a fraction of the time interval given by $1/\Delta f$, as discussed before, or correspondingly the NGD-bandwidth product quantity, NGD·Δf, can be used. When

comparing the presented topologies' NGD vs. the out-of-band gain characteristic, all resistive-matched circuits have the same expression given by (3.7), while the LC-matched expression is given by (3.24).

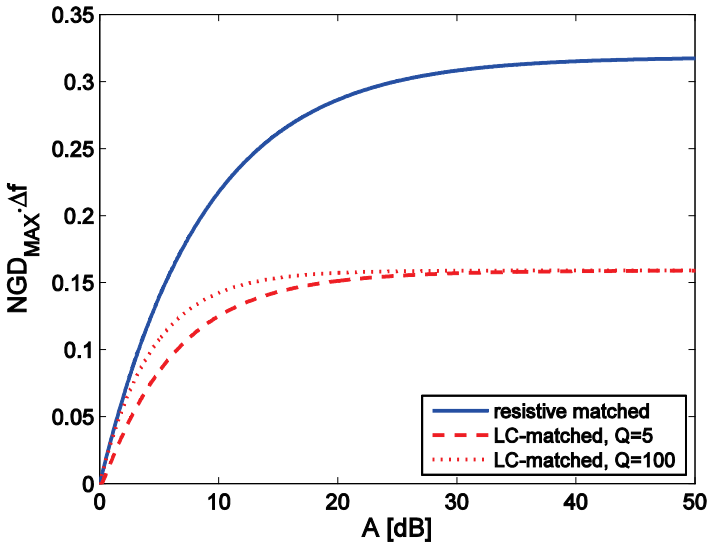

Figure 3-17: NGD vs. out-of-band gain for different circuit topologies.

These plots are shown in Fig. 3-17, including two variations for the *LC*-matched circuit with different values of Q. The characteristics showing NGD vs. transmission loss at the resonance frequency, A_0, however, will be different for all presented topologies. These expressions for single-stage unmatched, *R*-matched, π-matched and *LC*-matched circuits are given respectively by

$$NGD_{UNM}\,\Delta f = \frac{1}{\pi}\left(1 - A_0\right), \tag{3.27a}$$

$$NGD_{R-M}\,\Delta f = \frac{1}{2\pi}\left(2 - A_0\right)\left(1 - A_0\right), \tag{3.27b}$$

$$NGD_{\pi-M}\Delta f = \frac{1}{\pi}\left(\frac{1-A_0}{1+A_0}\right), \tag{3.27c}$$

$$NGD_{LC-M}\Delta f = \frac{1}{2\pi}\left(1-A_0^2-\frac{2-A_0^2}{Q}A_0^2\sqrt{1-A_0^2}\right). \tag{3.27d}$$

The corresponding plots are shown in Fig 3-18. It can be concluded that the unmatched *RLC* resonator circuit has the best NGD vs. transmission loss performance, followed by the *R*-matched, π-matched, and finally *LC*-matched circuits respectively. The unmatched resonator topology however cannot be cascaded, as will be discussed in the multi-stage resonator-based circuits section.

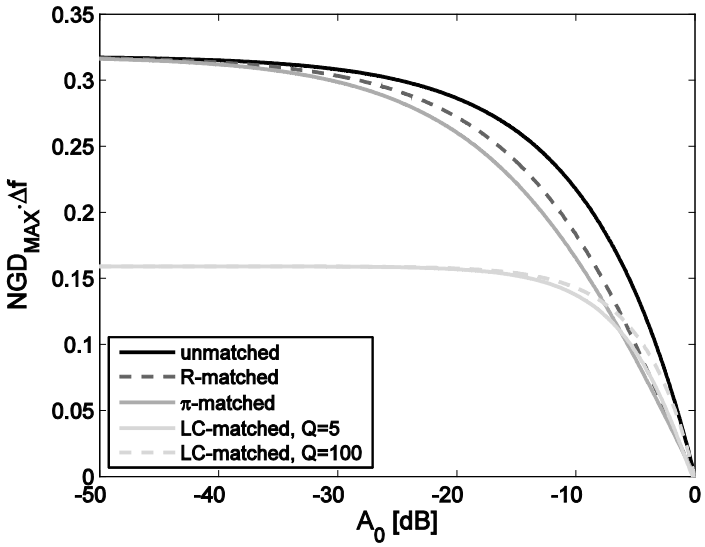

Figure 3-18: NGD vs. transmission loss for different circuit topologies.

Overall, resistive matched topologies are preferred to achieve the highest possible NGD for a given out-of-band gain and/or transmission loss. When both NGD and negative phase delay (LHM) are needed simultaneously, a separated LHM/NGD design is shown

to outperform the traditional *LC*-matched design, while also allowing independent designs of LHM and NGD values.

3.1.6 Gain-Compensated NGD Circuit

In this section an active NGD circuit is presented, which is used to compensate for the loss associated with the *RLC* resonators. An obvious solution is to connect a matched amplifier stage in cascade with one of the lossy NGD circuits discussed in the previous section. However, this configuration might require a large amplifier gain since the loss associated with any useful NGD is on the order of 10-20 dB. Having the signal attenuated that much before the amplifier stage can deteriorate the signal-to-noise-ratio (SNR) considerably. Amplifying the signal first and then cascading a lossy NGD circuit can produce a better SNR at the output. However, if the signal level at the input is relatively high, there is a limit in how much the signal can be amplified before the amplifier distortion and its overall output voltage and power limits become an issue. Alternatively, a circuit design [61] is proposed with the *RLC*-resonator embedded within the amplifier input branch, not cascaded separately, as shown in Fig. 3-19.

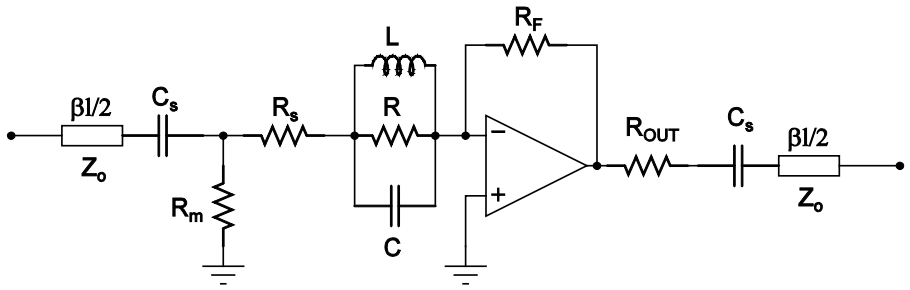

Figure 3-19: A gain-compensated, active *RLC*-resonator based NGD circuit.

This configuration has a better noise performance than the one with a de-embedded matched resonator preceding the amplifier, which will be confirmed later. At the same time, the amplifier gain required for full loss-compensation at the resonance frequency is low. The amplifier type used is an operational amplifier in the inverting configuration. The amplifier itself has a very large gain ideally, and therefore a feedback resistor, R_F, is used to control the overall gain. This will result in a very small voltage difference between the input terminals, which is virtually zero in the ideal case. Therefore, the negative terminal in the configuration in Fig 3-19 is referred to as "virtual ground", since the positive terminal is grounded. These approximations yield a simple relationship between the output and input voltages of an operational amplifier in the inverting configuration, given by

$$V_{OUT\_AMP} = -\frac{R_F}{Z_{IN}} V_{IN\_AMP}. \tag{3.28}$$

The input branch impedance is the impedance connected to the negative terminal of the amplifier, and the input voltage is the voltage at the input end of that branch. Applying the ideal operational amplifier approximations, the overall transmission coefficient of the circuit in Fig 3-19 is given by

$$S_{21}(\omega) = -\frac{R_F R_m}{(Z_{RES}(\omega) + R_s)(R_m + Z_0) + Z_0 R_m} e^{-j\beta \cdot L}, \tag{3.29a}$$

where

$$R_m = Z_0 \frac{R_s + R}{R_s + R - Z_0}. \tag{3.29b}$$

Alternatively, the circuit's transfer characteristic can be described by the generic expression (3.4), with parameters given by

$$A = \frac{R_F / Z_0}{1 + 2R_s / Z_0 - R_s / (R + R_s)}, \quad A_0 G = -1. \tag{3.30}$$

The matching shunt resistor R_m is employed to match the overall input impedance to the source impedance, Z_0, at the resonance frequency, given that the amplifier input impedance branch is larger than the source (R_s+R>Z_0). The series input branch resistor R_s is used optionally for cases where it is desirable to limit the overall gain at frequencies far away from the resonance, where the resonator impedance is small. Finally, an output resistance R_{OUT} is used, since the amplifier itself has very low output impedance. If the output resistor is chosen to match the load impedance (R_{OUT}=Z_0), then only half of the amplifier output voltage will appear at the terminal output. In that case the actual amplifier gain needs to be double the overall target gain.

3.1.6.1 Simulated and Measured Frequency Domain Results

The described gain-compensated circuit was designed, operating at a resonance frequency of 450 MHz, and fabricated on a microstrip line substrate, as shown in Fig 3-20. The operational amplifier used was a National Semiconductor LMH6703.

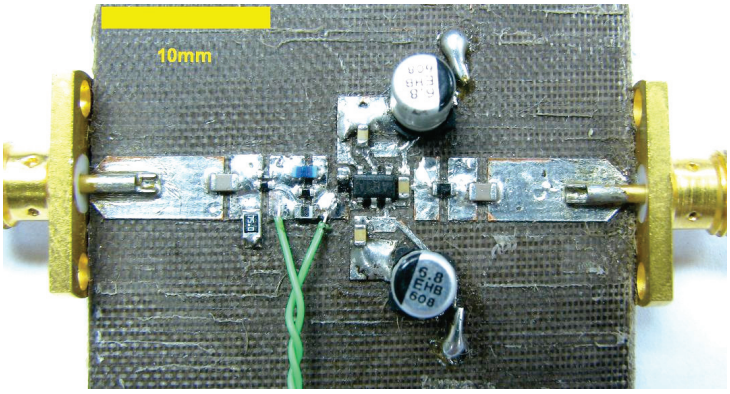

Figure 3-20: Fabricated active NGD circuit with a physical length of L=30 mm, operating at f_0=450 MHz.

Large series capacitors were added at the circuit input and output to isolate the DC voltages used as power supply for biasing the amplifier. These capacitors do not affect the circuit performance significantly within the resonator bandwidth. The amplifier voltage gain of 2 is chosen so that the overall gain, including half the voltage taken by the output resistor, will be equal to 1. For optimum amplifier performance, the manufacturer recommends a feedback resistor value of R_F=500 Ω, which yields a resonator resistance of R=250 Ω, for the desired overall gain of 1. Clearly, this embedded configuration is using only an amplifier gain of 2 (6 dB) at the resonance frequency, to fully compensate for the loss. Conversely, a resonance frequency gain of 20 dB or so might be needed in a topology where the amplifier stage is isolated from the passive NGD stage. In addition to the ideal case, this circuit was also simulated using the commercial software package "Ansoft Designer" [66]. In this case, the measured frequency response of the amplifier itself was used, and the rest of the circuitry was simulated. The ideal, simulated and actual measured input and output matching characteristics are shown in Fig. 3-21. The ideal case predicts perfect input matching at the resonance frequency of 450 MHz, and the actual simulated and measured results are in a good agreement, with the input mismatch below -20 dB.

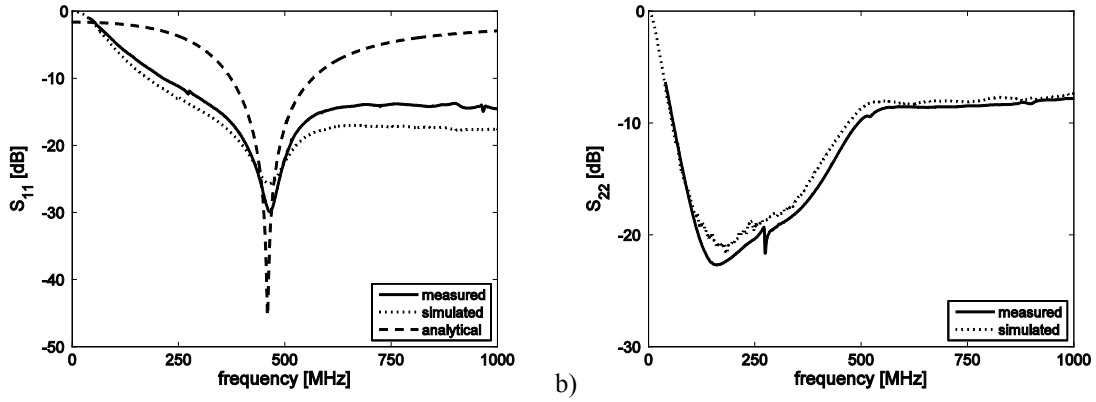

Figure 3-21: Ideal, simulated and measured a) input and b) output *S*-parameters of the gain-compensated circuit from Fig. 3-20.

The out-of-bandwidth disagreement of the ideal characteristic is due to ignoring the DC block capacitors in our model, to keep the derived expression relatively simple. The output matching characteristic for the ideal case is perfect (negative infinity in dB) and therefore not shown in Fig 3-21b. The measured and simulated characteristics are in good agreement with each other, but not close to the ideal case. The mismatch of about -15 dB at the resonance frequency is caused by the amplifier non-idealities, such as output capacitance. The transmission coefficient characteristics for the 3 cases are shown in Fig. 3-22. In order to make the overall gain of 1 (0 dB) at the resonance frequency in the actual fabricated design, a slightly larger ratio of the feedback and resonator resistors were required (an R of 150 Ω was used, instead of 250 Ω). Therefore, the overall gain for the ideal case is about 4 dB higher than the actual one, at the resonance frequency. Other than that, a good agreement within the bandwidth is observed.

The ideal characteristic disagreement at low frequencies is due to the DC block capacitors, while at high frequencies the output shunt capacitance of the amplifier starts attenuating the signal, which is not taken into account in the ideal case. The phase

characteristic plot of the ideal case is in a good agreement with the other two, since the positive delay due to the physical length and the amplifier delay are taken into account.

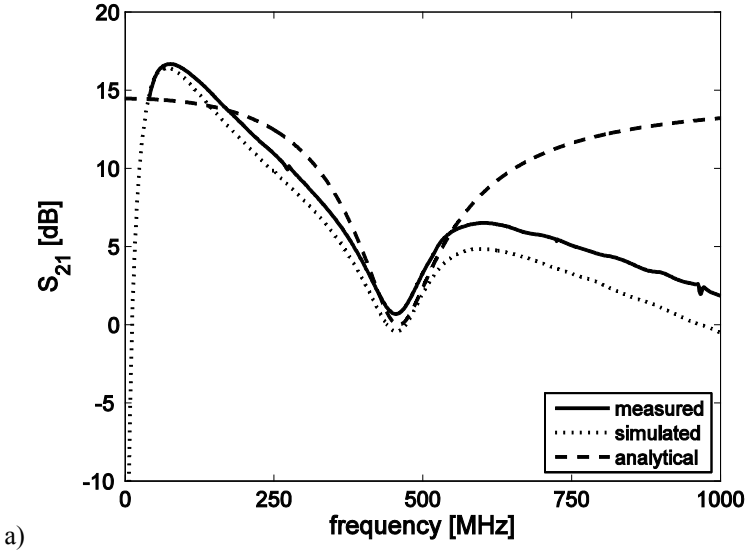

a)

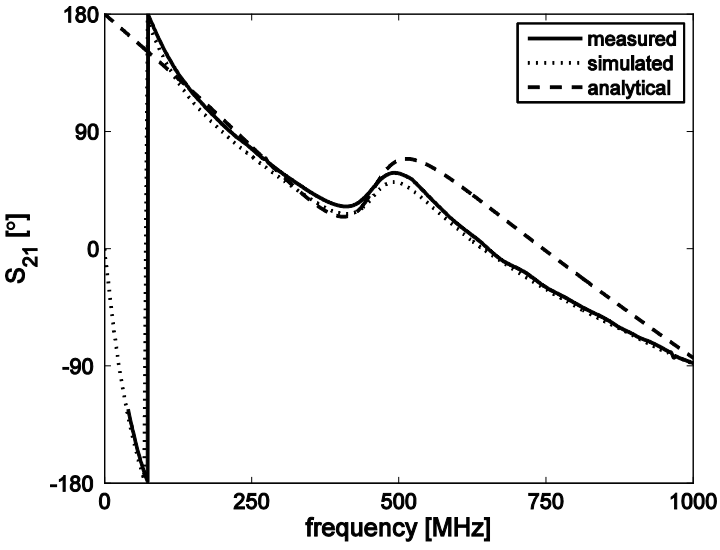

b)

Figure 3-22: The ideal, simulated and measured a) transmission magnitude and b) phase plots of the gain-compensated circuit from Fig. 3-20.

Group delay is also estimated as the tangent slope at all phase characteristic points, and it is shown in Fig. 3-23. The emphasized ripple in the group delay characteristic of

the measured and simulated circuit is due to error in numerical differentiation of the phase characteristic and added noise. The estimated group delay is about 2 ns, and for the resonator quality factor used (Q=5), the estimated bandwidth is about 90 MHz, making the relative NGD about 18% of $1/\Delta f$. This is in agreement with the absolute NGD limit for a single resonator circuit estimated in the previous chapter (32% of $1/\Delta f$).

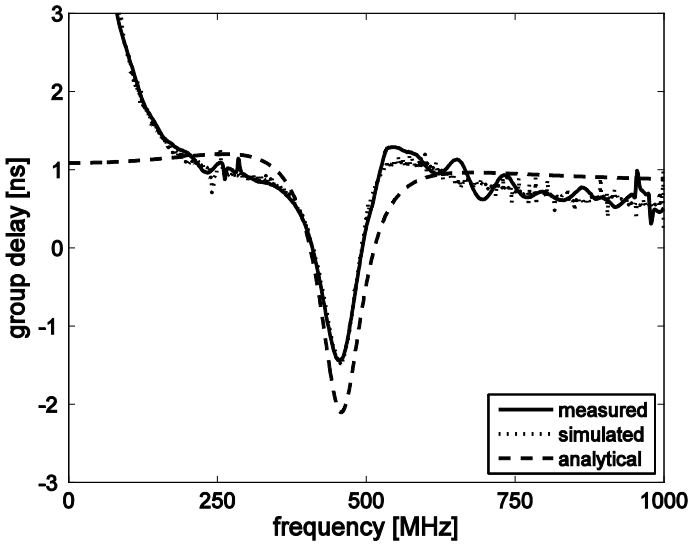

Figure 3-23: The ideal, simulated and measured group delay plots of the gain-compensated circuit from Fig. 3-20.

The relevant expressions derived from the ideal case transmission characteristics are given by

$$S_{21}(\omega_0) = -\frac{R_F}{2(R_s + R)}, \qquad S_{21}(0) = S_{21}(\infty) = -A, \tag{3.31a}$$

$$NGD_{MAX} = \frac{2Q}{\omega_0}\left(1 - \frac{1}{A}\right) - \beta l = \frac{2Q}{\omega_0}\frac{R}{R_S + R}\left(1 - \frac{Z_0/2}{R_S + R}\right) - \beta l, \tag{3.31b}$$

$$\lim_{A\to\infty} NGD_{MAX} = \frac{1}{\pi}\frac{1}{\Delta f} - \beta l \,. \tag{3.31c}$$

The results above obey the absolute NGD limit for a single-stage resonator circuit given by (3.8). In this case, the NGD limit is lowered by the positive delay, βl, which was taken into consideration (3.31c). The included positive delay of the circuit results from its finite dimensions, and an additional delay arising from the amplifier's electronics. The relatively simple expressions derived for the ideal case are in a good agreement with the actual results, proving to be useful in the design and analysis of this circuit type. These expressions can also be used in the time domain analysis.

The noise measurements were performed on the circuit shown in Fig. 3-20 using the noise figure personality of the Agilent PSA E4448A spectrum analyzer, and a calibrated Agilent 346C noise source. The narrow-band noise figure at the resonance frequency was measured at 19.8 dB while the estimated value is 19.5 dB. The estimated value calculations were based on the equivalent noise sources data supplied by the operational amplifier manufacturer, and by taking into account the external resistors and the circuit topology. Due to a good match between the measured and estimated noise figure values, the configuration with a de-embedded matched resonator preceding the amplifier has not been manufactured and its noise figure was estimated at 34 dB, using the same procedure. Therefore, the configuration with a resonator embedded in the amplifier input branch indeed exhibits a better noise performance than its de-embedded resonator alternative.

3.1.6.2 Time Domain Steady-State Measurement Results

For the purpose of analyzing the proposed circuit in the time domain, a simple experiment was set up as illustrated in Fig. 3-24.

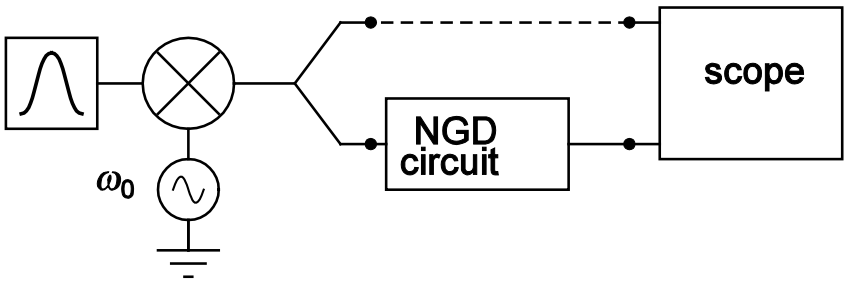

Figure 3-24: A steady-state time-domain experiment set up diagram.

A sinusoidal carrier waveform with a frequency of 450 MHz was used, and it was fed to a mixer, along with a baseband Gaussian pulse. The mixer multiplies these two waveforms, producing an amplitude-modulated (AM) waveform which is shown in Fig. 3-25. The output waveform is slightly amplified and distorted, as expected. The envelopes of the two waveforms were obtained through approximate curve fitting, assuming a Gaussian shape with a variable standard deviation. A non-ideal mixer also produces inter-modulation frequency components, which were filtered out by a bandpass filter employed at its output. The modulated waveform is fed to a 3 dB splitter, which splits the input waveform into 2 equal components, with 50% of the waveform power each (voltage lower by a factor of √2). One of the two obtained waveforms is fed directly into an oscilloscope (input voltage V_{in}). The other one is fed through the NGD circuit, with either one or two cascaded stages, producing an output waveform V_{out}, which is then also connected to the oscilloscope. Side by side comparison of the input and output waveform envelopes is shown in Fig. 3-25.

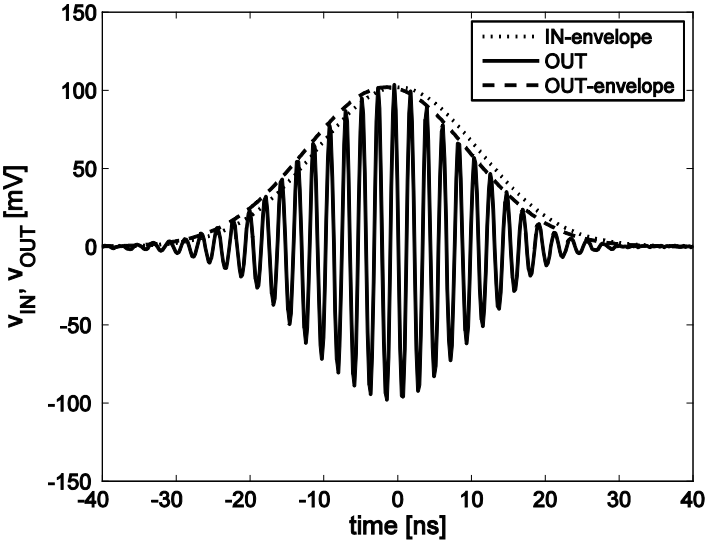

Figure 3-25: The waveform measured at the output of the gain-compensated circuit from Fig. 3-20, for a Gaussian modulated waveform applied at the input.

The NGD circuit makes the output peak precede the input one, overcoming the positive delay caused by the physical length of connecting transmission lines (estimated at approximately 0.3 ns), and the positive delay caused by the amplifier (estimated at approximately 0.5 ns, by isolated amplifier circuit measurement). The case shown in Fig. 3-25 has the output enveloped scaled in magnitude (lowered by a factor of $\sqrt{2}$ approximately), to have the same peak value as the input one, for a better comparison. The maximum NGD (at resonance frequency) predicted by the derived equations (3.31b) is 3.28 ns for the circuit parameters used, including the measured amplifier and connecting lines delay (total of approximately 0.8 ns). The actual measured maximum NGD in frequency domain was 2.7 ns, which is less than the predicted theoretical limit, as expected, due to the tolerance in component values and their non-idealities. The measured NGD in the time domain (estimated through curve fitting) was even smaller (approximately 2 ns), due to non-ideal magnitude and phase characteristics within the bandwidth of interest (82 MHz around the center frequency of 458 MHz, or 18%).

3.2 Multi-Stage Resonator-Based NGD Circuits

The circuits analyzed so far in this chapter, consist of a single NGD stage, which can be cascaded for a potentially cumulative NGD effect. The overall transmission coefficient for *N* ideally matched cascaded elements, can be obtained by multiplying the individual transmission coefficients as

$$S_{21-N}(\omega) = [S_{21}(\omega)]^N = |S_{21}(\omega)|^N e^{jN\phi(\omega)}. \tag{3.32}$$

Therefore, the individual transmission coefficient phase characteristics add up, as well as the magnitude characteristics (on a decibel scale). This will cause the individual phase characteristic slopes to add up as well, hence cumulating the NGD effect. The passive NGD circuits studied in the previous section are perfectly matched only at the resonance frequency, so the expression (3.32) is only an approximation over the entire bandwidth, for those topologies. However, when an ideal amplifier, such as the one discussed in Section 3.1.6, is considered to "isolate" the stages (prohibits propagation in the opposite direction, from output to input), and the amplifier output impedance is perfectly matched to the system impedance, $R_{OUT}=Z_0$, the expression (3.32) is valid.

In a general case, when the approximation (3.32) is not good enough, the exact transmission coefficient expressions can be obtained by converting the single-stage *S*-parameters into *ABCD* or transmission parameters first. The *ABCD*-parameter matrix relates the voltage and current at the input of an element, to the corresponding voltage and current at its output, so that the overall *ABCD* matrix of cascaded elements can be obtained simply by multiplying individual matrices regardless of the element's

impedances being matched or not. The overall *S*-parameters matrix of a cascaded network is then obtained by converting the overall *ABCD* matrix back to *S*-parameters [64].

The only circuit topology that does not produce a cumulative NGD effect is the unmatched *RLC*-resonator circuit, unless individual stages are isolated by an amplifier. This circuit is not matched even at the resonance frequency, and cascading N elements reduces to the same single-stage topology with overall parameters given by $R_{tot}=N\cdot R$, $L_{tot}=N\cdot L$, $C_{tot}=C/N$, and $Q_{tot}=Q$. Therefore, both the NGD and loss will increase, with slower NGD rate of increase for larger values of loss. This cascaded topology can never break the theoretical single-stage NGD limit of $1/(\pi\cdot\Delta f)$, since it always reduced to the single stage equivalent.

The other three topologies studied in Section 3.1 are matched and can effectively be cascaded, giving a total theoretical NGD limit of $1/(\pi\cdot\Delta f)$ per stage for *R*-matched and π-matched circuits, and $1/(2\pi\cdot\Delta f)$, per one stage for *LC*-matched circuit. However, achieving a cumulative phase characteristic slope (NGD) through cascaded stages also increases the swing (out-of-band gain) in transmission magnitude characteristic between the band edges and the resonance frequency, which causes distortion. The commonly accepted deviation in transmission magnitude characteristic is approximately 3 dB over the frequency bandwidth. This corresponds to a maximum ratio of $\sqrt{2}$ in voltage magnitudes of different frequency components, or a ratio of 2 in power ($10\cdot\log(2)\approx 3$ dB). The single stage topology has a maximum magnitude swing of 3 dB within the bandwidth, in the large loss case where the resonator dominates the rest of the circuit elements. This is due to the fact that the resonator impedance drops down by a factor of

√2 at the bandwidth edges. Therefore, an increased magnitude characteristic swing effectively reduces the overall 3 dB bandwidth, as it will be examined in more detail later. It will be shown that maintaining a constant bandwidth of an *N*-stage design, by reducing individual stage *Q*'s and therefore NGD's, still yields an overall cumulative NGD effect but at a slower than linear rate.

3.2.1 Cascaded, Non-Ideally Matched Design

The relationship between the input and output quantities of a two-port electrical network can be described with a number of different transfer parameters (matrices), such as impedance (*Z*) matrix, admittance (*Y*) matrix, scattering (*S*) matrix, transmission (*ABCD*) matrix etc.

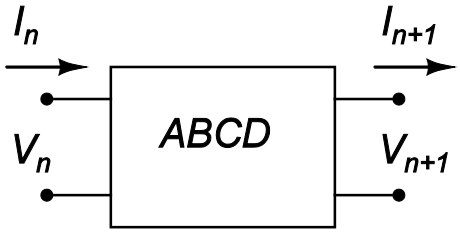

Figure 3-26: *ABCD* matrix representation of a network.

The *ABCD* matrix relates the input port voltage and current to the output voltage and current, as illustrated in Fig. 3-26 and given by

$$\begin{bmatrix} V_n \\ I_n \end{bmatrix} = \begin{bmatrix} A & B \\ C & D \end{bmatrix} \cdot \begin{bmatrix} V_{n+1} \\ I_{n+1} \end{bmatrix}. \tag{3.33}$$

The *ABCD* matrix analysis is preferred for cascaded networks, since the overall matrix of the system is obtained by a simple multiplication of individual cascaded element matrices [64]. The overall transmission matrix can then easily be converted into any other network parameters, such as *S*-parameters (scattering matrix), through conversion expressions [64].

When identical network elements are cascaded, they form a periodic structure. In the case of an infinitely long periodic structure, it is assumed that, for a steady-state sinusoidal applied voltage, the phase difference between the input and output of any cascaded element within the infinite structure will be the same. Similarly, the input to output voltage amplitude ratio will be the same for every element, as well as voltage to current ratio at the input or output of each element, which is referred to as Bloch's impedance (according to Bloch's theorem). Applying the described conditions to (3.33), it can be shown [64] that the transmission coefficient for an *N*-element block of an infinitely long periodic structure, is given by

$$e^{N\gamma} = \left[e^{\alpha+j\beta}\right]^N = \left[\frac{A+D}{2} \pm \frac{1}{2}\sqrt{(A-D)^2+4BC}\right]^N, \tag{3.34a}$$

$$Z_B = Z_0 \frac{B}{e^{\alpha+j\beta}-A} = Z_0 \frac{e^{\alpha+j\beta}-D}{C}, \tag{3.34b}$$

where A,B,C and D are transmission matrix parameters of individual (and identical) cascaded elements, and Z_B is the Bloch's impedance of the infinite structure. In essence, through expressions (3.34) an infinitely long periodic structure is described as a medium with a propagation constant γ and a characteristic impedance Z_B.

For example, applying (3.34) to an infinitely long periodic structure comprised of π-matched NGD elements presented in Section 3.1.3 yields propagation parameters given by

$$e^{\gamma} = A - \sqrt{BC} = 1 + \frac{Z}{R_{sh}} - \sqrt{\frac{2Z}{R_{sh}} + \frac{Z^2}{R_{sh}^2}}, \qquad Z_B = Z \Big/ \sqrt{\frac{2Z}{R_{sh}} + \frac{Z^2}{R_{sh}^2}}, \tag{3.35}$$

where Z is the resonator frequency-dependent impedance, given by (3.3b), and R_{sh} is the shunt matching resistance for this configuration, given by (3.18b).

If a periodic structure has a finite number of cascaded elements, N, and it is connected at both ends (source and load) to a system with characteristic impedance Z_0, which in a general case is different from the structure's Bloch's impedance, Z_B, the transmission coefficient of the overall network is then given by

$$S_{21} = \frac{(1-\Gamma^2)e^{N\gamma}}{1-\Gamma^2 e^{N\gamma}}, \qquad \Gamma = \frac{Z_B - Z_0}{Z_B + Z_0}, \tag{3.36}$$

where Γ is the incident reflection coefficient between the outside system and the periodic structure. If the system impedance is matched to the periodic structure impedance (the incident reflection coefficient Γ=0), then the overall transmission coefficient S_{21} in (3.36) reduces to $e^{N\gamma}$, as in the case of an infinite structure.

How well the periodic structure's impedance Z_B is matched to the system impedance Z_0, over a frequency band, depends on the structure topology. An example of the

impedance mismatch of a periodic structure comprised of π-matched NGD elements, is shown in Fig. 3-27.

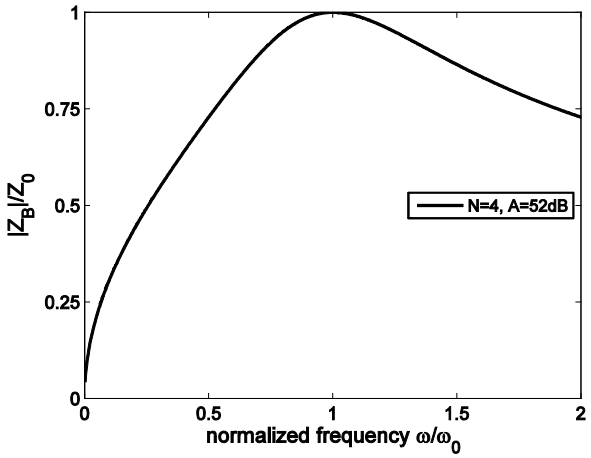

Figure 3-27: Bloch's impedance of a cascaded four-stage π-matched NGD circuit, with overall A=52 dB.

This particular structure's impedance is always matched at the resonance, and the mismatch increases away from this frequency. How small the mismatch is over the entire frequency band will depend on the number of stages, as well as the overall out-of-band gain.

3.2.2 Cascaded, Ideally Matched Design

As discussed in Section 3.1, any resistive matched resonator-based NGD circuit will have the same 2nd order transfer function form given by (3.4). In order to ensure ideal matching between cascaded NGD elements, an ideal amplifier can be cascaded with each element, as depicted in Fig. 3-28. In other words, the amplifier needs to provide an ideal output-to-input isolation (ideally unilateral), and needs to have an output impedance matched to the system impedance within the entire frequency band.

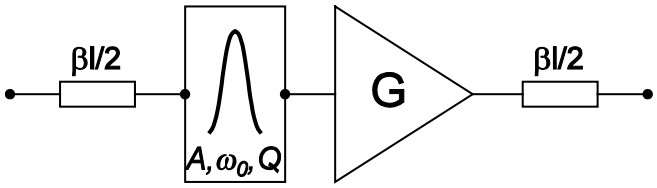

Figure 3-28: Schematic of a generic resonator-based gain-compensated NGD circuit, with physical length l and a propagation constant β.

For this generic, ideally matched gain-compensated case, the transmission coefficient of a cascaded N-stage design is given [60] by

$$S_{21}(\omega) = (A_0 G)^N A^N \left[\frac{\omega^2 - \omega_0^2 - j\frac{1}{Q}\omega_0\omega}{\omega^2 - \omega_0^2 - j\frac{1}{Q}A\omega_0\omega} \right]^N e^{-jN\beta \cdot l}, \tag{3.37}$$

where Q is the chosen quality factor of individual resonators, ω_0 is the resonance frequency, and A^N is the maximum out-of-band magnitude swing of the overall N-stage design. Here A_0 is the gain-uncompensated transmission coefficient at the resonance and G is the compensating amplifier gain. For the gain compensated case A_0G=1 and $S_{21}(0)$=$S_{21}(\infty)$=A^N. The $exp(-jN\beta l)$ term accounts for the phase shift due to finite physical dimensions.

Similarly to expression (3.7), the maximum NGD occurs at the resonance frequency approximately and can be derived as

$$NGD_{MAX} = -\tau_g\Big|_{\omega=\omega_0} = N\frac{2Q}{\omega_0}\left(1-\frac{1}{A}\right) - N\tau_{pd}, \tag{3.38}$$

where τ_{pd} is the positive group delay associated with the phase delay, βl, of each stage.

Comparison of the achieved NGD of an ideally matched design and the non-ideal one (presented in Section 3.2.1) is shown in Fig. 3-29. The same out-of-band gain is chosen for both designs, and the same number of stages. The ideally matched design exhibits a larger NGD, in addition to having a simpler expression for the transmission coefficient. Therefore, since one of the questions addressed in this thesis deals with establishing the maximum achievable NGD for a given out-of-band gain, only the ideally matched case will be considered for the remainder of this chapter.

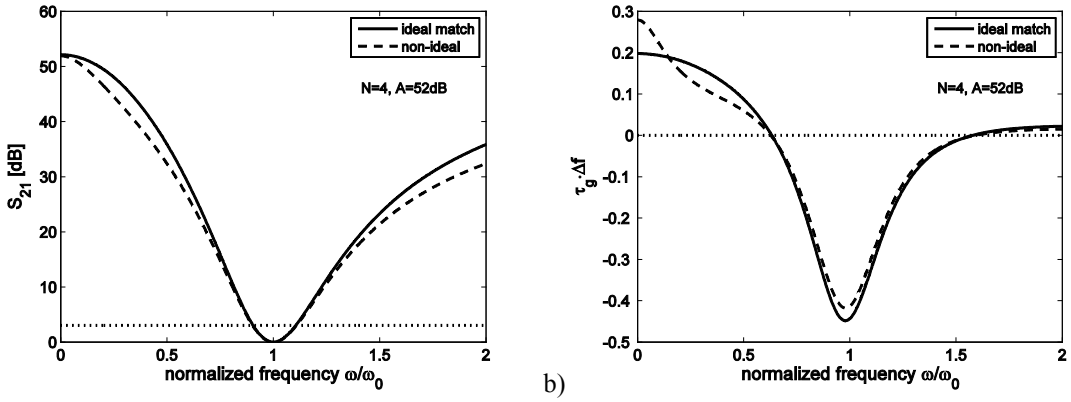

Figure 3-29: a) Transmission coefficient and b) group delay comparison of ideally and non-ideally matched cascaded NGD circuits.

3.3 NGD Asymptotic Limits of Multi-stage Resonator-based Circuits

When considering a multi-stage design, keeping the Q's of individual resonators constant as the number of stages increases results in an increasing overall Q (and thus a decreasing allowed signal bandwidth). This effect is demonstrated in Fig. 3-30, for ideally matched

cascaded designs with individual stages having A=20 dB and Q=5.

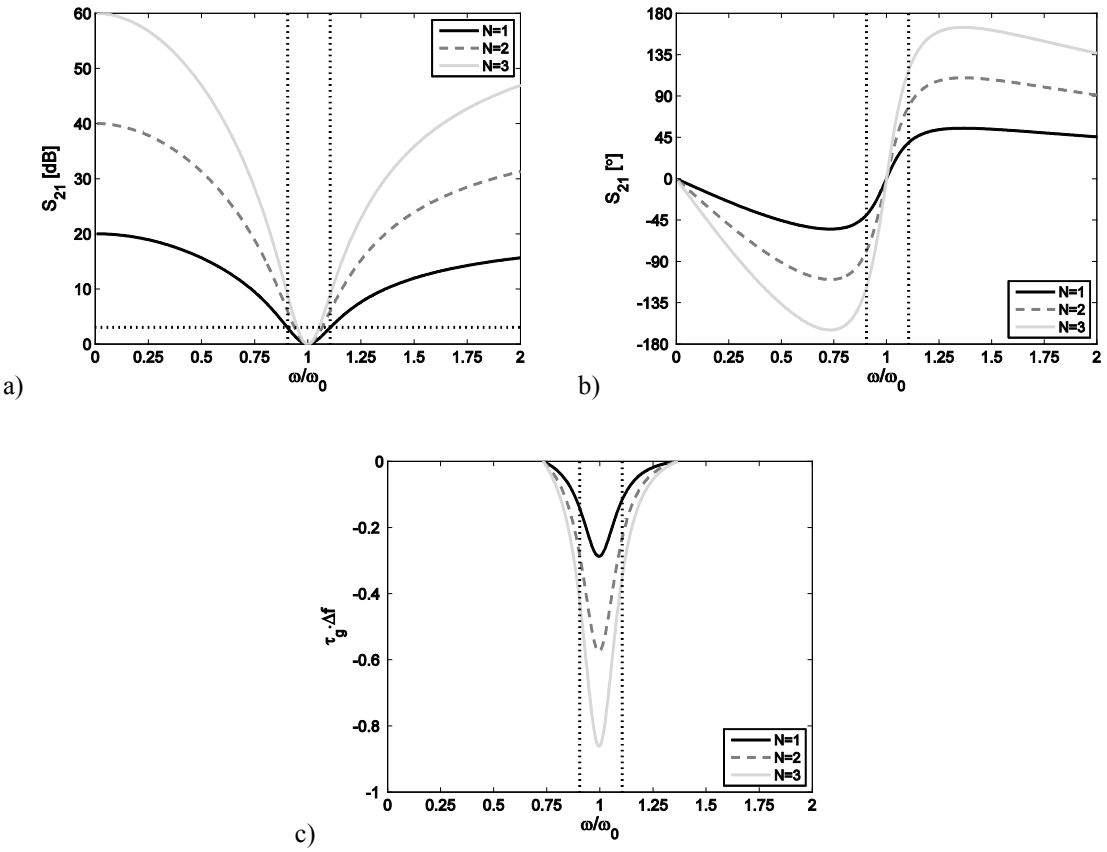

Figure 3-30: a) Transmission coefficient, b) transmission phase and c) group delay for ideally matched cascaded design with unadjusted Q-factor.

The achieved NGD is linearly increasing with the number of stages in this case (Fig. 3-30c), but the bandwidth is decreasing (Fig. 3-30a). It will be shown that the NGD is increasing at the higher rate than the rate of the bandwidth decrease, so the overall NGD-bandwidth product still increases with number of stages, but at a slower than linear rate.

In order to maintain a constant bandwidth for the overall N-stage design, the individual stage Q's need to be adjusted properly. As evident from Fig. 3-30, the individual stage Q's will need to be lower than the overall Q-factor, which will be called Q_{tot}. The condition to maintain a 3 dB N-stage transmission coefficient swing from the

upper band-edge to the center frequency, can be written as

$$\left|S_{21}\left(\omega_0+\frac{\Delta\omega}{2}\right)\Big/S_{21}(\omega_0)\right|^2=\left|S_{21}\left(\omega_0+\frac{\omega_0}{2Q_{tot}}\right)\Big/S_{21}(\omega_0)\right|^2=2. \tag{3.39}$$

Substituting S_{21} from (3.37), and assuming fully compensated case (A_0G=1), yields

$$\left|A\frac{1+jQ\left(1+\frac{1}{2Q_{tot}}-1\Big/\left(1+\frac{1}{2Q_{tot}}\right)\right)}{A+jQ\left(1+\frac{1}{2Q_{tot}}-1\Big/\left(1+\frac{1}{2Q_{tot}}\right)\right)}\right|^{2N}=2. \tag{3.40}$$

Assuming that the overall N-stage bandwidth is much smaller than the center frequency, $1/(2Q_{tot})<<1$, yields

$$\left|\frac{1+jQ\left(1+\frac{1}{2Q_{tot}}-1+\frac{1}{2Q_{tot}}\right)}{1+j\frac{Q}{A}\left(1+\frac{1}{2Q_{tot}}-1+\frac{1}{2Q_{tot}}\right)}\right|^2=\frac{1+\left(\frac{Q}{Q_{tot}}\right)^2}{1+\frac{1}{A^2}\left(\frac{Q}{Q_{tot}}\right)^2}\approx 2^{1/N}. \tag{3.41}$$

Finally, by introducing a variable for the overall N-stage out-of-band gain, $A_{tot}=A^N$, and solving (3.41), the approximate expression for individual stage Q-factor adjustment, required to maintain the overall bandwidth can be obtained as

$$Q \approx \frac{Q_{tot}\sqrt{2^{1/N}-1}}{\sqrt{1-2^{1/N}/A_{tot}^{2/N}}}. \tag{3.42}$$

Similar derivation can be performed at the lower bandwidth edge, yielding the same result. For large out-of-band gain values of individual stage resonators, $A=A_{tot}^{1/N}>>2^{1/(2N)}$, expression (3.42) reduces to

$$\lim_{A\to\infty} Q = Q_{tot}\sqrt{2^{1/N}-1}, \tag{3.43}$$

which matches the expression derived in [67]. In addition, expression (3.43) can be further simplified for large values of N, as

$$\lim_{\substack{A\to\infty \\ N>>1}} Q \approx Q_{tot}\frac{\sqrt{\ln 2}}{\sqrt{N}}, \tag{3.44}$$

in which case Q decreases proportionally to $1/N^{1/2}$. However, in this thesis the full expression (3.42) will be used to preserve accuracy in cases where A_{tot} is not large, or when both A_{tot} and N are large, so that $A=A_{tot}^{1/N}$ is not necessarily large.

In order to validate the derived expression (3.42), the Q-factors of three cases from Fig. 3-30 are adjusted accordingly, and the results are shown in Fig. 3-31. The N-stage maximum NGD-bandwidth product for the maintained bandwidth case can now be obtained by substituting (3.42) into (3.38), as

$$NGD_{MAX}\Delta f = \frac{1}{\pi} N\sqrt{2^{1/N}-1}\,\frac{1-1/A_{tot}^{1/N}}{\sqrt{1-2^{1/N}/A_{tot}^{2/N}}} - N\tau_{pd}\Delta f\,. \tag{3.45}$$

For N=1, $A\to\infty$ and neglecting the positive delay τ_{pd}, expression (3.45) yields the same limit of $1/\pi$, as derived previously.

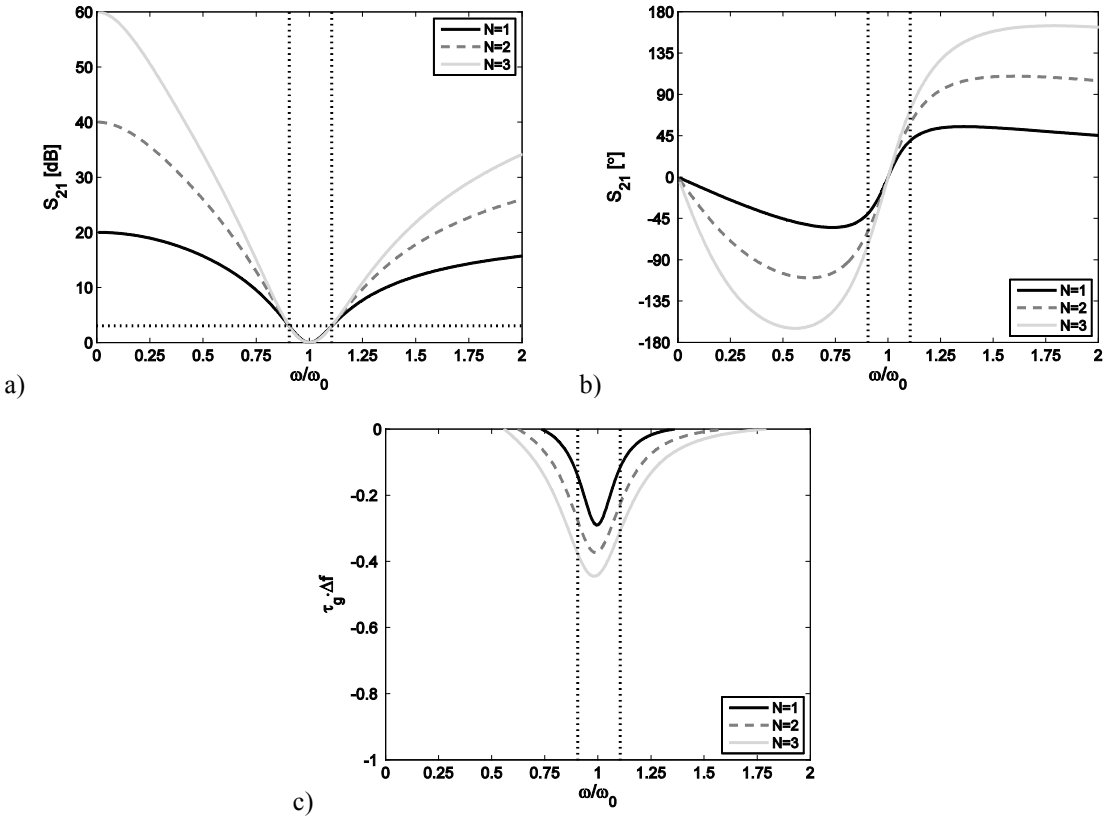

Figure 3-31: a) Transmission coefficient, b) transmission phase and c) group delay for ideally matched cascaded design with adjusted Q-factor.

The maximum NGD-bandwidth product as a function of two variables, number of stages N, and total out-of-band gain A_{tot}, is plotted in Fig. 3-32. As expected, NGD is a monotonically increasing function of both A_{tot} and N. The out-of-band gain A_{tot} is an undesirable effect since it is directly related to transient amplitudes of the circuit response

to finite duration signals, as it will be discussed in the next chapter. Therefore, there is a trade-off between increasing NGD, and A_{tot}.

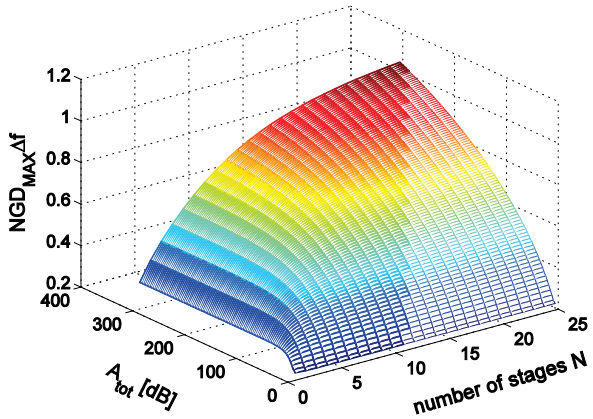

Figure 3-32: NGD-bandwidth product as a function of total out-of-band gain, A_{tot}, and the number of stages, N.

The NGD-bandwidth product as a single-variable function of A_{tot}, for several different values of N is shown in Fig. 3-33. Similarly, Fig. 3-34 depicts NGD-bandwidth product as a function of N, for several different values of A_{tot}.

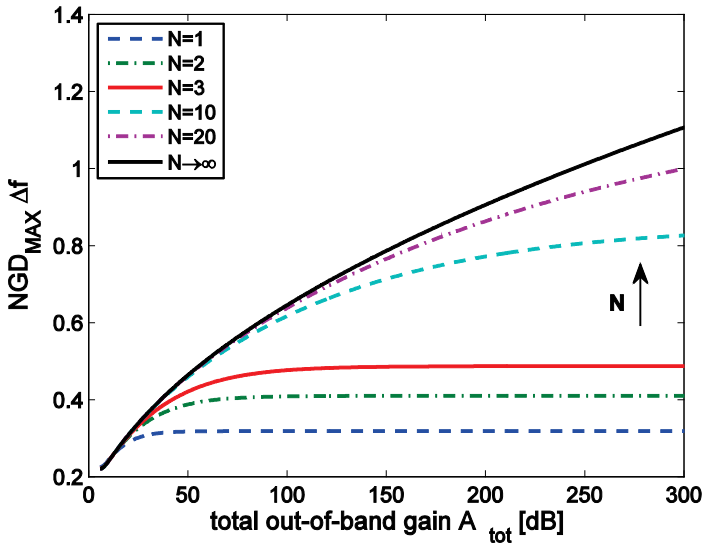

Figure 3-33: NGD-bandwidth product as a function of out-of-band gain, A_{tot}.

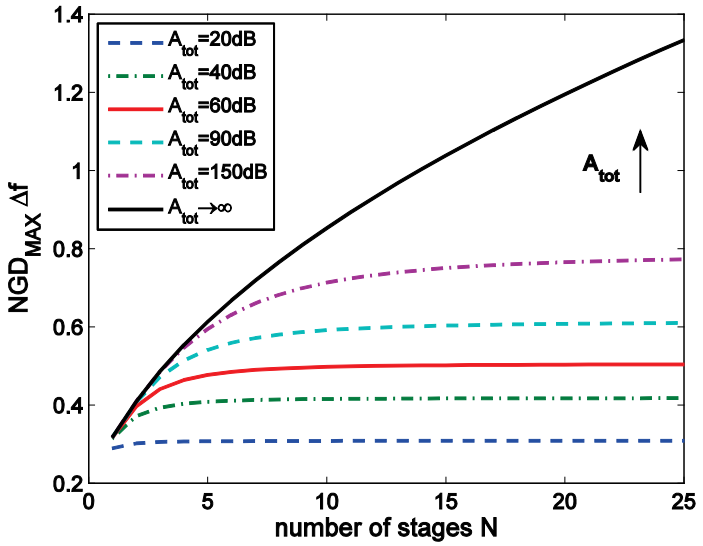

Figure 3-34: NGD-bandwidth product as a function of number of stages, N.

The family of curves in both Figs. 3-33 and 3-34 have an asymptotic limit for NGD, as one of the variables is fixed, and the other approaches infinity. This means that the largest NGD increase as a function of the trade-off quantities, A_{tot} and N, is given by these asymptotic curves. The first asymptotic limit can be derived from expression (3.45), as

$$\begin{aligned}
\lim_{N\to\infty} NGD_{MAX}\Delta f &= \lim_{N\to\infty} \frac{1}{\pi} N\sqrt{2^{1/N}-1}\,\frac{1-1/A_{tot}^{1/N}}{\sqrt{1-2^{1/N}/A_{tot}^{2/N}}} \\
&= \lim_{N\to\infty} \frac{1}{\pi} N\sqrt{\frac{\ln 2}{N}}\,\frac{A_{tot}^{1/N}-1}{\sqrt{A_{tot}^{2/N}-2^{1/N}}} \\
&= \lim_{N\to\infty} \frac{1}{\pi} \sqrt{\ln 2}\sqrt{N}\,\frac{\ln\left(A_{tot}\right)/N}{\sqrt{2\ln\left(A_{tot}\right)/N-\ln 2/N}} \\
&= \frac{1}{\pi}\sqrt{\ln 2}\,\frac{\ln\left(A_{tot}\right)}{\sqrt{2\ln\left(A_{tot}\right)-\ln 2}}, \qquad (3.46)
\end{aligned}$$

where the positive delay due to finite physical dimensions, τ_{pd}, is neglected, since only

the maximum achievable NGD values are of interest. The limit expression (3.46) can be further simplified for large out-of-band gain values, $A_{tot} >> \sqrt{2}$, as

$$\lim_{N\to\infty} NGD_{MAX}\Delta f \approx \frac{1}{\pi}\frac{\sqrt{\ln 2}}{\sqrt{2}}\sqrt{\ln\left(A_{tot}\right)}, \tag{3.47a}$$

or, when this limit is expressed in terms of the out-band-gain decibel value, $A_{tot\text{-}dB}=20\cdot\log(A_{tot})$, it becomes

$$\lim_{N\to\infty} NGD_{MAX}\Delta f \approx \frac{1}{\pi}\frac{\sqrt{\ln 2\cdot\ln 10}}{\sqrt{40}}\sqrt{A_{tot-dB}} \approx 0.0636\sqrt{A_{tot-dB}}\,. \tag{3.47b}$$

Similarly, the second asymptotic limit can be derived from (3.45), by neglecting the positive delay τ_{pd}, keeping N finite, and letting $A_{tot}\to\infty$, as

$$\begin{aligned}\lim_{A_{tot}\to\infty} NGD_{MAX}\Delta f &= \lim_{A_{tot}\to\infty}\frac{1}{\pi}N\sqrt{2^{1/N}-1}\,\frac{1-1/A_{tot}^{1/N}}{\sqrt{1-2^{1/N}/A_{tot}^{2/N}}}\\ &= \frac{1}{\pi}N\sqrt{2^{1/N}-1}\,.\end{aligned} \tag{3.48}$$

The limit expression (3.48) can be further simplified for large N values, $N >> 1$, as

$$\lim_{A_{tot}\to\infty} NGD_{MAX}\Delta f \approx \frac{\sqrt{\ln 2}}{\pi}\sqrt{N}\,. \tag{3.49}$$

From (3.47) and (3.49), it is evident that achievable NGD-bandwidth product is proportional to the square root of ln(A_{tot}), or square root of the out-of-band decibel value $A_{tot\text{-}dB}$, as well as to the square root of number of stages, respectively. It can alternatively be said that the magnitude of the total out-of-band gain, A_{tot}, increases exponentially with the square of NGD (A_{tot} is a reciprocal Gaussian function of NGD). This particular formulation will come in handy when discussing transients for Gaussian modulated signals in the next chapter. The results presented for multi-stage circuits in [40,41,42,48], all have NGD-bandwidth products that comply with the limits given by (3.47) and (3.49).

From Fig. 3-33, it can be noted that for a given NGD value, cases with larger number of stages, N, yield smaller out-of-band gain values, A_{tot}. This is also depicted in the frequency domain plots in Fig. 3-35, for a few selected cases. This result shows that having a larger number of stages (distributed case) is preferred, since it minimizes the undesirable out-of-band gain trade-off, for a given NGD-bandwidth.

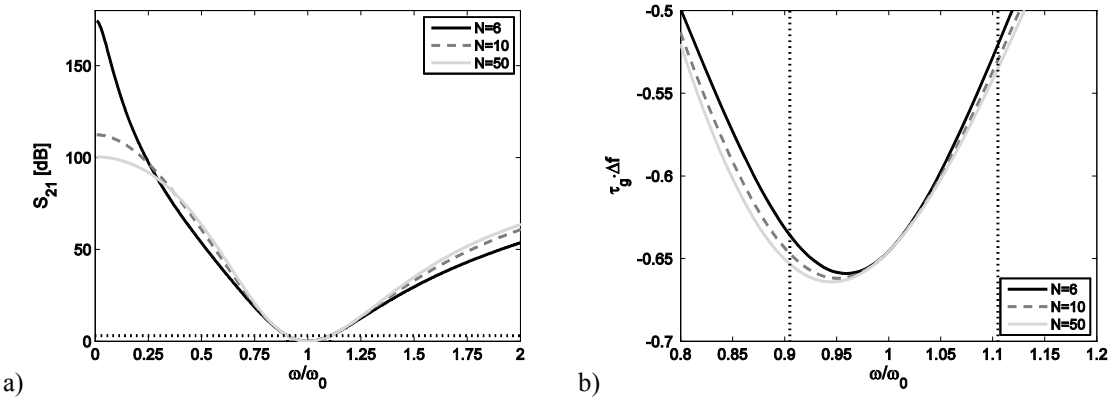

Figure 3-35: a) Transmission coefficient and b) group delay plots for a fixed NGD-bandwidth product value, and different number of stages N.

Similarly, the preference for larger number of stages can be demonstrated for a case when the out-of-band value is fixed, and the achieved NGD is to be maximized. From

Fig. 3-33 it can be observed again that the larger N values achieve this, which is also depicted in the frequency domain plots in Fig. 3-36, for a few selected cases.

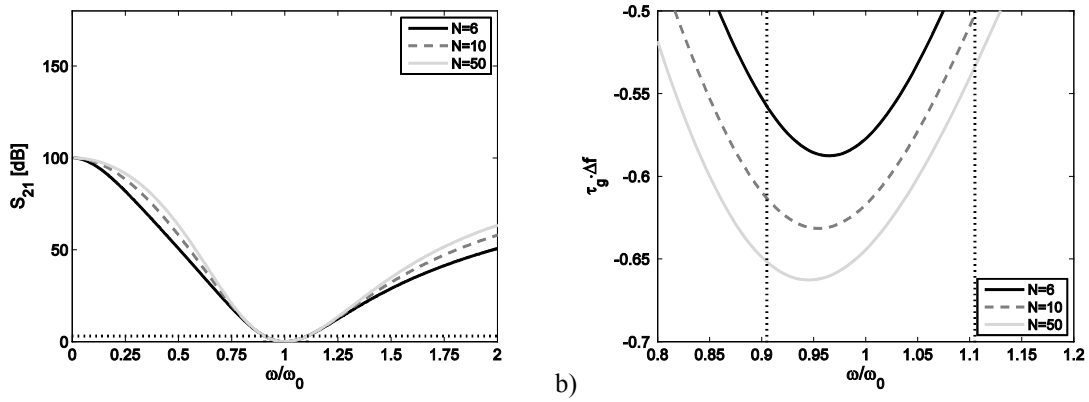

a) b)

Figure 3-36: a) Transmission coefficient and b) group delay plots for a fixed A_{tot} value, and number of stages N.

As expected, a larger number of stages (distributed case) maximizes the NGD-bandwidth, for a given out-of-band gain.

From Figs. 3-35b and 3-36b it can be noted that the maximum NGD does not occur exactly at the resonance, but at progressively lower frequency values as the number of stages increases. The minimum transmission magnitude value, however, stays at the resonance for all cases. The drifting NGD maximum is a consequence of resonator's asymmetric frequency response, which gets more pronounced for lower Q values of individual resonators, which is exactly the case with increasing number of stages, as given by (3.42) or (3.44). The frequency at which the drifting NGD maximum occurs could be quantified by finding the derivative of (3.6), as a function of number of stages and the out-of-band gain. However, there would be no apparent benefit in doing so, since trying to operate at frequencies where the NGD is exactly at its maximum would correspond to regions of larger transmission magnitude swings, as evident from Figs. 3-

35a and 3-36a, which would dramatically reduce the bandwidth. Therefore, it is still desirable to have the operating bandwidth around the resonance frequency, in spite of the fact that the NGD is not exactly at its maximum there. The preferred resonance frequency NGD value will still be referred to as NGD_{MAX} throughout this thesis, to avoid unnecessary nomenclature complexity.

3.3.1 Finite Positive Delay Considerations

Figure 3-34 shows an NGD plot as a function of number of stages for several selected overall out-of-band gain values, when the positive delay τ_{pd} is neglected in expression (3.45). The same shape of curves as in Fig. 3-34 would also hold if a constant positive delay, $N\tau_{pd}=const$, independent of the number of stages, was assumed. The curves would obviously be shifted downward by the constant value assumed. This would represent the case when a constant physical length (and electrical delay) of the medium is given and increasing the number of stages does not increase the overall delay (individual stages all fit into the given length for any number of stages considered).

Alternatively, a case is possible in which an additional positive delay is introduced with each added stage, regardless if the overall medium length is constant or not. For example, introducing an amplifier into each stage for the purpose of gain-compensation will also introduce positive delays (about 0.5 ns for the amplifier presented in Section 3.1.6). In this case, the curves produced from expression (3.45) will not be monotonically increasing as before, but have peak values instead as shown in Fig. 3-37.

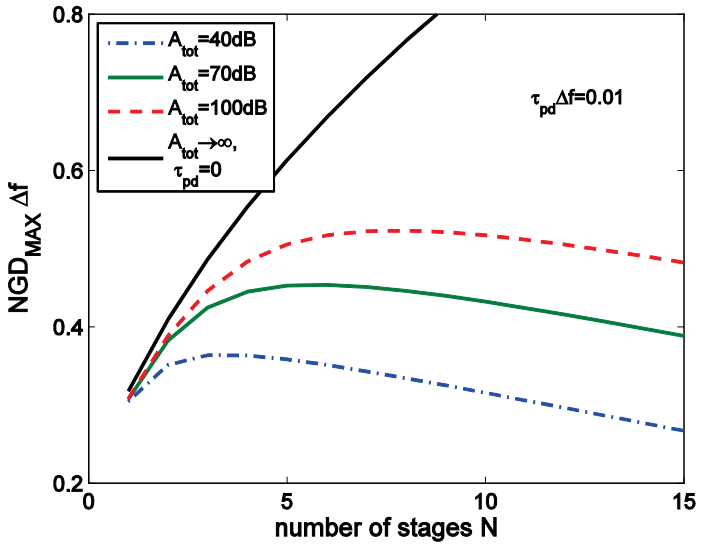

Figure 3-37: The effect of an added finite positive delay for each stage on the NGD-bandwidth product.

Based on the positive delay of each stage, τ_{pd}, there will be an optimum number of stages for each given overall out-of-band gain for which the NGD-bandwidth value is maximized. Therefore, derived expression (3.45) can also be used for optimum design purposes, when positive delay of each stage is considered. The overall asymptotic limit given by (3.49) still holds, since that case neglects the positive delay of each stage.

3.3.2 Bandpass Filter Effect on NGD Limits

In the analysis presented so far, it has been assumed that discussed NGD circuits have an unlimited bandwidth. However, some circuit components have a pronounced bandwidth limitation, such as the amplifier used in the NGD circuit presented in Section 3.6.1. The bandpass nature of this circuit is evident in the transmission coefficient plot in Fig. 3-22. This circuit attenuates high-end frequencies due to the low-pass nature of the amplifier

employed, while the low-end frequencies are attenuated due to the connecting DC block capacitors.

The bandpass nature of a circuit can be modeled by cascading a bandpass filter with the ideal, unlimited bandwidth circuit. This is demonstrated on an example depicted in Fig. 3-38. A bandpass filter introduces a positive group delay within the pass-band, which results in lowering the achieved NGD, as evident in an example depicted in Fig. 3-38b.

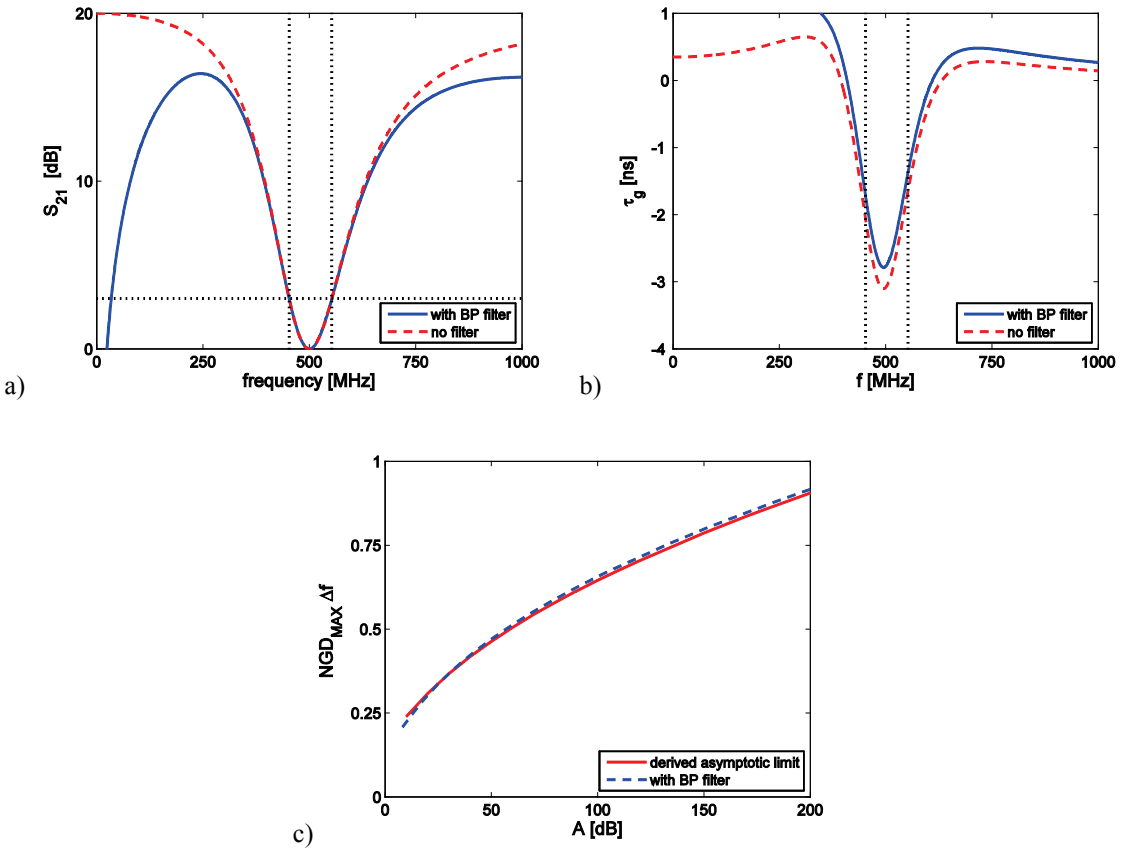

Figure 3-38: The effect of a bandpass filter on the a) NGD transmission coefficient, b) group delay and c) NGD-bandwidth product vs. out-of-band gain characteristic.

At the same time, the maximum out-of-band gain is lowered as well and the transmission coefficient has local maxima, as depicted in Fig. 3-38a for the same example. Since both the NGD and the maximum out-of-band gain are lowered, it cannot be said for certain if

the overall NGD vs. out-of-band asymptotic limit will increase or decrease as a result of introducing a bandpass filter. The bandpass filter impact on the asymptotic limit will vary depending on the type of filter used, its order, and its low and high-end cut-off frequencies. For the particular example shown in Fig. 3-38c, a bandpass filter has lowered the maximum out-of-band gain by a larger factor than it has lowered the achieved NGD, hence slightly surpassing the derived asymptotic NGD vs. maximum out-of-band gain limit.

This example demonstrates that introducing additional circuit elements can change the asymptotic NGD limit given by (3.47). Furthermore, one could argue that NGD-exhibiting circuit topologies other than the resonator-based ones might exist, for which the derived limit might not apply. This possibility was the motivation for the analysis presented in Chapter 4, where the NGD vs. out-of-band gain limits will be examined for a linear and causal medium, regardless of its topology.

3.3.3 Transfer Function of an Infinitely Distributed NGD Circuit

As discussed in Section 3.3 and as evident in Fig. 3-33, for a given overall out-of-band gain A_{tot}, the largest NGD-bandwidth product is achieved for an infinitely distributed case ($N\to\infty$). The asymptotic limit in this case is given by (3.47). In this section, the transmission coefficient approximation will be derived for this case. First, the original transfer function for the N-stage circuit (3.37) can be rewritten as

$$S_{21}(\omega)=A_{tot}\left[\frac{\omega_0\omega+jQ\left(\omega^2-\omega_0^2\right)}{\omega_0\omega A_{tot}^{1/N}+jQ\left(\omega^2-\omega_0^2\right)}\right]^N=A_{tot}\left[1+\frac{\omega_0\omega\left(1-A_{tot}^{1/N}\right)}{\omega_0\omega A_{tot}^{1/N}+jQ\left(\omega^2-\omega_0^2\right)}\right]^N, \quad (3.50)$$

where the gain-compensated case is assumed (A_0G=1) and the overall out-of-band gain is given by $A_{tot}=A^N$. The phase delay of the overall circuit, exp(-$jN\beta l$), is omitted and can be easily factored in at the end of derivation as a finite phase delay of the distributed circuit. By letting $N\to\infty$ in (3.50) and assuming that the overall out-of-band gain is finite, the factor (1-$A_{tot}^{1/N}$) will approach zero and the overall expression becomes an exponential function in this limit case as given by

$$\lim_{N\to\infty} S_{21}(\omega) = \lim_{N\to\infty} A_{tot} \exp\left[N \frac{\omega_0\omega\left(1 - A_{tot}^{1/N}\right)}{\omega_0\omega A_{tot}^{1/N} + jQ\left(\omega^2 - \omega_0^2\right)} \right]$$

$$= \lim_{N\to\infty} A_{tot} \exp\left[\frac{-\omega_0\omega \ln\left(A_{tot}\right)}{\omega_0\omega + jQ\left(\omega^2 - \omega_0^2\right)} \right]. \qquad (3.51)$$

The individual stage Q-factor in (3.51) is now substituted by (3.42) and its limit expression found by letting $N\to\infty$ as

$$\lim_{N\to\infty} Q \approx \lim_{N\to\infty} \frac{Q_{tot}\sqrt{2^{1/N}-1}}{\sqrt{1-2^{1/N}/A_{tot}^{2/N}}} = \lim_{N\to\infty} \frac{Q_{tot}\sqrt{\ln 2}}{\sqrt{N}\sqrt{2\ln\left(A_{tot}\right)/N - \ln 2/N}} \approx \frac{Q_{tot}\sqrt{\ln 2}}{\sqrt{2\ln\left(A_{tot}\right) - \ln 2}}. \qquad (3.52)$$

Finally, the overall transfer function for the distributed circuit is obtained by substituting (3.52) into (3.51) as

$$\lim_{N\to\infty} S_{21}(\omega) = A_{tot} \exp\left[\ln\left(A_{tot}\right) \frac{jb\omega}{\omega^2 - jb\omega - \omega_0^2} \right], \qquad (3.53a)$$

where

$$b = \Delta\omega\sqrt{\frac{2\ln(A_{tot})}{\ln 2} - 1}\,, \tag{3.53b}$$

and the overall distributed circuit bandwidth is given by $\Delta\omega=\omega_0/Q_{tot}$. Expression (3.53) is a connection between an NGD multi-stage discrete circuit model and its continuous medium equivalent in the limit case. By applying (3.5) to (3.53), the phase characteristic and the group delay can be extracted in this case. Finally, using the group delay value at the resonance, the same NGD_{MAX}-bandwidth product vs. total out-of-band expression as given by the asymptotic limit (3.47) can be obtained as expected.

3.4 Lorentzian Dielectric Modeling With Resonator-based NGD Circuits

The derived expression for an infinitely distributed NGD medium (3.53) can be modified to include a positive delay due to finite physical dimensions, t_0, as

$$\begin{aligned} S_{21}(\omega) &= A_{tot}\exp\left[\ln(A_{tot})\frac{jb\omega}{\omega^2 - jb\omega - \omega_0^2} - j\omega t_0\right] \\ &= A_{tot}\exp\left\{-j\omega t_0\left[1 - \frac{b\ln(A_{tot})/t_0}{\omega^2 - jb\omega - \omega_0^2}\right]\right\}. \end{aligned} \tag{3.54}$$

Assuming the NGD medium is embedded within a homogeneous host medium with an effective relative dielectric permittivity ε_{eff}, and a length z, expression (3.54) can be rewritten as

$$S_{21}(\omega) = A_{tot} \exp\left\{ - j\omega \frac{z}{c} \sqrt{\varepsilon_{eff}} \left[1 - \frac{b \ln(A_{tot}) \omega_0 / \phi(\omega_0)}{\omega^2 - jb\omega - \omega_0^2} \right] \right\}, \tag{3.55}$$

where c is the speed of light in vacuum, and the phase delay at the resonance is determined by the delay due to the host medium alone, as $\phi(\omega_0)=\omega_0 \cdot t_0$.

Refractive index of a medium is a measure of the medium's propagation characteristic deviation from the propagation characteristic of vacuum. In general, the refractive index of a medium, $n(\omega)$, is a frequency dependent, complex quantity when sinusoidal electric fields are considered, and it relates to the medium's transmission characteristic as

$$S_{21}(\omega) = K \exp\left\{ - j\omega \frac{z}{c} n(\omega) \right\}, \tag{3.56}$$

where K is an optional, frequency-independent amplification/attenuation factor. From (3.56), it can be noted that the real and imaginary parts of the refractive index contribute to medium's phase and amplitude responses, respectively. Comparing (3.56) to (3.55), the complex refractive index of the distributed NGD medium is given by

$$n_{NGD}(\omega) = \sqrt{\varepsilon_{eff}}\left[1 - \frac{b\ln(A_{tot})\omega_0/\phi(\omega_0)}{\omega^2 - jb\omega - \omega_0^2}\right]. \tag{3.57}$$

Expression (3.57) resembles the 1st order approximation of the refractive index of a Lorentzian dielectric model, which is given by

$$n_{Lorentz}(\omega) = \sqrt{1 - \frac{\omega_p^2}{\omega^2 - 2j\delta\omega - \omega_0^2}} \approx 1 - \frac{\omega_p^2/2}{\omega^2 - 2j\delta\omega - \omega_0^2}, \tag{3.58}$$

where ω_0 and ω_p are the medium's resonance and plasma frequencies, respectively, and δ is the damping factor, which is related to medium's absorption bandwidth around the resonance [7]. The approximation in (3.58) is accurate only for $\omega_p << \omega_0$, when the second term numerator is small compared to the denominator. This approximation is least accurate for frequencies around ω_0, when the denominator of the term is smallest.

At the resonance frequency, the refractive index of the Lorentzian dielectric approximation and the one of the NGD medium are, respectively, given by

$$n_{Lorentz}(\omega_0) \approx 1 - j\frac{\omega_p^2}{4\delta\omega_0}, \qquad n_{NGD}(\omega_0) = \sqrt{\varepsilon_{eff}}\left[1 - j\frac{\ln(A_{tot})}{\phi(\omega_0)}\right]. \tag{3.59}$$

Equating the two expressions in (3.59), the required out-of-band gain value for the NGD medium model in terms of the Lorentzian dielectric parameters is obtained as

$$A_{tot} \approx \exp\left[\frac{\phi(\omega_0)}{\sqrt{\varepsilon_{eff}}}\frac{\omega_p^2}{4\delta\omega_0}\right]. \tag{3.60}$$

The other parameter of the NGD medium that needs to be determined is the overall bandwidth, $\Delta\omega$, or equivalently, $Q_{tot}=\omega_0/\Delta\omega$. Comparing the denominators in (3.57) and (3.58), it can be noted that in order to make them equal it is required that $b=2\delta$, which can be further expanded by utilizing (3.53b), as

$$2\delta = b = \Delta\omega\sqrt{\frac{2\ln(A_{tot})}{\ln 2}-1}\,. \tag{3.61}$$

Finally, the required Q_{tot} for the NGD medium can be determined by substituting $\Delta\omega$ from (3.61), as

$$Q_{tot} = \frac{\omega_0}{\Delta\omega} = \frac{\omega_0}{2\delta}\sqrt{\frac{2\ln(A_{tot})}{\ln 2}-1}\,. \tag{3.62}$$

Therefore, for relatively low values of plasma frequency, $\omega_p<<\omega_0$, the Lorentzian dielectric model can be approximated by a distributed NGD circuit, embedded in a dispersionless host medium. If the host medium has an effective relative dielectric permittivity ε_{eff}, and a phase delay at the resonant frequency equal to that of the Lorentzian medium, $\phi(\omega_0)$, the distributed NGD parameters can then be determined from (3.60) and (3.62).

Further, the amplitude characteristics of the two models differ by a multiplication constant. The amplitude characteristic value of the NGD medium is 0 dB at resonance while it is equal to A_{tot} at both ω=0 and $\omega\to\infty$. On the other hand, the Lorentzian medium is passive, with a 0 dB amplitude characteristic value at ω=0 and $\omega\to\infty$, and an attenuation (negative decibel value) at resonance. Therefore, the NGD medium's amplitude characteristic needs to be divided by A_{tot} when comparing it to the original Lorentzian medium. The NGD model is verified for a chosen case and the resulting comparison plots are shown in Fig. 3-39. In this example, the NGD medium is chosen to have a finite number of stages, N=10, instead of being infinitely distributed to demonstrate that the results still exhibit a good agreement in this case.

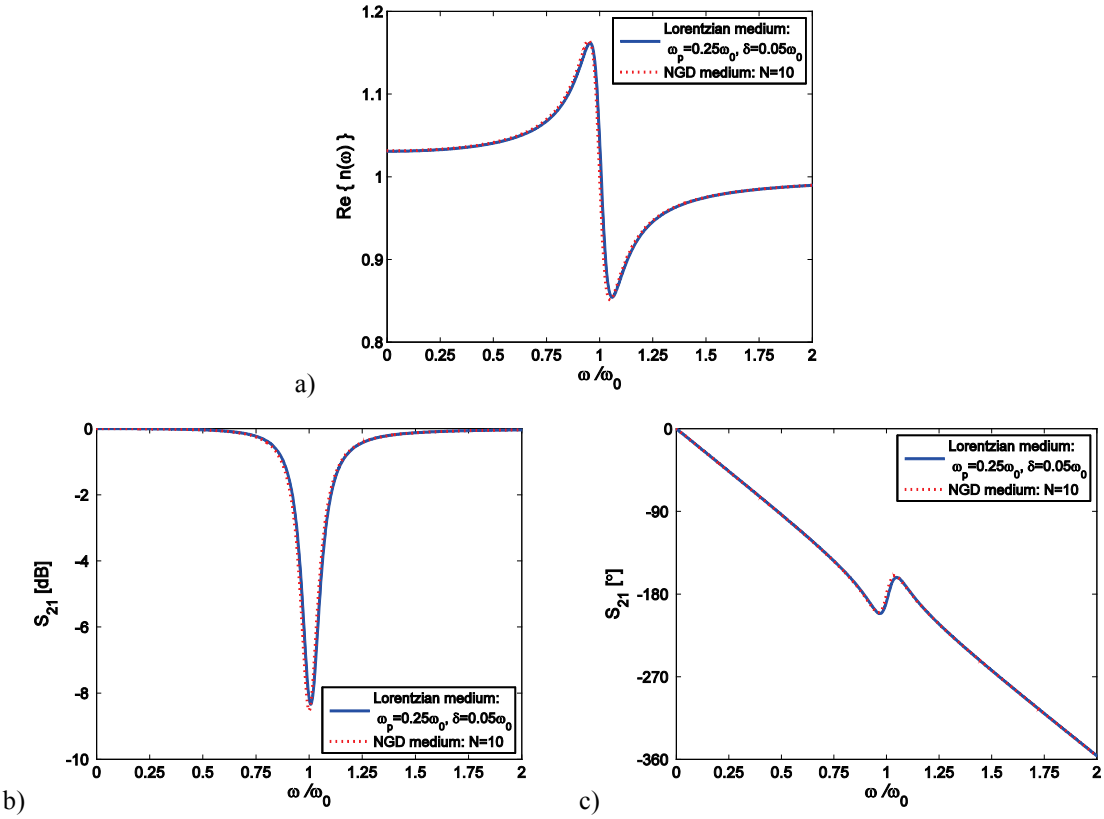

Figure 3-39: A ten-stage NGD medium and a Lorentzian dielectric model medium a) refractive index real part, b) amplitude and c) phase characteristics, for $\omega_0 \cdot t_0$=180°, ω_p=0.25 ω_0, and δ=0.05 ω_0.

The NGD circuit model of the Lorentzian dielectric medium can potentially be scaled down to relatively low frequencies, where the employed circuit components have smaller performance limitations. Furthermore, lower frequency waveforms propagated through the described NGD model can potentially be easier to measure and observe than their high frequency equivalents in the actual Lorentzian dielectric medium.

3.5 Baseband High-pass Filter-based NGD Circuits

NGD circuits presented so far in this chapter are based on *RLC* resonators, which are circuit components with a 2nd order frequency characteristic. Their NGD behavior is observed within a bandwidth $\Delta\omega$, centered around a non-zero resonant frequency, $\omega_0 \neq 0$. As discussed in Chapter 2, this phenomenon corresponds to a time-advancement of a smooth, relatively slow-varying envelope of an amplitude-modulated sinusoidal carrier with frequency ω_0. If, however, the NGD behavior is observed within a frequency bandwidth around a zero center frequency, i.e. within a baseband, a time-advancement will be observed for a low-frequency waveform whose frequency spectrum fits within the NGD bandwidth.

The NGD phenomenon at baseband frequencies can be achieved by replacing the *RLC* resonators (acting as stop-band filters), with high-pass filters [37,38]. The filters can, for example, be realized by a parallel *RC* element connected in series with the load or by a series *RL* element connected in shunt with the load, as shown in Fig. 3-40.

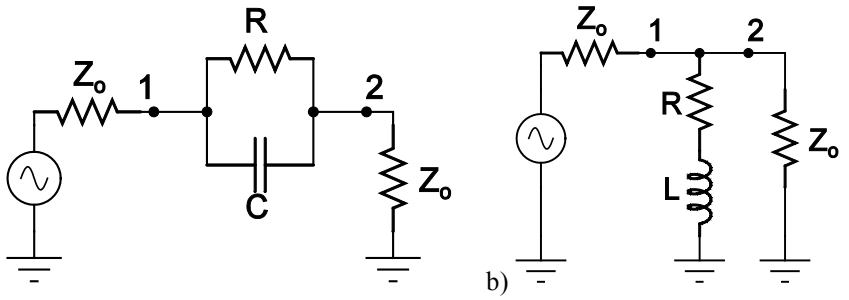

Figure 3-40: Baseband NGD circuits with a high-pass filter based on a) a parallel *RC* element connected in series, or b) a series *RL* element connected in shunt with the source/load.

The impedance of a parallel *RC* element and the corresponding bandwidth are given by

$$Z_{RC-par}(\omega)=\frac{R}{1+j2\dfrac{\omega}{\Delta\omega}},\quad \Delta\omega=\frac{2}{RC}. \tag{3.63}$$

Similarly, the impedance of a series *RL* element and the corresponding bandwidth are given by

$$Z_{RL-ser}(\omega)=R\left(1+j2\frac{\omega}{\Delta\omega}\right),\quad \Delta\omega=\frac{2R}{L}. \tag{3.64}$$

The bandwidth in each of the two baseband cases is equal to double the value of the cut-off frequency since the baseband characteristics symmetrically extend to negative frequencies. Similar to *RLC* resonators, the cut-off frequency is defined as the frequency where the real and imaginary parts of the element are equal in magnitude. This condition yields the bandwidth expressions in (3.63) and (3.64).

Using a similar reasoning as the one presented in Section 3.1, a generic transmission coefficient of any baseband NGD circuit based on a resistive-matched, single-stage *RC* or *RL* high-pass filter-based circuit can be written as

$$S_{21}(\omega) = (A_0 G) A \frac{\omega - j\frac{\Delta\omega}{2}}{\omega - j\frac{\Delta\omega}{2}A} e^{-j\beta l}, \tag{3.65}$$

where A is the single-stage out-of-band gain, A_0 is the gain-uncompensated transmission coefficient value at zero frequency, G is the optional compensating gain value, and βl is the phase delay due to finite dimensions if considered. The transfer function (3.65) is a ratio of 1st order functions of frequency in this case, in contrast to 2nd order functions for the resonator-based circuits. The group delay characteristic can be derived as

$$\tau_g(\omega) = -\frac{2}{\Delta\omega}\left(\frac{1}{4(\omega/\Delta\omega)^2 + 1} - \frac{A}{4(\omega/\Delta\omega)^2 + A^2}\right). \tag{3.66}$$

The maximum NGD value occurs exactly at the center frequency in this case and can be evaluated from (3.66) as

$$NGD_{MAX} = -\tau_g\big|_{\omega=0} = \frac{2}{\Delta\omega}\left(1 - \frac{1}{A}\right). \tag{3.67}$$

The maximum achievable NGD-bandwidth product in this case is obtained from (3.67) by letting $A \to \infty$ and it is equal to $1/\pi$, just as it was the case for single-stage resonator-based NGD circuits.

The transmission coefficient and group delay plots of a generic, single-stage baseband NGD circuit are shown in Fig. 3-41 for chosen values of A=20 dB and Δf=100 MHz.

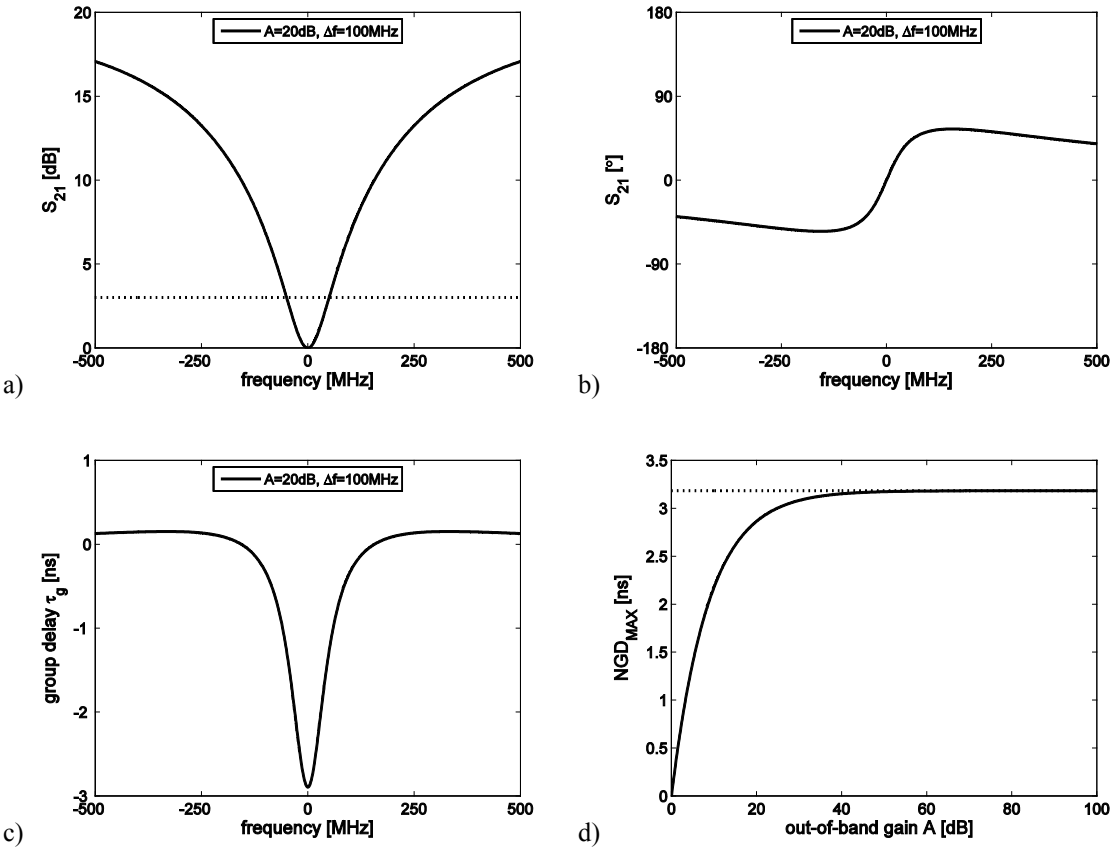

Figure 3-41: Baseband, single-stage NGD circuit a) amplitude, b) phase, c) group delay and d) maximum NGD vs. out-of-band gain characteristics, for A=20 dB and Δf=100 MHz.

The transmission coefficient and group delay characteristics of the baseband NGD circuits are similar in shape to those of the resonator-based NGD circuits, except that they are perfectly symmetric around the center frequency.

3.5.1 Multi-stage Baseband NGD Circuits

The transmission coefficient of an *N*-stage baseband NGD circuit with ideally matched cascaded stages can be derived as

$$S_{21}(\omega) = A_{tot}\left[\frac{\omega - j\dfrac{\Delta\omega'}{2}}{\omega - j\dfrac{\Delta\omega'}{2}A_{tot}^{1/N}}\right]^{N} e^{-jN\beta\cdot l}, \tag{3.68}$$

where $\Delta\omega'$ is the bandwidth of each individual stage, which needs to be adjusted to yield an overall desired bandwidth $\Delta\omega$ as given by

$$\Delta\omega' \approx \frac{\Delta\omega\sqrt{1-2^{1/N}/A_{tot}^{2/N}}}{\sqrt{2^{1/N}-1}}. \tag{3.69}$$

Expression (3.69) is derived by employing a similar procedure as the one used in the derivation of (3.42) for multi-stage resonator-based circuits. The difference here is that only bandwidths are dealt with, since the *Q*-factor is not defined for baseband circuits (using ω_0=0 in the expression for *Q* would always yield *Q*=0, regardless of the $\Delta\omega$ value).

By applying the standard procedure of extracting the phase characteristic to (3.68), finding its derivative to obtain the group delay and evaluating it at the center frequency, the maximum NGD-bandwidth product in this case can be written as

$$NGD_{MAX}\Delta f = \frac{1}{\pi} N\sqrt{2^{1/N}-1}\,\frac{1-1/A_{tot}^{1/N}}{\sqrt{1-2^{1/N}/A_{tot}^{2/N}}} - N\tau_{pd}\Delta f\,, \tag{3.70}$$

which is exactly the same as expression (3.45) for resonator-based circuits. Obviously, the asymptotic NGD limits for baseband circuits will be identical to those derived for resonator-based circuits as given by (3.47) and (3.48).

Finally, following a similar derivation as the one in Section 3.3.3, the transmission coefficient of an infinitely distributed baseband NGD circuit can be written as

$$\lim_{N\to\infty} S_{21}(\omega) = A_{tot}\exp\left[\ln(A_{tot})\frac{jb/2}{\omega - jb/2}\right], \tag{3.71a}$$

where

$$b = \Delta\omega\sqrt{\frac{2\ln(A_{tot})}{\ln 2}-1}\,, \tag{3.71b}$$

and is identical to the expression for b in (3.53b) for resonator-based circuits.

In conclusion, baseband NGD circuits have a transmission characteristic comprised of a ratio of lower order frequency functions, as compared with resonator-based circuits (1^{st} order vs. 2^{nd} order, respectively). The NGD-bandwidth product as a function of the out-of-band gain is identical for both types of circuits as well as the corresponding asymptotic limits. In Chapter 5, a time domain analysis will be performed for both types of circuits, showing further similarities in their responses to selected waveforms.

3.6 Chapter Conclusions

In this chapter, a comprehensive frequency domain analysis of different *RLC* resonator-based NGD circuits was presented. The motivation for this chapter emerged from reviewing the work on several different NGD circuit topologies reported in the literature (mostly *LC*-matched and π-matched circuits) and not finding a quantitative comparison model between them. Furthermore, most of the work reported in the literature emphasizes the NGD achieved cumulatively through several cascaded stages, often disregarding the decreased 3 dB bandwidth when individual stage *Q*-factors (and thus bandwidth) is kept constant.

By applying circuit analysis, explicit expressions for NGD as a function of loss were derived and presented for different *RLC* passive topologies. These expressions account for an easy quantitative comparison of different topologies, suggesting an *R*-matched topology (one-sided resistive match at the source side) as the preference in terms of the absolute NGD achieved in both single-stage or cascaded design.

A generic transmission coefficient expression was derived, which is applicable to any resistive-matched resonator-based NGD circuit topology, gain-compensated or not. It was shown that the ideally matched multi-stage case achieves the highest NGD for a given overall out-of-band gain. NGD as a function of number of stages and the out-of-band gain was derived for an ideally matched multi-stage design when overall bandwidth was maintained. Asymptotic upper NGD limits were derived as a function of the number of stages and the out-of-band gain, separately. The effect of cascading a band-pass filter with an NGD circuit was shown to be able to slightly increase the derived NGD limits,

but the overall square root relation between the NGD and out-of-band gain was preserved.

An infinitely distributed resonator-based NGD circuit was shown to yield the upper NGD limit and the transmission characteristic function was derived in this case. The similarities of the distributed NGD medium when a non-zero length is considered to the Lorentzian model of a dielectric medium was demonstrated, and the model parameters expressions were derived under certain approximations.

Finally, a generic transmission coefficient expression for baseband NGD circuits was derived in a similar fashion as for the resonator-based ones. Even though the individual stage frequency functions appearing in the baseband transmission coefficient are only of the 1^{st} order, compared to the 2^{nd} order functions of the resonator-based circuits, the NGD limits were shown to be the same.

In the next chapter, an upper NGD asymptotic limit as a function of the out-of-band gain will be derived for an optimally engineered linear causal medium. The derived limits will apply to all causal NGD circuits, regardless of their topology. The motivation for such analysis came from the fact that even cascading a simple band-pass filter with a resonator-based NGD circuit can change the achieved NGD as a function of the out-of-band gain, as demonstrated in Section 3.3.2. However, since the general square root asymptotic relationship between the NGD and the out-of-band gain was still preserved in that case, the analysis presented in the next chapter will explore the possibility that an optimally engineered linear causal medium will still have an asymptotic limit of the same functional dependence.

4. NGD Asymptotic Limit for an Optimally Engineered Linear Causal Medium

In the previous chapter, NGD circuits based on *RLC* resonators (operating around a non-zero center frequency), and NGD circuits based on high-pass filters (operating at baseband frequencies) were analyzed. For single-stage circuits, the maximum achievable NGD value at the center frequency was shown to be a $1/\pi$ fraction of $1/\Delta f$, which is a measure of the pulse width. For multi-stage circuits, NGD values at the center frequency as a function of the number of stages and the total out-of-band gain were derived, and given by (3.45). Distributed circuits (having a theoretically infinite number of stages) were shown to exhibit an upper asymptotic limit for NGD, given as a square root function of the logarithm of the out-of-band gain magnitude, as given by (3.47).

One could wonder if some different circuit topologies can perform better than those presented in Chapter 3, in terms of the achieved NGD-bandwidth product as a function of out-of-band gain. For example, it was demonstrated in Section 3.3.2 that cascading a band-pass filter with a resonator-based NGD circuit can increase the achieved NGD to out-of-band gain ratio. Rather than experimenting with different circuit topologies, in this chapter the propagation characteristic will be engineered for a linear and causal medium which exhibits an optimal asymptotic NGD limit as a function of the out-of-band gain.

It is well known that the complex transfer function of a causal, physically realizable medium does not have independent real and imaginary parts [7, 8, 33]. If the medium was initially at rest, there cannot be any response at the output of a causal medium before an

input signal is applied. This requirement translates into causal medium's response to a Dirac delta function input being equal to zero, before the point in time when the input signal is applied. If the Dirac delta function is applied at t=0 and the considered medium is linear and causal, the following will apply

$$h(t<0)=\int_{-\infty}^{\infty}H(\omega)e^{j\omega\cdot t}d\omega=0\,, \tag{4.1a}$$

where

$$H(\omega)=P(\omega)+jQ(\omega)=A(\omega)e^{j\varphi(\omega)}\,. \tag{4.1b}$$

Since the medium's response to Dirac delta function in this case takes non-zero values only for $t\geq 0$, it can be decomposed into an odd and an even function of time as

$$h(t)=h_{eve}(t)+h_{odd}(t)\,, \tag{4.2a}$$

where

$$h_{eve}(t)=\begin{cases}\dfrac{1}{2}h(-t), & t<0\\[2ex] \dfrac{1}{2}h(t), & t\geq 0\end{cases}\qquad\text{and}\qquad h_{odd}(t)=\begin{cases}-\dfrac{1}{2}h(-t), & t<0\\[2ex] \dfrac{1}{2}h(t), & t\geq 0\end{cases}\,. \tag{4.2b}$$

It is clear from (4.2b) that the even and odd components of a causal medium's response are not independent of each other, but can rather be expressed as $h_{eve}(t)=\text{sgn}(t)\cdot h_{odd}(t)$, or alternatively $h_{odd}(t)=\text{sgn}(t)\cdot h_{eve}(t)$, where sgn(·) denotes a signum function. As evident from the Fourier integral (2.4a), an even function in time yields a purely real frequency

response, while an odd function in time yields a purely imaginary frequency response. Therefore, by comparing (4.1b) and (4.2a) it can be noted that the real part of a causal medium's transfer function, $P(\omega)$, is correlated with $h_{eve}(t)$ only, while the imaginary part of the transfer function, $Q(\omega)$, is correlated with $h_{odd}(t)$ only. Since $h_{eve}(t)$ and $h_{odd}(t)$ are dependent in this case, then $P(\omega)$ and $Q(\omega)$ will be dependent of each other as well. Furthermore, since the exact functional relationship between $h_{eve}(t)$ and $h_{odd}(t)$ is known in this case (a signum function), it can be shown [7] that the real and imaginary parts of a linear causal medium's transfer function are related through Kramers-Kronig relations, given by Cauchy Principal Value integrals as

$$Q(\omega) = V.P.\left\{-\frac{1}{\pi}\int_{-\infty}^{\infty}\frac{P(\nu)}{\nu-\omega}d\nu\right\} \quad \text{and} \quad P(\omega) = V.P.\left\{\frac{1}{\pi}\int_{-\infty}^{\infty}\frac{Q(\nu)}{\nu-\omega}d\nu\right\}. \tag{4.3}$$

Since NGD phenomenon stems from the phase response characteristic, it is more useful to relate the amplitude and phase characteristic of a causal medium's transfer function in this case, rather than its real and imaginary parts. Further manipulation of expressions (4.3) yields [68]

$$A_{dB}(\omega) = -\frac{20}{\pi\ln 10}V.P.\left\{\int_{-\infty}^{\infty}\frac{\varphi(\nu)}{\nu-\omega}d\nu\right\} \quad \text{and} \quad \varphi(\omega) = \frac{\ln 10}{20\pi}V.P.\left\{\int_{-\infty}^{\infty}\frac{A_{dB}(\nu)}{\nu-\omega}d\nu\right\}. \tag{4.4}$$

Therefore, if an arbitrary phase characteristic is set for a linear and causal medium's transfer function, the corresponding amplitude characteristic is not arbitrary. It is rather

uniquely defined (up to an integration constant). This fact can be taken advantage of and a suitable phase characteristic, and therefore the NGD, can be assumed and the corresponding magnitude characteristic can then be evaluated from (4.4). Then, an attempt can be made to extract the maximum out-of-band gain in that case, and to find its relationship to the achieved NGD.

4.1 Piece-wise Linear Phase Response

In order to simplify the analysis, a transfer function phase characteristic exhibiting NGD within the signal baseband (around ω=0) is chosen. However, the obtained results and conclusions can be extended to NGD phenomena occurring within an arbitrary frequency band. Moreover, a zero-length medium is considered in order to further simplify the analysis. The finite medium length can easily be taken into account by adding a constant positive delay t_0 at the end of the analysis. However, since upper NGD asymptotic limits are of interest in this work, the added positive delay will not be considered. For analytical simplicity, in this section a piece-wise linear phase response will be considered, which is given by

$$\phi(\omega) = \begin{cases} t_g \omega, & 0 \le \omega < \omega_M \\ (\omega - \omega_E)\dfrac{t_g \omega_M}{\omega_M - \omega_E}, & \omega_M \le \omega \le \omega_E \\ 0, & \omega \ge \omega_E \end{cases}, \tag{4.5}$$

and $\phi(-\omega)=-\phi(\omega)$, with t_g being the positive phase response slope (NGD) at the center frequency, ω_M is the frequency at which the slope changes sign, and at ω_E the phase characteristic reaches zero, and stays there beyond this frequency. The phase response is always an odd function around $\omega=0$, and it is shown in Fig. 4-1 along with the corresponding group delay plot.

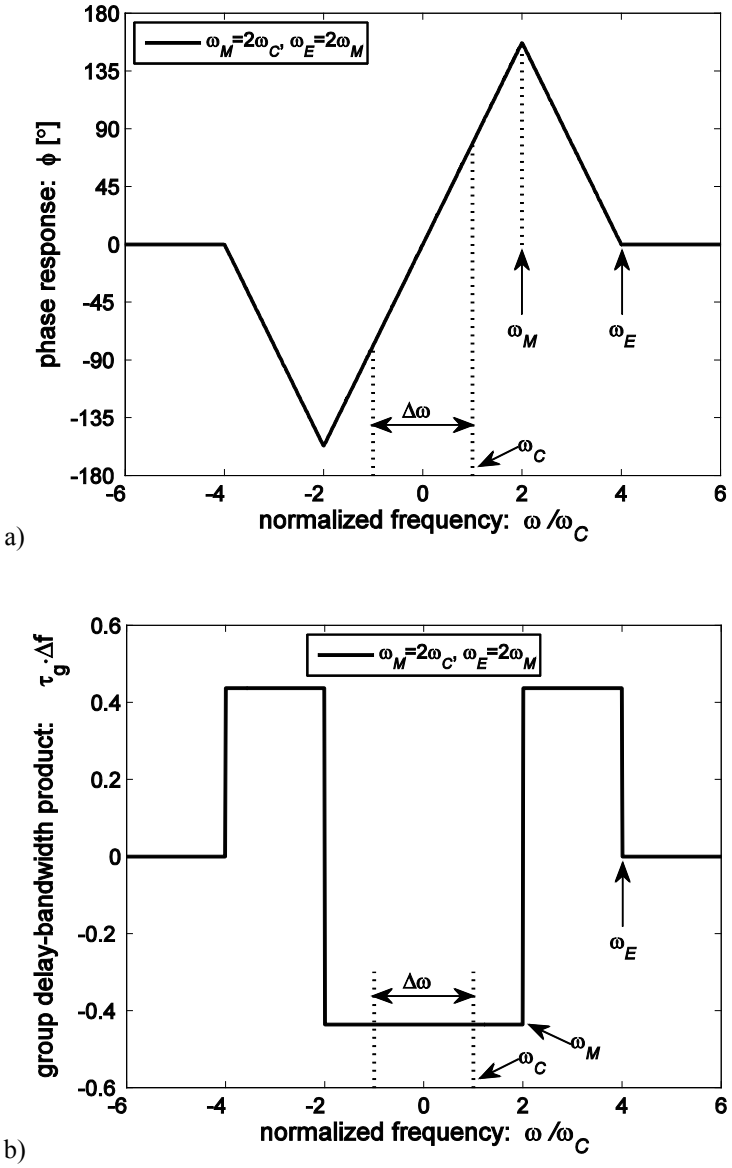

Figure 4-1: Piece-wise linear phase response a) and group-delay-bandwidth product b) for $\omega_M=2\omega_C$ and $\omega_E=2\omega_M$.

The phase characteristic is zero at high frequencies, which is equivalent to phase characteristic approaching a constant-slope line ("light-line") if a non-zero length medium was considered in the model. At high frequencies, the phase characteristic approaches the "light-line" for all physical media, as discussed in Chapter 2. Therefore, the phase characteristic shown in Fig. 4-1 has a general shape resembling the phase of actual media which exhibit NGD. A constant NGD is achieved over the entire frequency band ($-\omega_M$, ω_M). For a more general discussion the NGD bandwidth is allowed to be defined within a smaller band $\Delta\omega=2\pi\Delta f=(-\omega_C,\ \omega_C)$ and the bandwidth is solely determined by a 3 dB swing in the system amplitude response in this case (all distortion comes from the amplitude characteristic deviation, since the phase is linear within entire bandwidth).

The amplitude response obtained through integration using (4.4) is shown in Fig. 4-2 and given by

$$A_{dB}(\omega) = (t_g \Delta f)\frac{20}{\ln 10}\frac{\omega_M}{\omega_C}a(\omega), \tag{4.6a}$$

where

$$a(\omega) = \left\{ \frac{2\omega_E}{\omega_E - \omega_M}\ln\left(\frac{\omega_E}{\omega_M}\right) + \frac{\omega_E + \omega}{\omega_E - \omega_M}\ln\left(\frac{\omega_M + \omega}{\omega_E + \omega}\right) + \frac{|\omega|}{\omega_M}\ln\left(\frac{\omega_M + \omega}{|\omega_M - \omega|}\right) + \frac{\omega_E - \omega}{\omega_E - \omega_M}\ln\left(\left|\frac{\omega_M - \omega}{\omega_E - \omega}\right|\right)\right\}. \tag{4.6b}$$

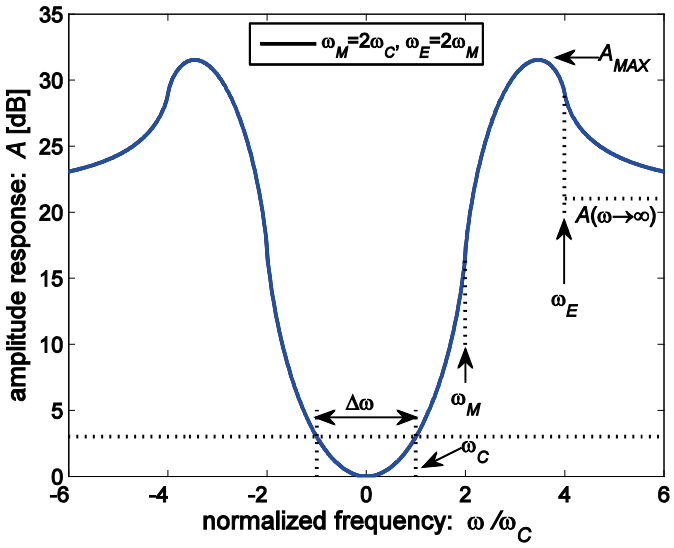

Figure 4-2: Amplitude response satisfying Kramers-Kronig relations for the given phase response, Fig. 4-1, with $\omega_M=2\omega_C$ and $\omega_E=2\omega_M$.

The integration constant is chosen so that $A_{dB}(0)=0$. By setting the 3 dB bandwidth of the obtained amplitude characteristic to be at $\omega=\pm\omega_C$, the negative group delay at the center frequency t_g is uniquely defined as

$$t_g \Delta f = \frac{\ln 2}{2}\frac{\omega_C}{\omega_M}\frac{1}{a(\omega_C)}. \tag{4.7}$$

The out-of-band gain can be obtained from (4.6a) as

$$A_{dB}(\omega \to \infty) = (t_g \Delta f)\frac{\omega_M}{\omega_C}\frac{20}{\ln 10}\frac{2\omega_E}{\omega_E - \omega_M}\ln\left(\frac{\omega_E}{\omega_M}\right). \tag{4.8}$$

Selecting smaller values for ω_M in (4.7) yields higher values for the NGD at the center frequency. However, this comes at the expense of larger out-of-band gain $A(\infty)$. Large

out-of-band gain is undesirable, since it amplifies transients when signals with defined "turn on" and/or "turn off" times are applied, as it will be demonstrated in Chapter 5.

A family of NGD-bandwidth product versus $A_{dB}(\infty)$ functions can be obtained from expressions (4.7) and (4.8), where discrete values of ω_E correspond to different functions. In this case, ω_M is an independent parameter which is continuously swept and substituted into (4.7) and (4.8). Such obtained family of functions is shown in Fig. 4-3, indicating that for any given out-of-band gain the maximum NGD is achieved when $\omega_E \rightarrow \omega_M$.

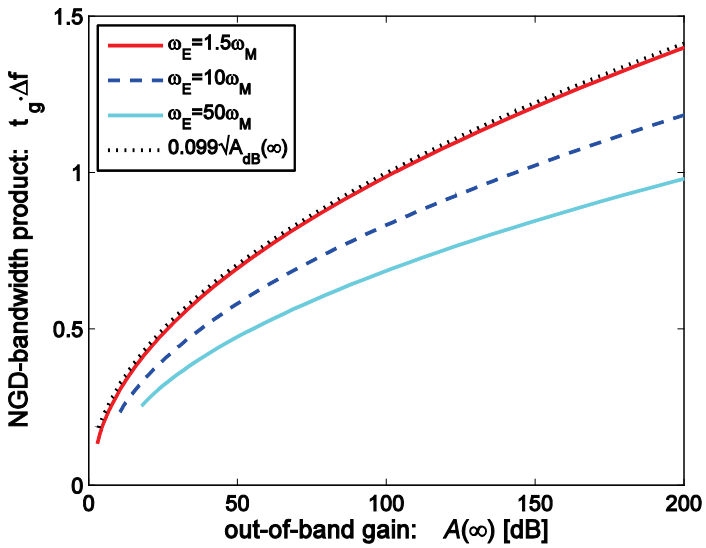

Figure 4-3: Maximum NGD-bandwidth product as a function of out-of-band gain $A(\infty)$, for different values of ω_E.

Moreover, an asymptotic relationship can be found between the maximum NGD and out-of-band gain, for $\omega_E \rightarrow \omega_M$ and large values of ω_M / ω_C (large out-of-band gain). First, expression (4.7) can be simplified in this case as

$$t_g \Delta f \approx \frac{\ln 2}{2} \frac{\omega_M}{\omega_C} \frac{\omega_E}{\omega_E + \omega_M}. \tag{4.9}$$

Substituting ω_M / ω_C from (4.9) into (4.8), and by letting $\omega_E \to \omega_M$, the asymptotic upper limit for NGD is obtained as a function of $A_{dB}(\infty)$ as

$$t_g \Delta f \le \sqrt{\frac{(\ln 2)(\ln 10)}{160}} \sqrt{A_{dB}(\infty)} \approx 0.099 \sqrt{A_{dB}(\infty)} \,. \tag{4.10}$$

However, for the piece-wise linear phase response the maximum value of the out-of-band gain, A_{MAX}, is always higher than the $A_{dB}(\infty)$ value as shown in Fig. 4-2. Finding the zeros of the first derivative of (4.6a) involves solving a transcendental equation, which also depends on the ω_E / ω_M ratio. By numerically solving this equation and manipulating (4.6a), it can be shown that the maximum NGD/A_{MAX} ratio is obtained when $\omega_E \approx 3.368\,\omega_M$. Now (4.6a) and (4.7) can be combined to produce NGD-bandwidth product versus A_{MAX} curves, which are shown in Fig. 4-4.

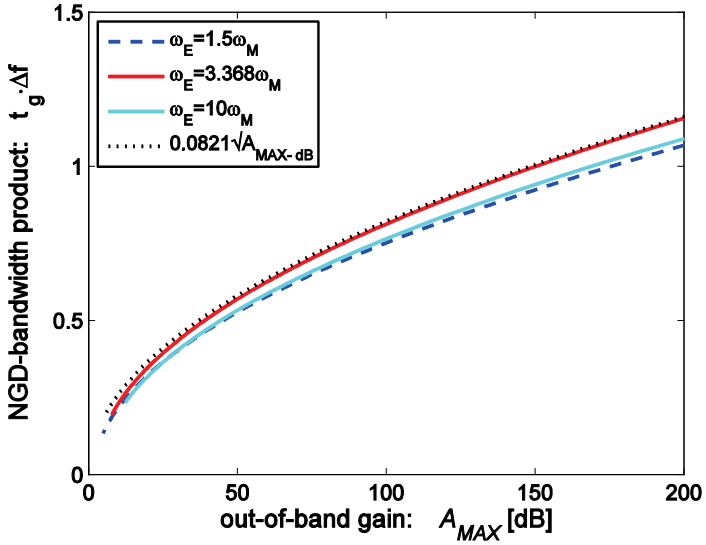

Figure 4-4: Maximum NGD-bandwidth product as a function of out-of-band gain $A_{MAX\text{-}dB}$, for different values of ω_E.

The upper asymptotic limit in this case is given by

$$t_g \Delta f \leq 0.0821 \sqrt{A_{MAX-dB}} \ . \tag{4.11}$$

Comparing this limit to the one for resonator-based circuits (3.47b), it can be noted that this asymptotic limit has the same square root relationship only with a higher multiplying coefficient, and therefore does not contradict the limit derived for resonator-based or filter-based (at baseband frequencies) circuits. This is a promising result since resonator-based media are just a subset of causal media, so any limits derived for causal media in general should also apply to resonator-based circuits, by extension.

4.2 Frequency-Reciprocal Decay of the Phase Response

As is evident from (3.6) and (3.66), the group delay as a function of frequency of the media presented in Chapter 3 has a reciprocal square decay, $(1/\omega^2)$, at high frequencies. Since the group delay is essentially a derivative of the phase response, this means that at high frequencies the phase response of these media has a reciprocal decay, $(1/\omega)$. The 1st order approximation of a general linear causal medium phase response analyzed in Section 4.1, however, has a linear, not reciprocal decay past the phase slope reversal point, ω_M. In this section, phase approximations with the same linear phase response around the center frequency will be examined, but with different order reciprocal phase decays, $(1/\omega^k)$, past the ω_M frequency. The decay functions parameters are chosen such that the phase characteristics are continuous at the reversal point, ω_M, and the decay

slopes at the same point, $\tau_g(\omega_M)$, are related to the center frequency phase slope, t_g, such that the NGD/A_{MAX} ratio is maximized in each case.

Figure 4-5 shows phase and corresponding group delay responses for the reciprocal phase decay cases of orders k=1/2, k=1, k=2 and $k\to\infty$ (equivalent to a linear decay).

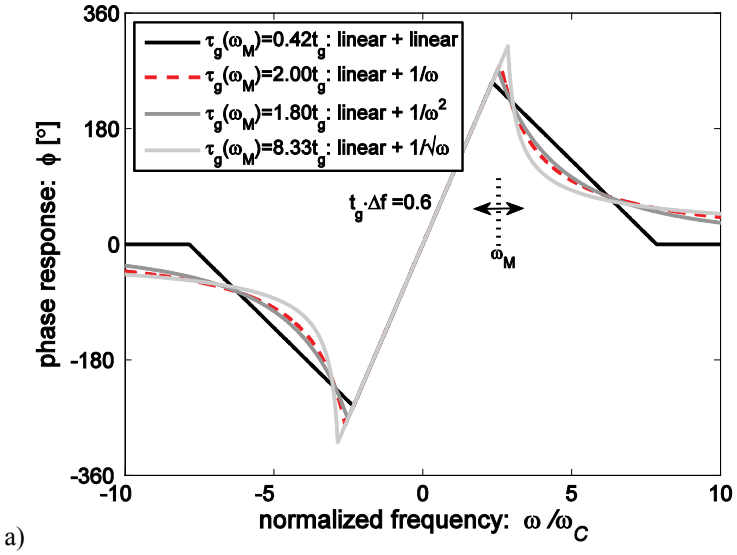

a)

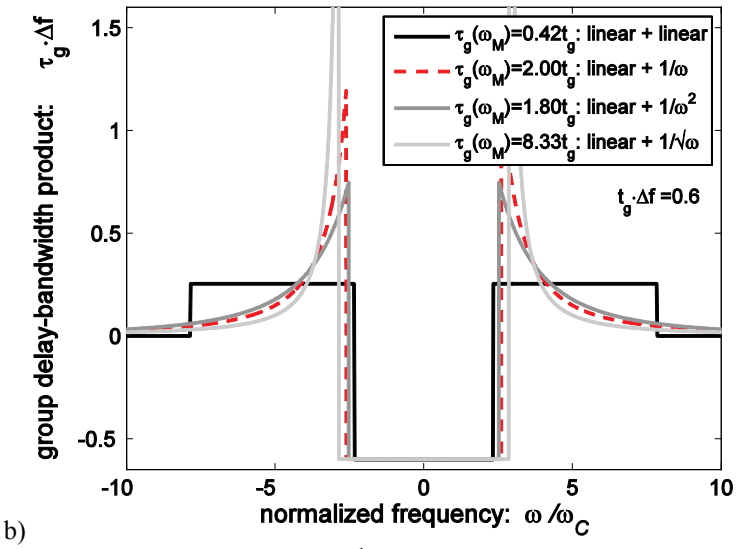

b)

Figure 4-5: Piece-wise linear and reciprocal ($1/\omega^k$) decay a) phase responses and corresponding b) group-delay-bandwidth products for k=1/2, k=1, k=2, and $k\to\infty$ (linear decay). Each case shown corresponds to the maximized NGD/A_{MAX} ratio, and it has $t_g\cdot\Delta f$=0.6.

For comparison purposes, each case has the same NGD-bandwidth product value at the center frequency, $t_g \cdot \Delta f = 0.6$. The amplitude responses corresponding to Fig. 4-5 cases are derived following a similar procedure as in Section 4.2, and they are shown in Fig. 4-6. Since all cases have the same NGD-bandwidth product, $t_g \cdot \Delta f = 0.6$, the case with the smallest A_{MAX} value will have the largest NGD/A_{MAX} ratio (optimum case).

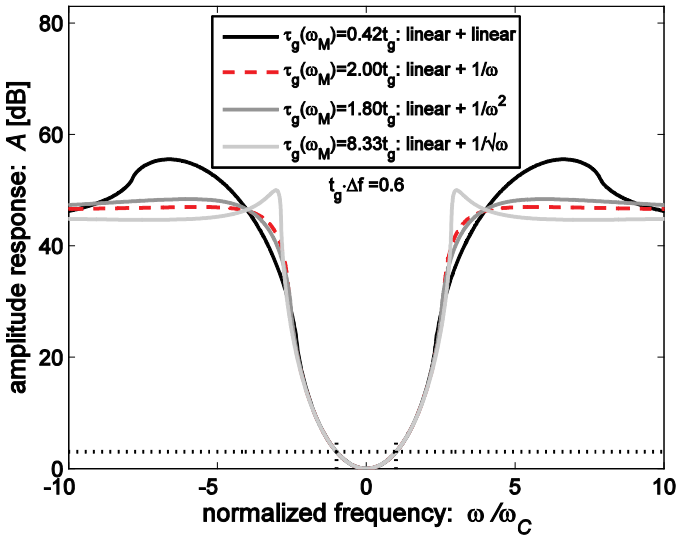

Figure 4-6: Magnitude responses for piece-wise linear and reciprocal ($1/\omega^k$) phase decays with k=1/2, k=1, k=2, and $k \to \infty$ (linear decay). Each case shown corresponds to the maximized NGD/A_{MAX} ratio, and it has $t_g \cdot \Delta f = 0.6$.

As evident from Fig. 4-6, the reciprocal decay case ($1/\omega$) has the smallest out-of-band gain, and it is therefore optimal. This is confirmed in Fig. 4-7, where curves relating NGD-bandwidth versus maximum out-of-band gain are produced, in a similar manner as those in Section 4.1. The asymptotic limit for the optimum case is determined numerically as

$$t_g \Delta f \le 0.089\sqrt{A_{MAX-dB}}\,. \tag{4.12}$$

The asymptotic limit given by (4.12) does not contradict limits given by (4.11) and (3.47b). Changing the order of phase decay to a higher ($1/\omega^2$), or a lower ($1/\omega^{1/2}$) value from the optimum case ($1/\omega$) produces asymptotic limits smaller than (4.12).

All cases shown in Fig. 4-6 have their maximum out-of-band values, A_{MAX}, larger than their corresponding out-of-band values at high frequencies, $A_{dB}(\infty)$. Therefore, amplitude characteristics are not monotonic functions of frequency, unlike the media presented in Section 3. Decay slopes at the phase reversal points, $\tau_g(\omega_M)$, can be adjusted for the k=1 and k=1/2 cases to make their amplitude characteristics monotonic functions in frequency half-planes (A_{MAX} is at $A_{dB}(\infty)$). However, changing the decay slopes from the optimum values shown in Fig. 4-5 would result in lowering the NGD/A_{MAX} ratio for each case. For example, the limit for the optimal case (k=1) given by (4.12) would decrease by 2.25%, if the phase slope at the reversal point, $\tau_g(\omega_M)$, was changed to make the corresponding amplitude characteristic monotonic.

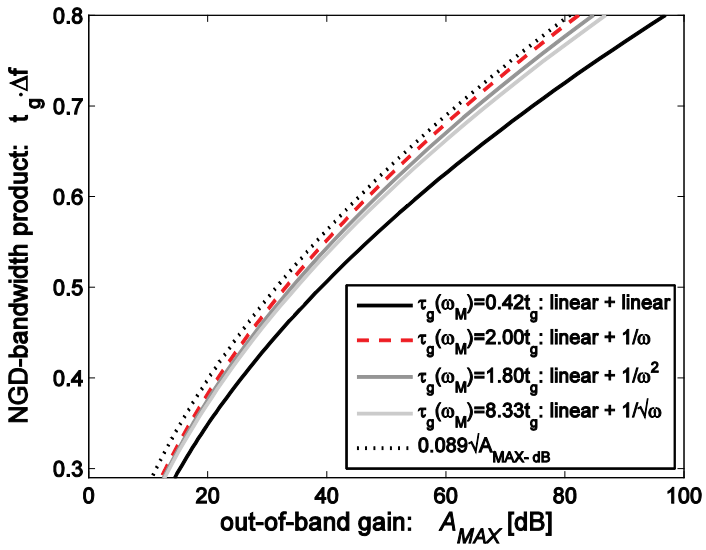

Figure 4-7: Center frequency NGD-bandwidth product as a function of out-of-band gain A_{MAX}, for piece-wise linear and reciprocal ($1/\omega^k$) phase decays with k=1/2, k=1, k=2, and $k\to\infty$ (linear decay).

Since the primary objective of this chapter was to derive the upper asymptotic limit, the limit given by expression (4.12) will be retained.

Similar derivations as the ones presented in the last two sections were performed for several other types of phase responses, such as a 2^{nd} order phase characteristic around the center frequency combined with a reciprocal decay phase at high frequency, with a continuous phase derivative (group delay) over the entire frequency domain. However, the upper limit given by expression (4.12) still holds for the analyzed cases. The same is expected for any higher order phase response around the center frequency, combined with any order of the decay response at high frequencies.

The optimally engineered phase and amplitude responses shown in Fig. 4-5 and Fig. 4-6, respectively, are used to characterize a fictitious but causal medium which exhibits an upper asymptotic limit given by (4.12). It attempts to set an upper NGD limit for any other causal, physically realizable medium. Synthesis of an actual medium with amplitude and phase characteristics that are close to those of the optimal medium is out of scope for this thesis. However, since the analytical expression for the transfer function of the optimal medium is known, numerical methods can be employed to approximate it with a rational function of polynomials and the poles and zeros of the approximated transfer function can be determined. The knowledge of poles and zeros then opens the possibility of the medium synthesis via the use of cascaded electrical circuit elements.

4.3 Asymptotic Limit Verification with Physical Media

In this section, the asymptotic limit for the distributed high-pass filter-based NGD

medium presented in Section 3.5, and a Lorentzian model dielectric medium are both compared with the optimally engineered medium from Section 4.2 corresponding to the asymptotic limit given by (4.12). The comparison is carried out for both amplitude and phase frequency responses, for a selected case.

In the first comparison, an infinitely distributed high-pass filter-based medium exhibiting an NGD-bandwidth product of $t_g \cdot \Delta f = 0.6$ is chosen, corresponding to a maximum out-of-band gain A_{MAX}=86 dB. This is compared to a medium with an within-band linear phase approximation with a reciprocal ($1/\omega$) decay at high frequencies, which is chosen to have the same NGD-bandwidth product and with $\tau_g(\omega_M)=2t_g$, yielding a maximum NGD/A_{MAX} ratio as in Section 4.2. The amplitude characteristic for this case is obtained by Kramers-Kronig relations as before. The phase and amplitude response plots for this case are shown in Figs. 4-8a and 4-8b, respectively.

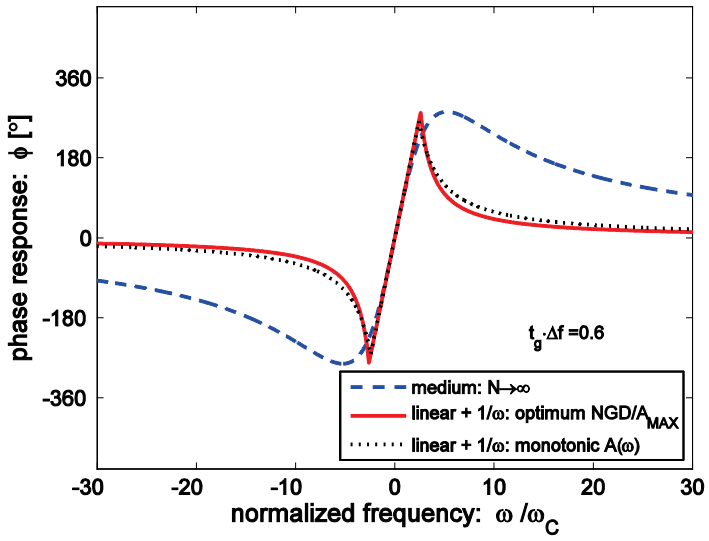

a)

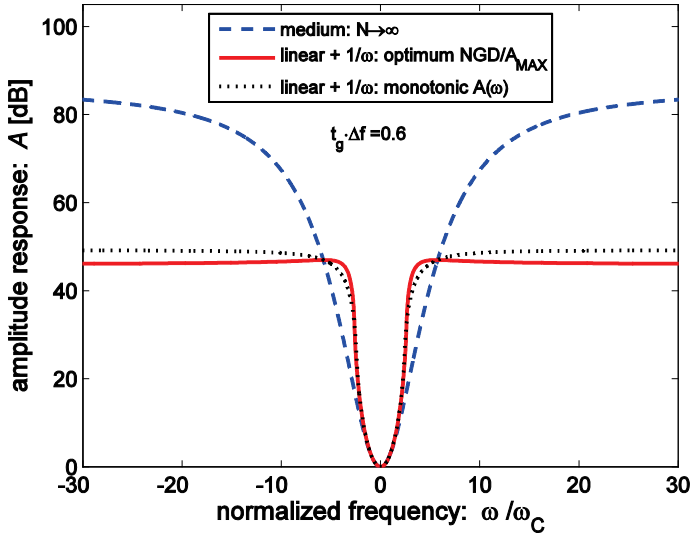

b)

Figure 4-8: a) Phase and b) amplitude response characteristics of a distributed high-pass filter-based medium, and a piece-wise linear and reciprocal decay phase approximation medium with NGD-bandwidth product $t_g \cdot \Delta f$=0.6.

It can be noted that for the same NGD-bandwidth product chosen for both cases, the optimum medium from Section 4.2 (linear and reciprocal phase decay combination) has a much smaller maximum out-of-band gain of A_{MAX}=47 dB. If the parameters of the same optimum medium type from Section 4.2 are slightly adjusted to yield a monotonic amplitude characteristic, a slightly larger out-of-band gain value of A_{MAX} =49 dB results. This case is also shown in Figs. 4-8a and 4-8b.

In the second comparison, a passive Lorentzian dielectric model medium is chosen for $\phi(\omega)$=Re$\{-\omega \cdot n(\omega)/c\}$. As in Section 3.4, the refractive index of this medium is given by

$$n(\omega) = \sqrt{1 - \frac{\omega_p^2}{\omega^2 - 2j\delta\omega - \omega_0^2}}, \tag{4.13}$$

where ω_0 and ω_p are the medium's resonance and plasma frequencies, respectively, and δ is the damping factor, which is related to medium's absorption bandwidth around the resonance. The chosen example has ω_p=0.53ω_0, δ=0.05ω_0, and a physical length corresponding to a 360° phase shift of a sinusoidal waveform of frequency ω_0, travelling the same distance in vacuum (light-line). The NGD bandwidth of this medium is not centered around ω=0, but around a point in the vicinity of the resonance frequency instead. The phase and magnitude responses are not symmetric around the center frequency either. The chosen example exhibits the same NGD-bandwidth product of $t_g \cdot \Delta f$=0.6, corresponding to a maximum out-of-band gain A_{MAX}=99 dB as shown in Fig. 4-9b. This medium has an even larger maximum out-of-band gain (or equivalently, center frequency loss, since it is a passive medium) for a given NGD-bandwidth product, as compared with the medium from Section 3.5.

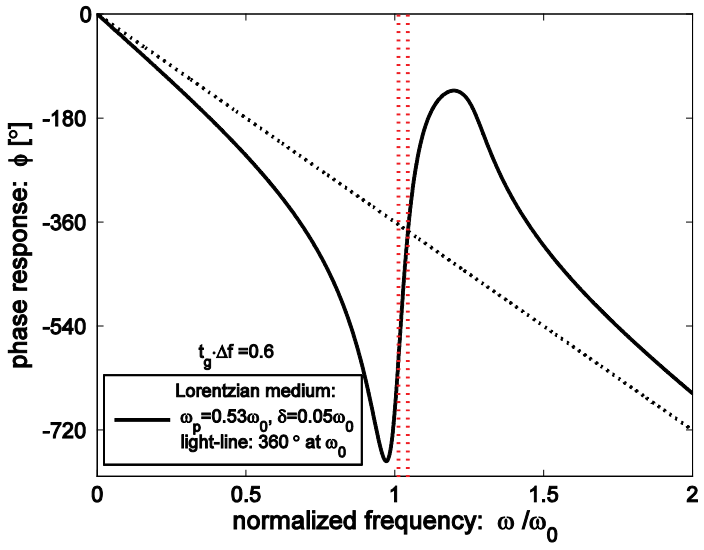

a)

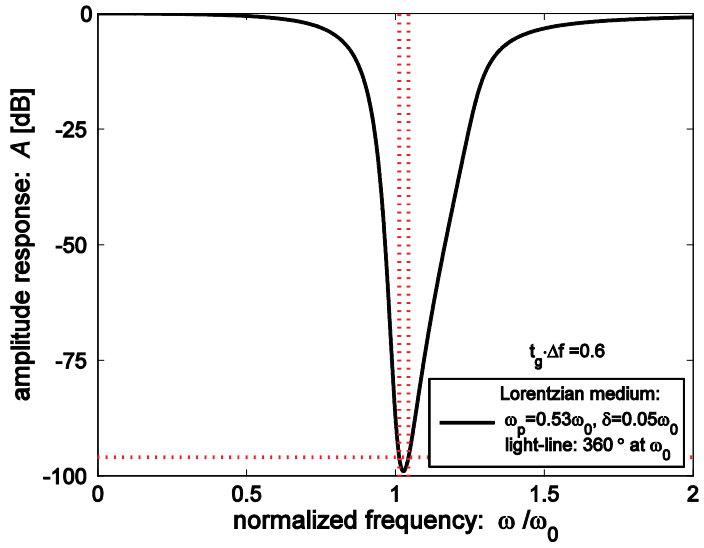

b)

Figure 4-9: a) Phase and b) amplitude response characteristics of a Lorentzian medium with an NGD-bandwidth product $t_g \cdot \Delta f = 0.6$, $\omega_p = 0.53\,\omega_0$, $\delta = 0.05\,\omega_0$, and medium length corresponding to a 360° light-line phase at ω_0.

The asymptotic limit for this medium will therefore be even smaller, and it is numerically evaluated as shown in Fig. 4-10. The same upper limit holds for Lorentzian media with different light-line phase shifts than the one shown. The asymptotic limit is given by

$$t_g \Delta\omega \le 0.061\sqrt{A_{MAX-dB}}\,, \tag{4.14}$$

and it is smaller than the limit given by (4.12). Therefore, the optimally engineered linear and causal medium with a linear phase response around the center frequency and a reciprocal ($1/\omega$) phase decay at high frequencies, indeed has the highest asymptotic NGD limit given by (4.12), compared to all considered media.

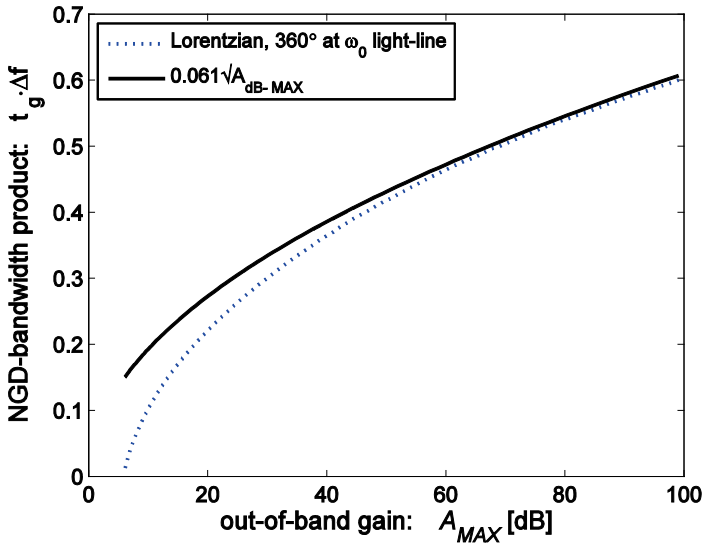

Figure 4-10: Center frequency NGD-bandwidth product as a function of out-of-band gain A_{MAX}, for a Lorentzian medium with δ=0.05ω_0, and medium length corresponding to a 360° light-line phase at ω_0.

4.4 Chapter Conclusion

In this chapter, an asymptotic NGD-bandwidth limit as a function of maximum out-of-band gain was derived, for an optimally engineered linear causal medium. Several approximation functions of the phase response of an arbitrary linear causal medium were examined, and their corresponding amplitude responses were derived, satisfying Kramers-Kronig relations. The optimal phase response function was identified, comprised of a linear part around the center frequency, and reciprocal decay at high frequencies. The corresponding causal amplitude responses were analytically obtained in each case.

It was shown that there is a trade-off between the maximum NGD value within a specified bandwidth on one hand, and the undesirable maximum out-of-band gain in the amplitude response on the other. Moreover, an upper limit for NGD-bandwidth product

was shown to be an asymptotic square root function of a logarithm of the maximum out-of-band gain. Alternatively, it can be said that the out-of-band gain and therefore transient response amplitude of finite-duration signals increase exponentially with the square of the achieved NGD. The obtained asymptotic NGD limit was shown to apply to a distributed gain-compensated NGD medium comprised of ideally matched high-pass filters, as well as to a Lorentzian dielectric model medium.

It was shown that the NGD-bandwidth product as a function of the maximum out-of-band gain has an upper limit given by expression (4.12) for an optimally engineered linear and causal medium. The motivation for the establishment of such a limit was to quantify how far the NGD-bandwidth product can be pushed in physically realizable media, and not to provide a guideline for synthesizing such a medium. However, since the analytical expression for the transfer function of the optimal medium is known, numerical methods can be employed to approximate it with a rational function of polynomials. The poles and zeros of the approximated transfer function can then be determined, which opens the possibility of synthesis via the use of cascaded electrical circuit elements.

5. Transient Analysis of NGD Circuits

In previous chapters the NGD phenomenon has been studied in the frequency domain, and its time-domain interpretation was demonstrated on selected steady-state waveforms. However, achieving an NGD effect for a steady-state waveform which has been turned on at a point far back in time has little practical importance since the steady-state part of the waveform does not carry any new information compared with the early waveform part just after the "turn on" point. Waveforms used in information transfer have defined "turn on" and "turn off" points in time and can therefore cause transients as they propagate through the information channel. As mentioned in Chapter 2, one of analytically simplest such waveforms is a semi-infinite (or step-modulated) sinusoid, and is commonly used in transient analysis of a medium [1] to determine the early part of the output response. This waveform will be used in this chapter to determine transient responses of single-stage resonator-based and high-pass filter based NGD circuits analytically, while transient responses of multi-stage and distributed NGD circuits will be determined numerically.

A correlation between the frequency-domain out-of-band gain and the transient amplitude will be demonstrated, which will give rise to a time-domain interpretation of the NGD asymptotic limits derived in Chapter 2. The trade-off between the NGD and the transient amplitude will also be demonstrated on an example where a maximum allowable transient magnitude is predefined, which then translates into a trade-off between the NGD and the waveform temporal duration between the "turn on/off" points.

5.1 Single-stage Resonator-based NGD Circuit Transient Response

To facilitate the transient analysis for resonator-based NGD circuits, the transmission coefficient expression (3.4) of a generic single-stage circuit with neglected physical length can be rewritten in the canonical form as

$$S_{21} = A\left[\frac{(\omega-\omega_{z1})(\omega-\omega_{z2})}{(\omega-\omega_{p1})(\omega-\omega_{p2})}\right], \tag{5.1a}$$

$$\omega_{z1,2} = \frac{\omega_0}{2Q}\left[j \pm \sqrt{4Q^2-1}\right], \tag{5.1b}$$

$$\omega_{p1,2} = \frac{\omega_0}{2Q} A\left[j \pm \sqrt{\frac{4Q^2}{A^2}-1}\right]. \tag{5.1c}$$

The zeros of the transfer function are a complex pair in the frequency domain, and only depend on Q and ω_0 (5.1b). On the other hand, the transfer function poles are dependent on the out-of-band gain, A, as well.

For values $A<2Q$, the poles can be visualized as lying on the $|\omega|=\omega_0$ circle in a 2-D complex plane, as depicted in Fig. 5-1. The zeros will also be on this circle, but closer to the real-ω axis. It will be shown later that when the poles are in this region the transients' initial values are lower but they also decay slower. For $A=2Q=A_{cr}$, the out-of-band gain reaches a critical value and the two poles become a single 2nd order pole at $\omega_p=j\omega_0$ (critically damped case), which yields a single, purely exponential decaying transient.

Finally, $A>2Q$ values yield two purely imaginary poles, with their magnitude product $|\omega_{p1}||\omega_{p2}|=\omega_0^2$. These poles yield two exponentially decaying transients, one with large magnitude and fast decay and the other one with smaller magnitude and slower decay.

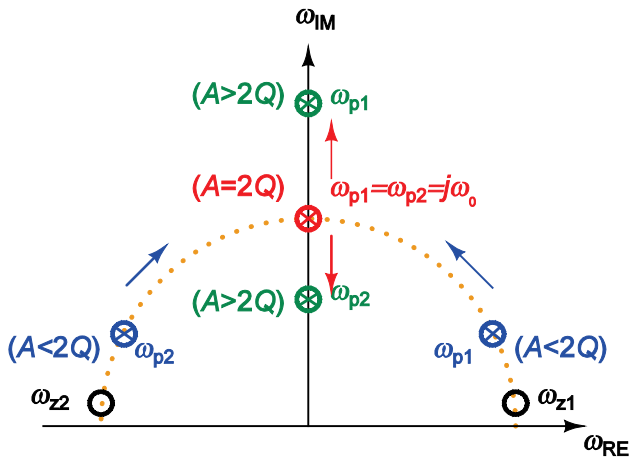

Figure 5-1: Transfer function zeros, O, and poles, X, in the complex plane, for different out-of-band gain $A<A_{cr}$, $A=A_{cr}$, and $A>A_{cr}$, with $A_{cr}=2Q$.

For a trivial case in (5.1c) when $A=1$ (the resonator L and C are removed and only resistor R remains), the poles will coincide with zeros and therefore cancel each other in (5.1a), resulting in a constant, frequency-independent transfer function with no NGD effect.

Now the output response of a single-stage resonator-based generic NGD circuit can be determined for these particular three cases (two complex poles, a single 2nd order purely imaginary pole, or two purely imaginary poles) when a step-modulated sinusoidal input with frequency ω_s is applied. According to (2.12) and (2.15), the input waveform and the medium's output response are, respectively, given by

$$u_{IN}(t)=\begin{cases}0, & t<0\\ \sin(\omega_s t), & t\geq 0\end{cases}, \tag{5.2}$$

$$u_{OUT}(t)=\frac{1}{2\pi}\int_{-\infty}^{\infty}\frac{-\omega_s}{(\omega-\omega_s)(\omega+\omega_s)}A\frac{(\omega-\omega_{z1})(\omega-\omega_{z2})}{(\omega-\omega_{p1})(\omega-\omega_{p2})}e^{j\omega\cdot t}d\omega. \tag{5.3}$$

The output waveform is given by the inverse Fourier integral (5.3) and in this case can be obtained by applying the Cauchy Residue Theorem. The output waveform consists of two main components, a steady-state part, $u_{STE}(t)$, due to the contribution to integral (5.3) from the signal poles, and a transient part, $u_{TR}(t)$, due to the contribution from the medium poles. Therefore, the output waveform can be written as

$$u_{OUT}(t)=u_{STE}(t)+u_{TR}(t). \tag{5.4}$$

The output response to excitation given by (5.2) will be equal to zero for times $t<0$ for any causal medium as discussed in Section 2.1. For all 3 cases depicted in Fig. 5-1, the steady-state part can be determined by the residues at the two signal poles, as given by (2.14a). Due to the symmetry of signal pole locations, the two residues will have equal real parts and their imaginary parts will cancel. The steady-state part of the output response can therefore be written as

$$u_{STE}(t)=A\cdot\mathrm{Re}\left\{-j\frac{(\omega_s-\omega_{z1})(\omega_s-\omega_{z2})}{(\omega_s-\omega_{p1})(\omega_s-\omega_{p2})}e^{j\omega_s t}\right\}=\left|S_{21}(\omega_s)\right|\sin\left(\omega_s t+\phi_{21}(\omega_s)\right), \tag{5.5}$$

for times $t>0$, and zero otherwise. As evident from (5.5), the steady-state part of the output response is a sinusoid with the same frequency ω_s, whose magnitude and phase are modified by the medium's transmission coefficient value at that frequency, as expected. For example, if $\omega_s=\omega_0$, then the transmission coefficient is $S_{21}(\omega_0)=1$, at that frequency, and the steady-state output signal is equal to the input signal.

The transient parts will be different for the 3 cases of the medium's pole locations (two complex poles, a single 2nd order purely imaginary pole at $\omega_p=j\omega_0$, and two purely imaginary poles), which can, respectively, be evaluated as

$$u_{TR1}(t)=A\cdot\mathrm{Re}\left\{-2j\omega_s\frac{1}{\omega_{p1}^2-\omega_s^2}\frac{(\omega_{p1}-\omega_{z1})(\omega_{p1}-\omega_{z2})}{\omega_{p1}-\omega_{p2}}e^{j\omega_{p1}t}\right\}, \tag{5.6a}$$

$$u_{TR2}(t)=\oint\frac{f(\omega)}{(\omega-\omega_p)^2}d\omega=j2\pi f'(\omega_p)=2\omega_0\omega_s\frac{A-1}{\omega_0^2+\omega_s^2}\left(\frac{\omega_0^2-\omega_s^2}{\omega_0^2+\omega_s^2}+\omega_0 t\right)e^{-\omega_0 t}, \tag{5.6b}$$

where $f(\omega)=-\dfrac{A\omega_s}{2\pi}\dfrac{(\omega-\omega_{z1})(\omega-\omega_{z2})}{(\omega-\omega_s)(\omega+\omega_s)}e^{j\omega\cdot t}$,

$$u_{TR3}(t)=\frac{j\omega_s A}{\omega_{p1}-\omega_{p2}}\left[\frac{(\omega_{p2}-\omega_{z1})(\omega_{p2}-\omega_{z2})}{\omega_{p2}^2-\omega_s^2}e^{j\omega_{p2}t}-\frac{(\omega_{p1}-\omega_{z1})(\omega_{p1}-\omega_{z2})}{\omega_{p1}^2-\omega_s^2}e^{j\omega_{p1}t}\right]. \tag{5.6c}$$

All (5.6) expressions are purely real functions of time. Further, it can be shown that at time $t=0$, they are all equal in magnitude and opposite in sign to the steady-state part

given by (5.5), so the total output signal is equal to zero at this instance just as the input signal is. This result is expected due to causality.

For $\omega_s=\omega_0$, expressions (5.6) become substantially simplified so the total output signal for the three cases reduces to

$$u_{OUT1}(t)=\sin(\omega_0 t)+e^{-A\frac{\omega_0}{2Q}t}\left((A-1)\Big/\sqrt{1-\frac{A^2}{4Q^2}}\right)\sin\left(\omega_0 t\sqrt{1-\frac{A^2}{4Q^2}}\right), \qquad (5.7a)$$

$$u_{OUT2}(t)=\sin(\omega_0 t)+\omega_0 t(A-1)e^{-\omega_0 t}\ , \qquad (5.7b)$$

$$u_{OUT3}(t)=\sin(\omega_0 t)+\left(\frac{A-1}{2}\Big/\sqrt{\frac{A^2}{4Q^2}-1}\right)\left(e^{-A\frac{\omega_0}{2Q}\left(1-\sqrt{1-\frac{4Q^2}{A^2}}\right)t}-e^{-A\frac{\omega_0}{2Q}\left(1+\sqrt{1-\frac{4Q^2}{A^2}}\right)t}\right). \qquad (5.7c)$$

The transient output signals, as well as total output signals are shown in Fig. 5-2 and Fig. 5-3, respectively, for the three pole location cases. As expected, the steady-state parts of the output responses are the same in magnitude and phase as the input, since the transfer function value at the resonance is $S_{21}(\omega_0)=1$. Furthermore, at $t=0$, the steady-state part and all of the three transients parts are equal to zero and therefore the total output signals are also equal to zero (causality is satisfied).

As evident from Fig. 5-2, the transient for the case of two complex poles (a lower value of the out-of-band gain, $A=0.5A_{cr}$) is smaller in magnitude (the medium poles are close to zeros, Fig. 5-1), but it also decays slower (poles are close to real-ω axis).

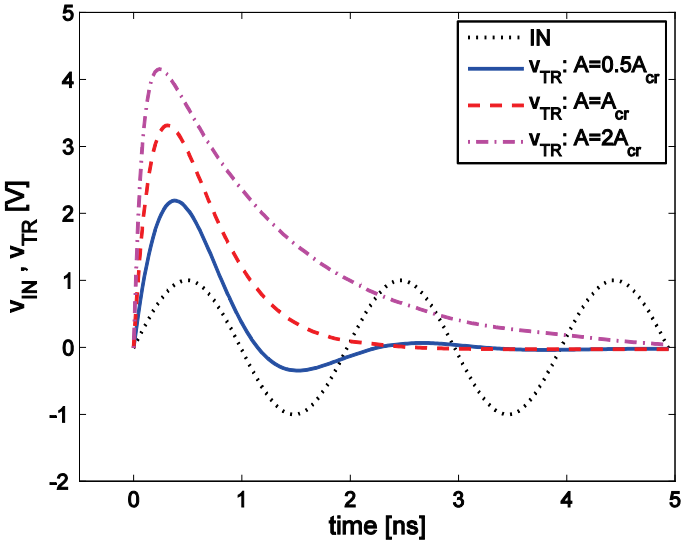

Figure 5-2: Transient parts of the output responses for $\omega_s=\omega_0$, and $Q=5$, $A=0.5A_{cr}$, $A=A_{cr}$, and $A=2A_{cr}$.

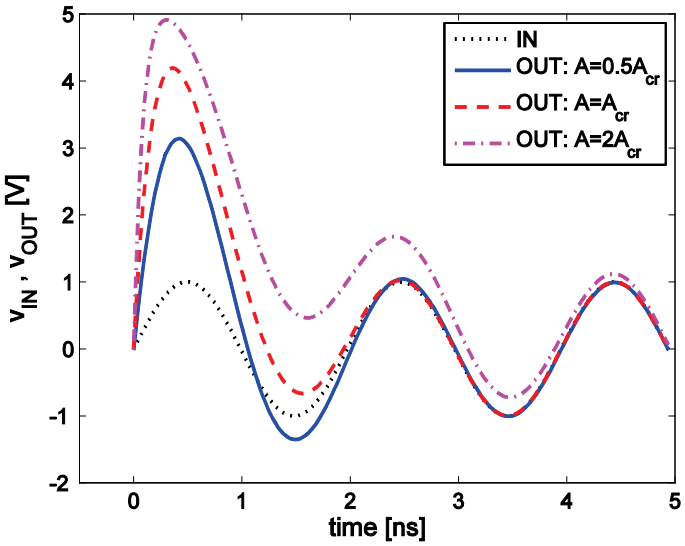

Figure 5-3: Total output responses for $\omega_s=\omega_0$, and $Q=5$, $A=0.5A_{cr}$, $A=A_{cr}$, and $A=2A_{cr}$.

On the other hand, the transient for the case of a single purely imaginary 2nd order pole ($A=A_{cr}$) is larger in magnitude but it also decays faster, which can be explained following the same argument of the pole position relative to the zeros and to the real-ω axis. Finally, the case with two purely imaginary poles ($A=2A_{cr}$) is the least desired since it has

a large magnitude (due to one of the poles being far away from zeros, Fig. 5-1) and also a slower decay (the other pole is closer to real-ω axis).

In order to demonstrate an analytically simple NGD example in the time domain, the single-stage circuit response to a signal obtained by an amplitude modulation of a high-frequency sinusoidal carrier by a low-frequency sinusoidal waveform can be examined. The input signal is given by

$$u_{IN}(t)=\frac{\cos(\omega_{lo}t)-\cos(\omega_{hi}t)}{2}=\sin\left(\frac{\Delta\omega}{2}t\right)\sin\left(\frac{\omega_{hi}+\omega_{lo}}{2}t\right)\approx\sin\left(\frac{\Delta\omega}{2}t\right)\sin(\omega_0 t), \quad (5.8)$$

for times $t>0$, and zero otherwise, where ω_{lo} and ω_{hi} are the lower and upper band edge frequencies, respectively. The "envelope" (or modulation) part of the input signal is a slow varying sinusoidal waveform with a frequency given by $\Delta\omega/2$, while the carrier is a sinusoid with frequency ω_0, as noted from (5.8). Alternatively, this input signal can be thought of as a linear combination of two cosine waveforms with their respective frequencies being the lower and the upper band edge frequency. A step-modulated cosine function and the single-stage NGD circuit's response to it are, respectively, given by

$$u_{IN-COS}(t)=\begin{cases}0, & t<0\\ \cos(\omega_s t), & t\geq 0\end{cases}, \quad (5.9a)$$

$$u_{OUT-COS}(t)=\frac{1}{2\pi}\int_{-\infty}^{\infty}\frac{-j\omega}{(\omega-\omega_s)(\omega+\omega_s)}A\frac{(\omega-\omega_{z1})(\omega-\omega_{z2})}{(\omega-\omega_{p1})(\omega-\omega_{p2})}e^{j\omega\cdot t}d\omega. \quad (5.9b)$$

Applying (5.9b) to the linear combination of two cosine waveforms in (5.8) yields the circuit's response to the described modulated waveform, as shown in Fig. 5-4. The chosen out-of-band gain of the circuit was A=15, the applied signal carrier frequency was f_0=500 MHz and the "envelope" waveform frequency was Δf=100 MHz. The frequency of the actual sinusoidal modulation according to (5.8) is $\Delta f/2$, but that includes the change of sign of the carrier phase at $2/\Delta f$ time intervals. However, considering the "envelope" part only of the signal, it repeats after every $1/\Delta f$ time interval, or 10 ns in the chosen case as shown in Fig. 5-4.

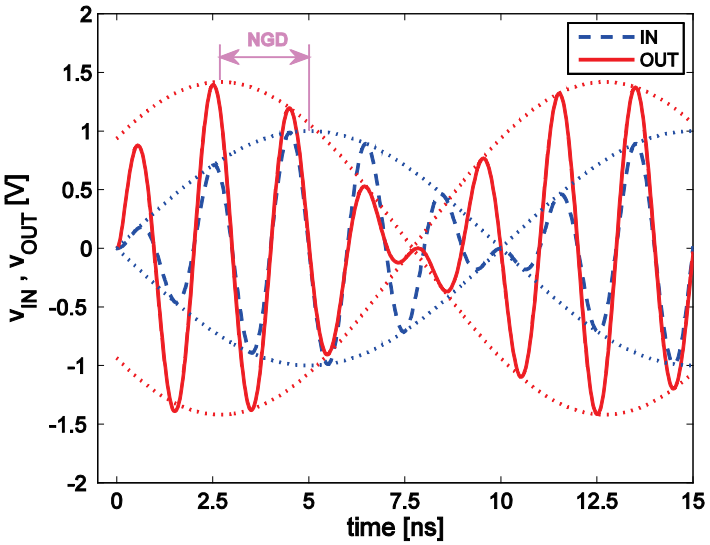

Figure 5-4: Total output response of a single-stage NGD circuit with A=15, to a step-modulated sinusoidal modulated input with f_0=500 MHz and Δf=100 MHz.

Further, Fig. 5-5 shows only the transient part of the output response, which has a relatively low amplitude, and short settling time. The steady-state NGD, obtained from the time shift between the output and input signal envelopes, is about 23% of the modulating "envelope" width (2.3 ns of $1/\Delta f$=10 ns).

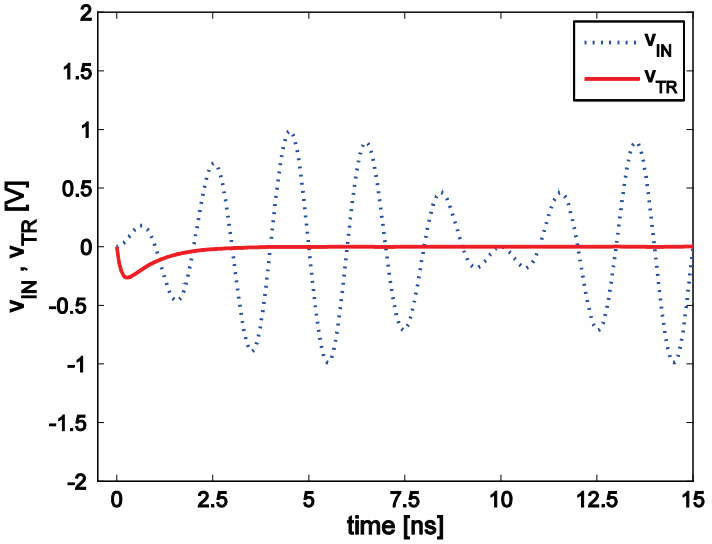

Figure 5-5: Transient response of a single-stage NGD circuit with A=15, to a step-modulated sinusoidal modulated input with f_0=500 MHz and Δf=100 MHz.

The estimated value for NGD at the center frequency is NGD_{MAX}=2.97 ns, according to (3.7). Since the applied signal in our case is comprised of two single-frequency components which are at band edge frequencies, not at the center frequency, the observed NGD is considerably lower than the limit given by (3.7). Therefore, rather than considering the maximum phase characteristic slope (NGD) at the center frequency, the average phase slope over the bandwidth should be considered in this particular case. The bandwidth average NGD can be shown to be smaller than the center frequency NGD by a factor of $4/\pi$, which brings it down to NGD_{AVE}=2.33 ns, and it is in a good agreement with the value observed in Fig. 5-4.

For waveforms other than step-modulated sinusoidal signals, it could be very difficult, or in many cases impossible to find the exact analytical output responses of NGD circuits. In such cases numerical techniques can be employed. First, the frequency spectrum of the applied signal can be obtained by numerically evaluating the corresponding Fourier integral, and then the output response can be obtained by

evaluating the corresponding inverse Fourier integral. Numerically solved examples to follow in this chapter were all obtained through the "Matlab" software application. For example, the response of a single-stage NGD circuit with an out-of-band gain of A=20 to a Gaussian modulated signal with f_0=500 MHz and a temporal standard deviation of σ_t=10 ns was numerically evaluated and shown in Fig 5-6. The signal was turned-on/off at instances $3\sigma_t$ away from the instance of the signal peak value.

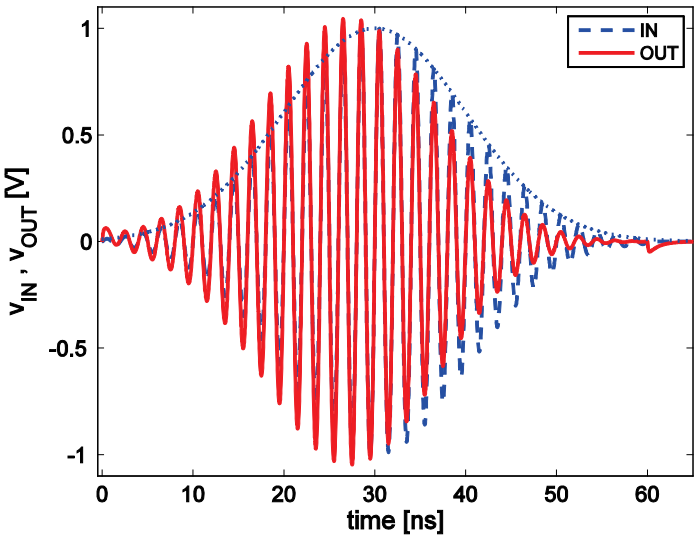

Figure 5-6: Response of a single-stage circuit with A=20 and a Gaussian modulated input with f_0=500 MHz and σ_t=10 ns.

As expected, an NGD effect is observed, and the response signal envelope is advanced in time. The transient part of the signal is relatively small compared to the signal peak value in this case, and it is shown in Fig. 5-7. Also shown in Fig. 5-7 is the circuit's transient-only response to a step-modulated sinusoidal input. The sinusoidal input amplitude is constant and equal to the value of the Gaussian envelope value at the "turn on" time. It is evident from Fig. 5-7 that the transient responses for the two signals match very closely,

which emphasizes the usefulness of studying transient responses to step-modulated sinusoidal signals, which are more suitable for analytical evaluation.

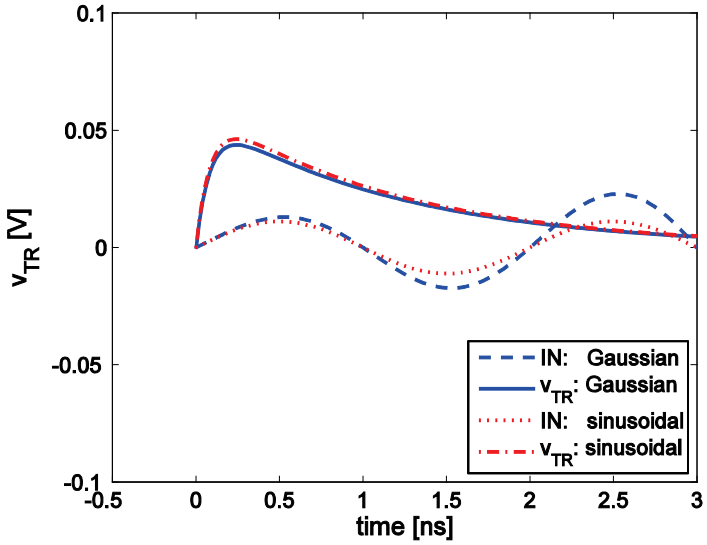

Figure 5-7: Transient response of a single-stage circuit with A_{tot}=20 and a Gaussian modulated input with f_0=500 MHz and σ_t=10 ns, turned on $3\sigma_t$ away from the signal peak.

5.2 Multi-stage NGD Circuit Transient Response

As demonstrated for a single-stage resonator-based NGD circuit in Fig. 5-2, increasing the out-of-band gain past the critically damped value results in large transients with slow settling time. For an N-stage circuit, the condition for the critically damped case can be obtained by substituting $A_{tot}=A^N=(2Q)^N$ into (3.42) and solving for Q, which yields

$$Q_{cr} = \frac{1}{2}\sqrt{4Q_{tot}^2(2^{1/N}-1)+2^{1/N}}\ . \tag{5.10a}$$

Now the overall out-of-band gain can be found for the critically damped case of an N-stage circuit as

$$A_{tot-cr} = A^N = (2Q)^N = \left(4Q_{tot}^2\left(2^{1/N}-1\right)+2^{1/N}\right)^{N/2}, \tag{5.10b}$$

as well as the NGD-bandwidth product in this case, by substituting (5.10b) into (3.45), which yields

$$NGD_{MAX-cr}\Delta f = \frac{1}{\pi} N \frac{1}{2Q_{tot}}\left(\sqrt{4Q_{tot}^2\left(2^{1/N}-1\right)+2^{1/N}}-1\right). \tag{5.10c}$$

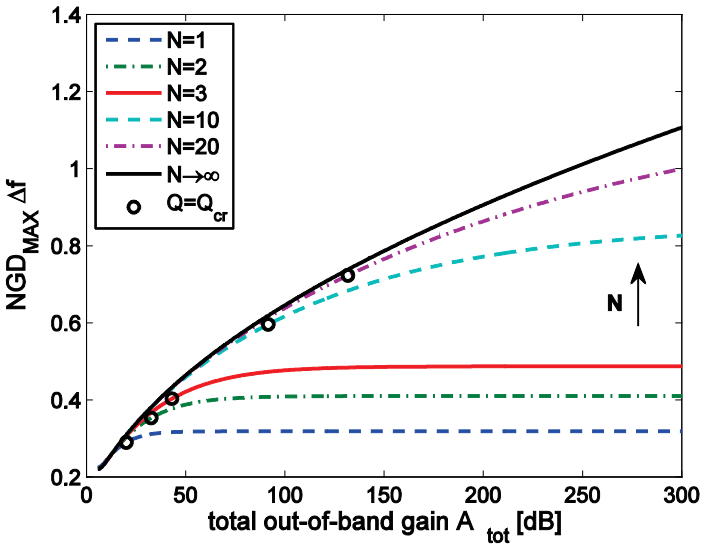

Figure 5-8: NGD vs. out-of-band gain for multi-stage NGD circuits, including critically-damped case points.

Therefore, a critically damped resonator-based NGD circuit with a given number of stages, N, and an overall Q-factor, Q_{tot}, will have a uniquely defined overall out-of-band gain and NGD-bandwidth product given by (5.10b) and (5.10c), respectively. The NGD-

bandwidth product and out-of-band gain discrete values associated with selected critically damped cases are shown in Fig. 5-8, along with the continuous curves previously shown in Fig 3-33. As the number of stages approaches infinity, limits of expressions (5.10) can be found as

$$\lim_{N\to\infty} Q_{cr} = \frac{1}{2}, \tag{5.11a}$$

$$\lim_{N\to\infty} A_{tot-cr} = 2^{\frac{4Q_{tot}^2+1}{2}}, \tag{5.11b}$$

$$\lim_{N\to\infty}\left(NGD_{MAX-cr}\Delta f\right) = \frac{1}{\pi}(\ln 2)\left(Q_{tot} + \frac{1}{4Q_{tot}}\right). \tag{5.11c}$$

For example, for Q_{tot}=5, the critically damped, infinitely distributed circuit would have A_{tot}≈304 dB, and $NGD_{MAX}\cdot\Delta f$≈1.1. By employing expressions (5.10) and (5.11), operating point of any particular N-stage resonator-based NGD circuit can be determined in regards to the critically damped case.

The output time domain response of a two-stage resonator-based NGD circuit, to a step-modulated sinusoid excitation of frequency ω_s can be analytically obtained by solving

$$u_{2OUT}(t) = \frac{1}{2\pi}A^2\int_{-\infty}^{\infty}\frac{-\omega_s}{(\omega-\omega_s)(\omega+\omega_s)}\frac{(\omega-\omega_{z1})^2(\omega-\omega_{z2})^2}{(\omega-\omega_{p1})^2(\omega-\omega_{p2})^2}e^{j\omega\cdot t}d\omega. \tag{5.12}$$

Due to the 2nd order poles, the residue evaluation for the transient part of the output signal requires tedious first derivative evaluations similar to (5.6b), yielding a somewhat longer explicit solution to (5.12).

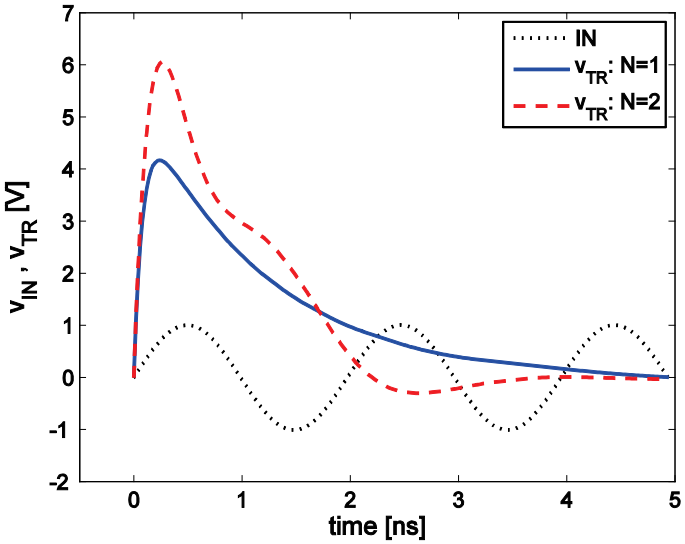

Figure 5-9: Transient signals for single-stage and two-stage circuits with A_{tot}=15 and $\omega_s=\omega_0$.

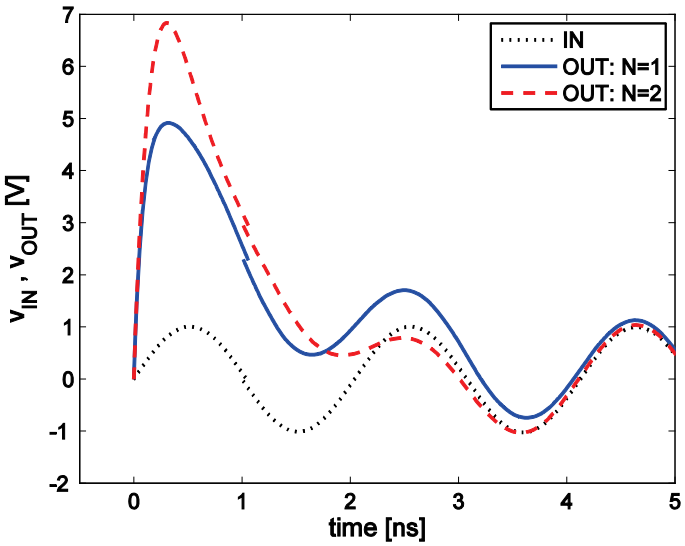

Figure 5-10: Total output signals, for single-stage and two-stage circuits A_{tot}=15 and $\omega_s=\omega_0$.

The solution expression is omitted from this thesis due to its length, but it was used for generating plots in Figs. 5-9 and 5-10 which, respectively, show the output signal transients and the total output signals for the single-stage and two-stage circuits. The transient for the single-stage circuit has a smaller amplitude and also appears to settle faster, as evident from Fig. 5-9, even though the same out-of-band gain value (A_{tot}=15) is chosen for both circuits. Further, transient responses were numerically evaluated for several cases having different numbers of stages, as well as different overall out-of-band gain values. Transient amplitudes were recorded for each simulated case and the results are shown in Fig. 5-11.

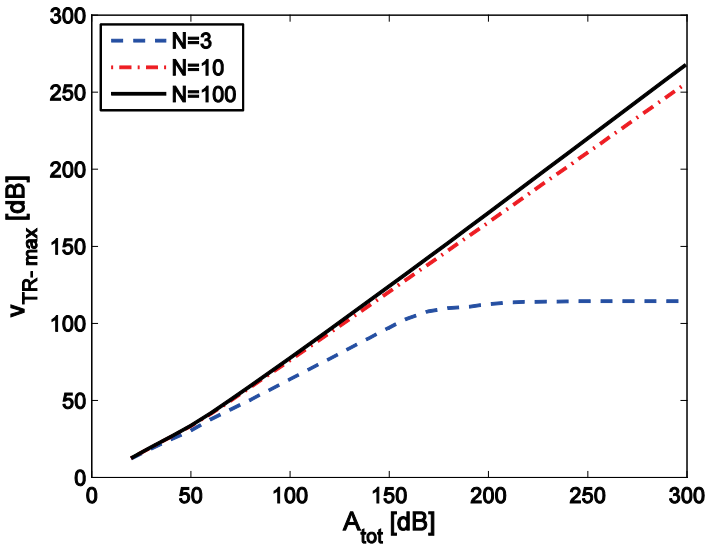

Figure 5-11: Transient amplitude vs. A_{tot} for a step-modulated sinusoidal input, and the number of stages N=3, N=10 and N=100.

The fact that circuits with larger number of stages yield larger transients, for the same given overall out-of-band gain, can be explained by Fig. 3-36a. There, the cases with a larger number of stages have a faster changing amplitude characteristic in the region just outside the bandwidth, which causes larger transients. However, these cases also exhibit a

larger NGD (Fig. 3-36b) and therefore an NGD to transient amplitude ratio is a more suitable quantity for comparing the performance of cases with different number of stages. The results of this analysis are depicted in Fig. 5-12, which demonstrates the preference of having a larger number of stages. The shape of the curves in Fig. 5-12 resemble closely the ones for NGD vs. out-of-band gain shown in Fig. 3-33, which is not surprising given the approximately linear relationship between the out-of-band gain and the transient amplitude response to the step-modulated sinusoidal excitation shown in Fig. 5-11. Therefore, an interpretation of the derived asymptotic NGD limits as a function of the frequency domain out-of-band gain has been demonstrated in the time domain.

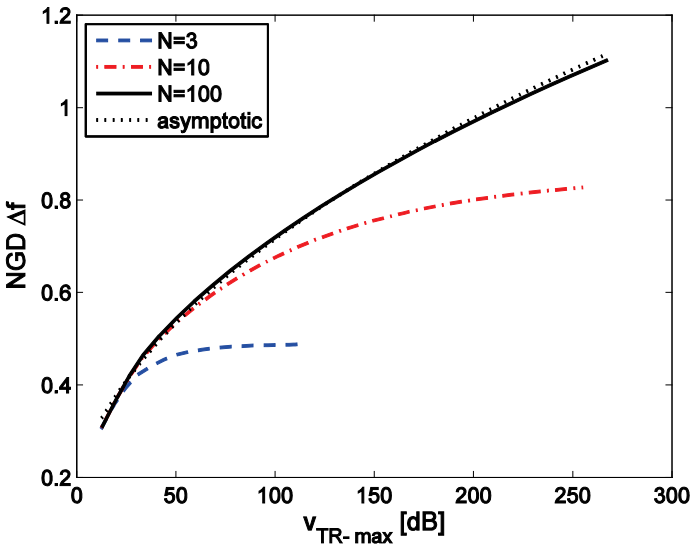

Figure 5-12: NGD-bandwidth product vs. transient amplitude for a step-modulated sinusoidal input, and the number of stages N=3, N=10 and N=100.

The preference for having a larger number of stages is also demonstrated using a Gaussian modulated signal example as shown in Fig. 5-13. Two cases were chosen, one with N=3 and the other with N=10 stages. The total out-of-band gains were adjusted for each case (A_{tot}=60 dB and A_{tot}=45.6 dB, respectively) to yield the same NGD=4.41 ns.

Temporal standard deviation of the Gaussian envelope was σ_t=5 ns and the signal was turned on/off at instances $3\sigma_t$ away from the peak.

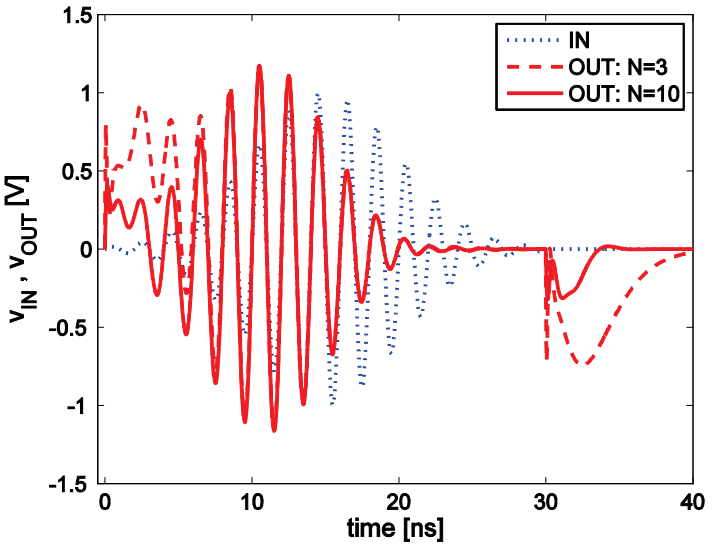

Figure 5-13: Output response to a Gaussian step-modulated sinusoidal signal, with σ_t=5 ns, $t_{on}=t_{peak}-3\sigma_t$, NGD=4.41 ns (NGD·$\Delta f$=0.441), N=3, A_{tot}=60 dB, v_{tr}=0.74, and N=10, A_{tot} =45.6 dB, v_{tr} =0.32.

Even though both cases yield the same NGD value, the case with larger number of stages has much smaller transients as evident from Fig. 5-13, and it is therefore preferred.

5.3 Pulse Duration Adjustment for Constant Transient Amplitude

According to expression (3.45) and as shown in Fig. 3-33, one might conclude that the output of a distributed NGD circuit could be negatively delayed to any desired value, by increasing out-of-band gain, A_{tot}. If the transients are ignored, the pulse may "seem" to be detectable before the input is observable. An example is shown in Fig. 5-14, where the

transient response of an infinitely distributed circuit, $N\rightarrow\infty$, with an out-of-band gain A_{tot}=230 dB is simulated using expression (3.53), for an applied Gaussian modulated signal with "turn on/off" relatively far away from its peak.

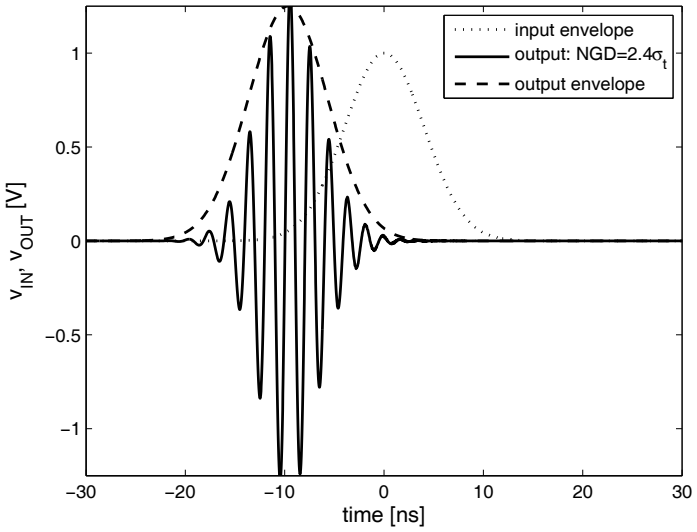

Figure 5-14: A Gaussian pulse modulated input signal and simulated output signal for infinitely distributed case ($N\rightarrow\infty$), with Q_{tot}=5, A_{tot}=230 dB, f_0=500 MHz and σ_t=4 ns. Turn-on/off times are chosen far away from the peak (±32 ns), yielding no visible transients.

However, as it has been demonstrated earlier in this chapter, waveforms with a defined "turn on" and "turn off" points in time cause transients as they propagate through NGD circuits. In the following examples a finite duration Gaussian-modulated sinusoidal signal will be considered with the turn-on/off times at the carrier zero-crossing (to ensure the lowest transient amplitude, since the "best case" scenario is of interest here, in terms of defining an upper limit of NGD vs. transient amplitude). The simulated response of an ideal single-stage resonator circuit, with Q=5 and A=10, to a signal comprised of a 500 MHz sinusoidal carrier modulated by a Gaussian pulse with σ_t=4 ns (92% of signal power is within Δf=100 MHz) is shown in Fig. 5-15.

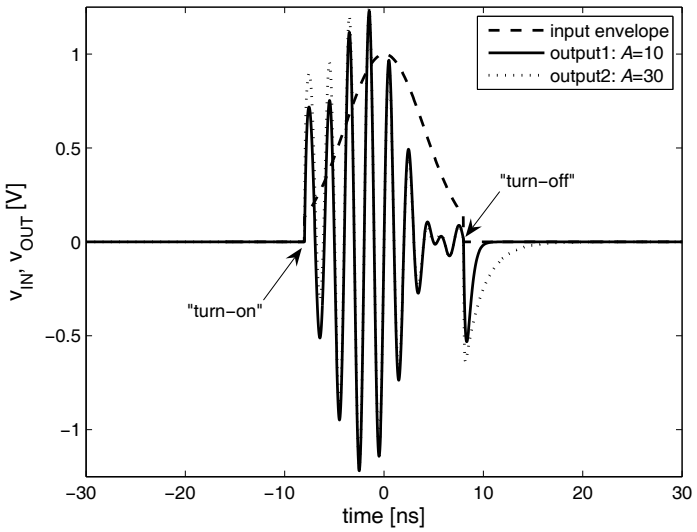

Figure 5-15: A Gaussian pulse modulated input signal and simulated output signals for an ideal single-stage circuit with Q_{tot}=5 and A =10 and A =30. Pulse turn-on and turn-off is at t=±2σ_t=±8 ns.

It was chosen that the input signal has defined turn-on (t=-2σ_t) and turn-off (t=2σ_t) times, at the carrier zero-crossing, yielding output transients at both ends of the pulse (at ±2σ_t the Gaussian pulse amplitude is at approximately 0.135 of the peak value). The NGD observed in the time domain is approximately 2.47 ns. The NGD at the resonance frequency for this circuit is 2.89 ns according to expression (3.45), which is close to the observed time-domain value. The transient amplitude for the single-stage A=10 case is 53% of the input signal peak level, as shown in Fig. 5-15, and begins to interfere with the output signal. Increasing A past this value increases the transient amplitude and the settling time significantly, while the increase in NGD is negligible, as shown in Fig. 5-15 for A=30.

To examine the transient interference with the modulated signal in multi-stage designs, three infinitely distributed NGD circuits were chosen with different total out-of-band gain values A_{tot}=17 dB, A_{tot}=51 dB, and A_{tot}=86 dB, respectively. In all cases Q_{tot}=5, so that a constant bandwidth was maintained.

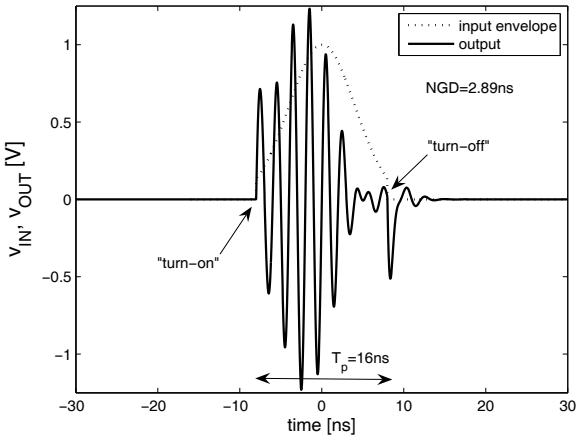

a)

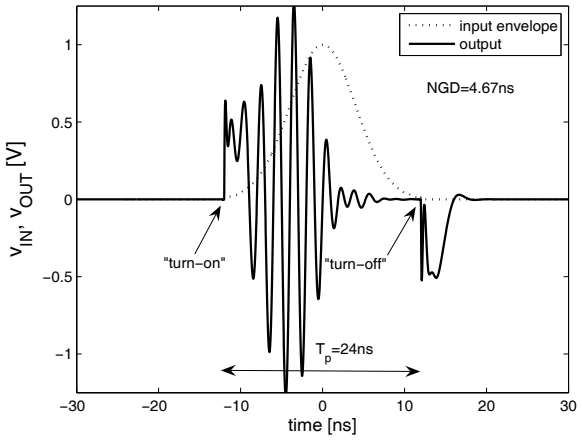

b)

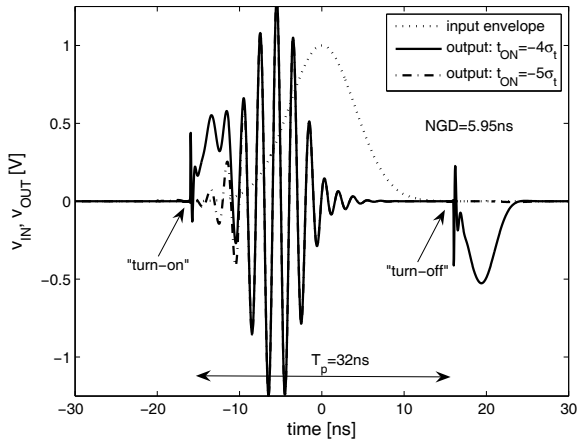

c)

Figure 5-16: A Gaussian pulse modulated input signal and simulated output signal for infinitely distributed case ($N\rightarrow\infty$), with Q_{tot}=5 and a) A_{tot}=17 dB, b) A_{tot}=51 dB, and c) A_{tot}=86 dB. Turn-on/off times are chosen to yield transient amplitude of $v_{TR}\approx 0.5V_{peak}$ in each case.

The three cases yield NGD values of 2.89 ns, 4.67 ns and 5.95 ns, respectively, using

expression (3.47). Figure 5-16 shows the transient responses for the three cases to a Gaussian modulated signal with σ_t=4 ns, 500 MHz carrier frequency, and different "turn on/off" times for each case. The transient amplitude is directly related to the out-of-band gain, A_{tot}, since a part of the frequency spectrum of a limited time-duration signal falls outside the bandwidth, and gets amplified. In Fig. 5-16 the turn-on/off times have been chosen so that transient amplitudes are equal (50% of the pulse peak value, which would be the typical choice for a decision circuit). In order to satisfy this condition, the turn-on/off times for the three cases are adjusted accordingly ($\pm 2\sigma_t$, $\pm 3\sigma_t$ and $\pm 4\sigma_t$, respectively), which yield input signal magnitudes at the turn-on/off times of e^{-2}, $e^{-4.5}$ and e^{-8} of the peak level, respectively.

In order to keep the transient amplitudes constant in Fig. 5-16, it is required that the "turn on/off" signal levels decrease exponentially with the square of NGD (this follows from expression 3-47). For a Gaussian modulated signal in particular, with a temporal width from turn-on to turn-off points in time, T_p, the following can be written [60] for the transient amplitude

$$v_{TR} \propto A_{tot} v_{ON} \propto \exp\left(k_1 NGD^2\right) \times V_{MAX} \exp\left(-k_2 T_p^2\right), \tag{5.13}$$

where k_1 and k_2 are proportionality constants and v_{ON} is the Gaussian pulse value at the turn-on time. For a constant transient amplitude to the Gaussian peak ratio, v_{TR}/V_{MAX}, it is required that

$$NGD \propto \sqrt{k_2 T_p^2 + \ln\left(\frac{v_{TR}}{V_{MAX}}\right)}. \tag{5.14}$$

For transient amplitudes on the order of the Gaussian signal peak, v_{TR}/V_{MAX}~1, expression (5.14) reduces to

$$\frac{NGD}{T_p} = a, \tag{5.15}$$

where a is a constant. For the specific cases shown in Fig. 5-16, the NGD-to-signal-duration ratio is a≈0.19. Thus, it can be concluded that even though it is possible to achieve an NGD-bandwidth product that increases with the number of stages and/or out-of-band gain, the final achievable NGD-to-signal-duration ratio will be constant for fixed transient amplitude. As discussed by several others [25,33], genuine information is conveyed by the points of non-analyticity in the waveform (such as "turn on/off" points), and these propagate luminally through a medium at the "front" velocity. Further, any attempt to create a finite-duration waveform and a channel medium that reshapes it to produce a negative group delay (in an attempt to speed up the propagation of certain features of the analytical part of the waveform, such as its peak), is thwarted by a corresponding increased transient.

5.4 Baseband NGD Circuit Transient Response

The single-stage baseband NGD circuit transmission coefficient given by (3.65), neglecting the physical delay, can be written in a canonical form as

$$S_{21}(\omega) = A\frac{(\omega-\omega_z)}{(\omega-\omega_p)}, \tag{5.16a}$$

where

$$\omega_z = j\frac{\Delta\omega}{2}, \qquad \omega_p = j\frac{\Delta\omega}{2}A. \tag{5.16b}$$

Comparing the obtained expression (5.16) to the corresponding one for resonator-based circuits given by (5.1), it can be noted that now there is only a single zero and a single pole in the complex frequency domain. They are both of the 1st order and purely imaginary. For a trivial case of A=1, the pole and the zero coincide and cancel each other, forming a constant with frequency response with no observed NGD. In Section 5.1, a step-modulated sinusoid excitation was used to study the single-stage resonator-based circuit's transient response, since most of the frequency spectrum of this signal falls within the circuit's bandwidth. For the single-stage baseband NGD circuit, however, the transient response to a step function will be derived, whose time domain waveform and the corresponding frequency spectrum (mostly concentrated within baseband frequencies) are given by

$$u_{IN}(t)=\begin{cases}0, & t<0\\ 1, & t\geq 0\end{cases}, \qquad U_{IN}(\omega)\approx\frac{1}{j\omega}. \tag{5.17}$$

The baseband NGD circuit's response is then given by

$$u_{OUT}(t)=\frac{1}{2\pi}\int_{-\infty}^{\infty}\frac{1}{j\omega}A\frac{(\omega-\omega_z)}{(\omega-\omega_p)}e^{j\omega\cdot t}d\omega, \tag{5.18}$$

which yields an output response comprised of a constant with time steady-state part and a decaying exponential transient part. The total output response in this case is shown in Fig. 5-17a for different values of the out-of-band gain A and given by

$$u_{OUT}(t)=1+(A-1)e^{-A\frac{\Delta\omega}{2}t}, \tag{5.19}$$

and equal to zero for $t<0$. As expected, the response transient amplitude increases proportionally to the out-of-band gain (the total output response at $t=0$ is $u_{OUT}(0)=A$, while the transient part alone is given by $u_{TR}(0)=A-1$.

The exact output response of a single-stage baseband circuit to a low-frequency step-modulated sinusoid can also be analytically determined. For example, a step-modulated sinusoid excitation having a frequency of exactly the baseband edge frequency, $\Delta\omega/2$, is given by

$$u_{IN2}(t)=\begin{cases}0, & t<0\\ \sin(\Delta\omega\cdot t/2), & t\geq 0\end{cases}. \tag{5.20}$$

The single-stage circuit response can now be determined by evaluating the inverse Fourier integral given by

$$u_{OUT2}(t)=\frac{1}{2\pi}\int_{-\infty}^{\infty}\frac{-\Delta\omega/2}{(\omega-\Delta\omega/2)(\omega+\Delta\omega/2)}A\frac{(\omega-\omega_z)}{(\omega-\omega_p)}e^{j\omega\cdot t}d\omega, \tag{5.21}$$

which yields a steady-state sinusoidal part of the same frequency and a decaying exponential transient part, as shown in Fig. 5-17b and given by

$$u_{OUT2}(t)=\frac{A\sqrt{2}}{\sqrt{A^2+1}}\sin\left(\frac{\Delta\omega}{2}t+\tan^{-1}(A)-\frac{\pi}{4}\right)-\left(\frac{A(A-1)}{A^2+1}\right)e^{-A\frac{\Delta\omega}{2}t}. \tag{5.22}$$

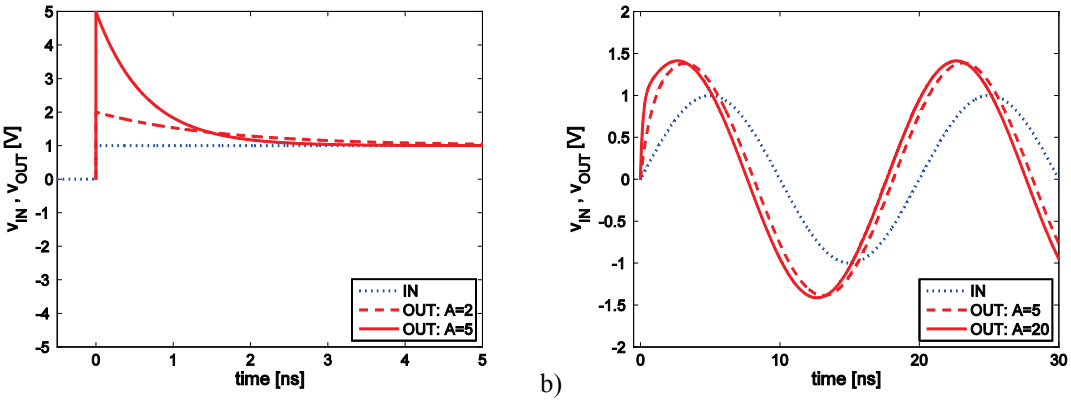

Figure 5-17: Single-stage baseband circuit response to a) step function and b) baseband frequency sinusoid.

The steady-state part of the response given by (5.22) has the form of the input sinusoidal function amplified in magnitude and advanced in time according to the transmission coefficient (5.16) value at the band edge frequency, $\omega=\Delta\omega/2$. For example, in an extreme case when $A\to\infty$, the steady-state sinusoidal part from (5.22) has a magnitude of exactly $\sqrt{2}$ (3 dB) and it is advanced in time exactly by $\pi/4$, as expected. In the other extreme case when $A=1$ the entire output response from (5.22) reduces to exactly the input waveform given by (5.20) with no amplification, time-shift or transients, as expected.

The difference between baseband and modulated-band (resonator-based) NGD circuit responses to correspondingly chosen inputs can now be checked. For example, a Gaussian modulated input was chosen for a resonator-based circuit, and it is "turned on/off" at carrier zero-crossing times which are three standard deviations away from the pulse peak. The corresponding input for the baseband circuit (with the same out-of-band gain as the resonator-based one) is comprised of the same Gaussian envelope pulse only without the carrier, so its frequency spectrum falls mostly within the baseband. The two circuit responses to their respective inputs are shown in Fig. 5-18a.

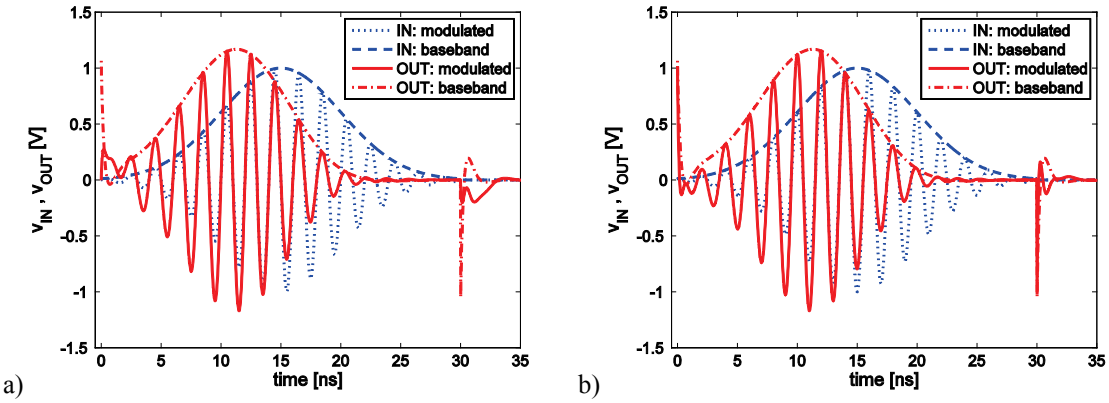

Figure 5-18: Gaussian vs. baseband, a) sine-modulated (carrier zero-crossing) and b) cosine modulated (carrier peak at "turn on/off").

As expected, the envelope of the modulated response steady-state part is in good agreement with the baseband response. However, the baseband response has much larger initial transients. The reason is that the input baseband Gaussian waveform suddenly jumps from zero to the small, but still a non-zero, pulse tail value at turn-on time while the modulated-band input starts exactly at zero due to carrier zero-crossing at that instance. A similar argument follows at the turn-off time. Intuitively, if the carrier waveform is shifted to have its peak values at "turn on/off times" (from a sine to a cosine function) an increase in the transient amplitude is expected, close to the one of the baseband case. Indeed, this effect is observed in Fig. 5-18b. Therefore, previously observed similarities between modulated-band and baseband NGD circuits in Chapter 3 are now confirmed and interpreted in the time domain as well.

5.5 Bandpass Filter Effect on NGD and Transients

In Section 3.3.2, the effects of adding a bandpass filter to resonator-based NGD circuits was examined. It was demonstrated that a bandpass filter results in lowering the achieved NGD but also lowers the out-of-band gain. For selected filter parameters (order of the filter and cut-off frequency points), the out-of-band gain can be reduced by a larger factor than the factor by which the NGD is reduced. Therefore, the overall NGD to out-of-band gain ratio can increase.

The same effect is demonstrated in the time domain, as shown in Figs. 5-19 and 5-20. A Gaussian modulated pulse, turned on/off at three standard deviations away from the pulse peak, was applied to a 100-stage resonator-based circuit with an out-of-band gain of

A_{tot}=49 dB. The simulated circuit's response is shown in Fig. 5-19, along with a response when a 5th order filter is applied. The transient amplitudes are considerably reduced while the reduction in the NGD is less pronounced.

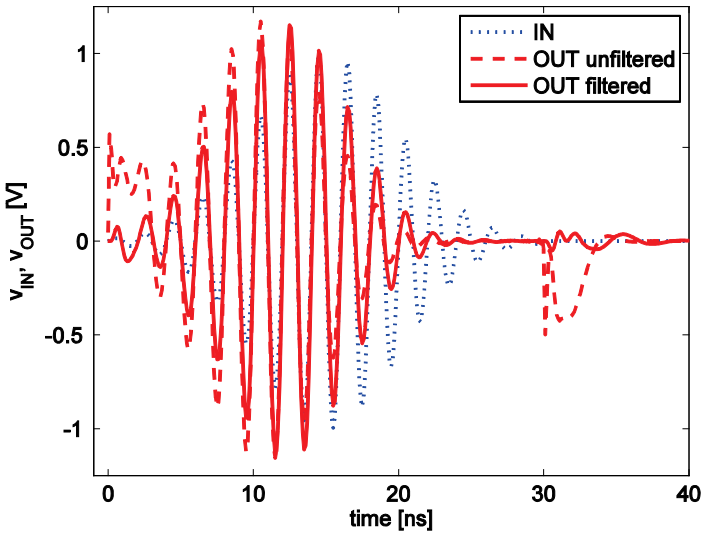

Figure 5-19: Unfiltered and 5th order filtered NGD circuit (A_{tot}=49 dB, N=100) response to a Gaussian modulated signal, σ_t=5 ns, t_{on}= t_{peak} -3σ_t.

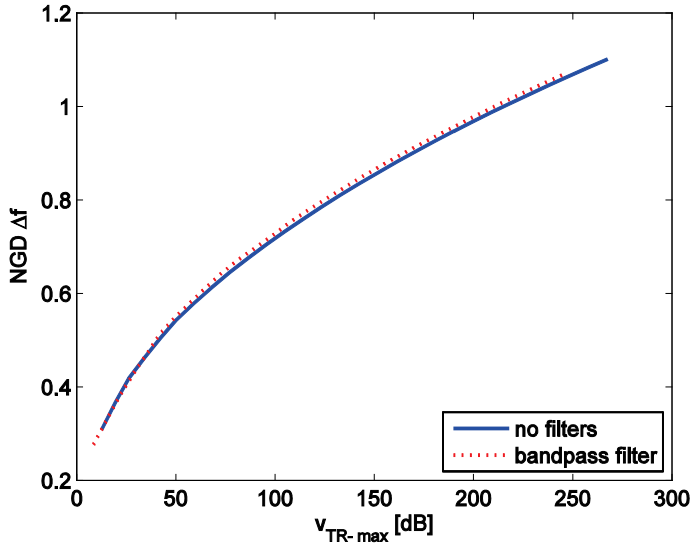

Figure 5-20: NGD vs. transient amplitude for a 1st order filtered and unfiltered response to a step-modulated sinusoidal signal, for an infinitely distributed resonator-based NGD circuit.

Finally, to examine the bandpass filter effect over a wide range of out-of-band gain values, and therefore transient amplitudes, the response of an infinitely distributed NGD circuit was simulated. The transient amplitudes and achieved NGD values for each simulated case were recorded and are shown in Fig. 5-20 for both the unfiltered circuit and the topology when a 1st order filter was cascaded. Similar to Fig. 3-38, a slight increase in the asymptotic limit of the achieved NGD was observed, demonstrating once again the connection between the out-of-band gain, and the transient amplitudes when finite duration waveforms are applied.

5.6 Measured Transients in a Resonator-based NGD Circuit

So far in this chapter all NGD circuits and the applied signals were assumed ideal, and the responses were either evaluated analytically, or in more complicated cases, numerically. In order to confirm some of the obtained results and conclusions, an experiment was set up as shown in Fig. 5-21.

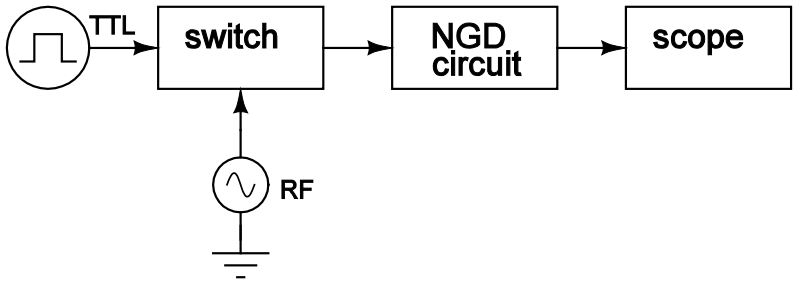

Figure 5-21: An experiment setup for a step-modulated sinusoidal excitation measurement.

A non-ideal step-modulated sinusoid input was produced by applying a 460 MHz

continuous wave to a Mini-Circuit ZASWA-2-50DR switch with a 4 ns rise-time, controlled by a square-wave signal, and then applying this waveform to the gain-compensated NGD circuit presented in Section 3.16. The measured input signal and the corresponding measured single-stage NGD circuit's transient response are shown in Fig. 5-22. The simulated time-domain response, obtained by Fourier analysis, and using the measured circuit frequency-domain transmission response is shown. The simulated response for the 4 ns-rise-time input is in close agreement with the measured response, demonstrating that the Fourier analysis of the known frequency responses yields accurate results in the time domain in this case. This fact can be used to obtain simulated responses for other input waveforms without actually applying them and expect the results to be representative.

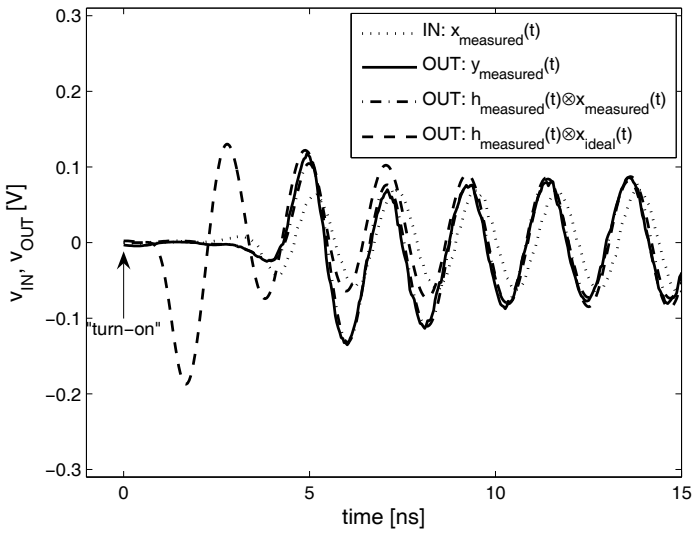

Figure 5-22: Single-stage NGD circuit measured and simulated responses to a step-modulated sinusoidal excitation. The circuit's impulse response $h_{measured}(t)$ used in simulated response is calculated from the circuit's measured frequency response.

The described approach was used to predict the circuit response to an ideal, zero rise-

time, step-modulated excitation (ideal switch) and is also shown in Fig. 5-22. The steady-state part of the simulated response matches well the measured one. Further, larger transient amplitude in the early part of the simulated response is now visible, which was suppressed in the measured response due to the rise-time of the non-ideal switch. Therefore, using the measured frequency response of the circuit, and simulating its response to an ideal step-modulated signal, brings us one step closer to the overall ideal responses presented earlier in this chapter.

Finally, the simulated response of the ideal circuit model to an ideal step-sinusoid is shown in Fig. 5-23, along with the simulated response of the actual circuit (from Fig. 5-22) to the same ideal excitation. Transients are larger in the ideal case, due to the ideal op-amp response at high frequencies (the absence of low-pass roll-off in the amplitude response).

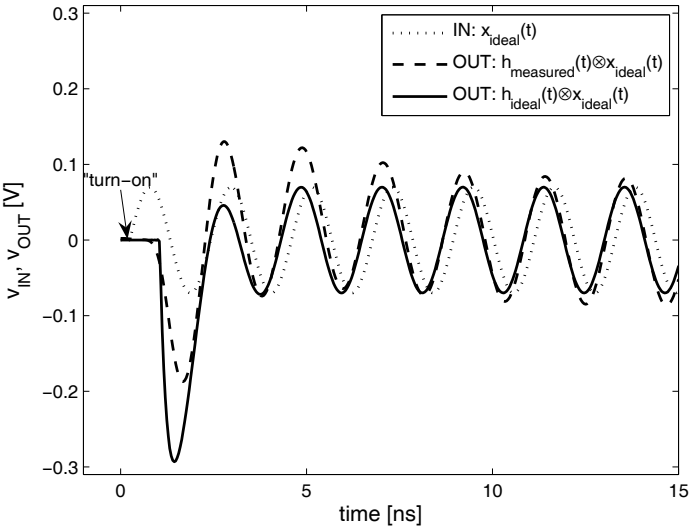

Figure 5-23: Single-stage NGD circuit simulated responses to an ideal step-modulated sinusoidal excitation. The circuit's impulse responses $h_{measured}(t)$ and $h_{ideal}(t)$ used in simulated responses are calculated from the circuit's measured and ideal frequency responses, respectively.

As expected, the ideal circuit model response to the ideal step-modulated excitation yields the largest transient amplitude, and shows a good match with the steady-state part of the measured response. The upper limits of NGD as a function of the transient amplitude, which were established from the previously presented analysis in this chapter, still hold for the measured circuit response. Due to the circuit's bandwidth limitations (a bandpass filter effect), the transients were considerable reduced, but the achieved NGD was reduced even more so. Furthermore, assuming that the NGD asymptotic limits for an optimally engineered causal medium derived in Chapter 4 apply, by the connection between the out-of-band gain and the transient amplitude demonstrated in this chapter, the limits derived in Chapter 4 can be extended to the transient response to step-modulated waveforms as well.

5.7 Chapter Conclusions

In conclusion, detailed transient analysis is performed on single-stage and multi-stage resonator-based and baseband NGD circuits, for several finite duration waveforms. The connection between the out-of-band gain from Chapter 4 and the transient amplitude has been demonstrated for both types of circuits. The derived asymptotic NGD limits as a function of the out-of-band gain have been extended to NGD limits as a function of the transient amplitude. It was shown that the limits have the same square root functional behavior and that distributed circuits (or the ones with larger number of stages, in general) yield larger NGD for a given transient amplitude, and thus are preferred.

The effect of the trade-off between an increase in NGD on one hand, and increased transients on the other hand, was demonstrated using a Gaussian modulated signal excitation. If the transient level is specified, increasing the NGD requires a linear overall increase in the pulse duration, therefore making the NGD-to-signal-duration ratio constant.

Finally, an experiment was set up to demonstrate the transient effects for a real circuit and compare the measured results to the derived ones. Good agreement was observed when circuit's and applied signal's non-idealities were taken into account and the overall derived NGD limits still hold.

In the next chapter, a bilateral gain compensated circuit which was designed and fabricated will be presented to demonstrate a novel application of NGD circuits as a part of the contribution resulting from the work completed in this thesis.

6. Bilateral Gain-Compensated NGD Circuit

Gain-compensated NGD circuits reported in literature can propagate signals only in a single direction, due to the unilateral nature of the employed active elements. In order to overcome this shortcoming a dual-amplifier NGD configuration shown in Fig. 6-1 is proposed, which supports a gain-compensated NGD propagation in both directions.

a)

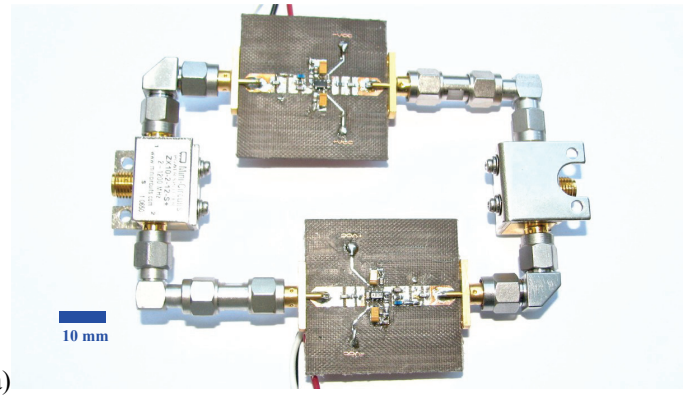

b)

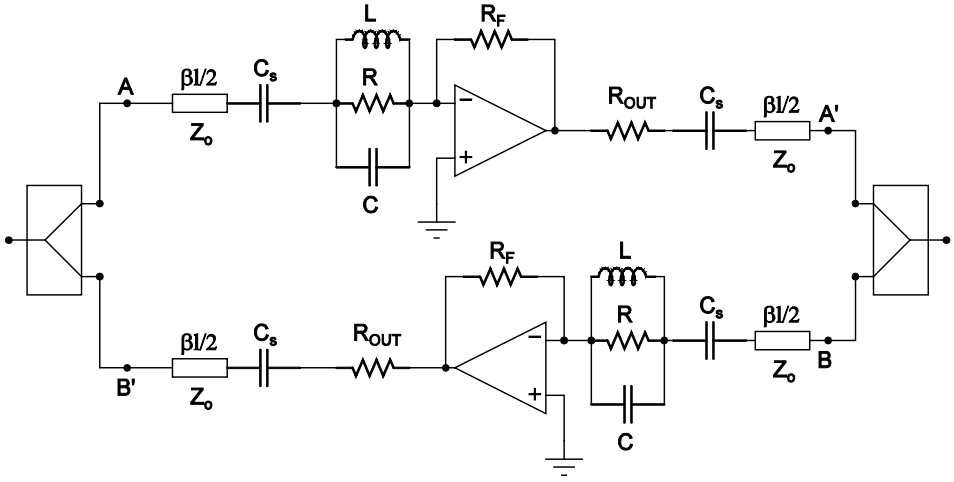

Figure 6-1: a) Fabricated single-stage, reciprocal gain-compensated NGD circuit and b) the equivalent circuit model.

Bilateral gain-compensated NGD propagation can be used to support both transmit and receive modes in numerous microwave applications, for instance, gain-compensated constant phase shifters, phased array antenna systems with a reduced beam-squint, antenna feeds which require a constant phase shift over a bandwidth such as a 90° feed for a circularly polarized antenna or a 180° feed (balun) for a dipole antenna, and others.

The proposed bilateral gain-compensated NGD circuit consists of two 3 dB power splitters with high isolation, and two amplifiers, one for each propagation direction [63]. Two National Semiconductor LMH6703 op-amps are used to produce the gain-compensated NGD. They operate in inverting configurations with *RLC* resonators embedded in their respective input branches. The transmission coefficient of the individual NGD circuits found in each branch of Fig. 6-1 (A-A' or B-B'), assuming op-amps with non-ideal gain factor K, and neglecting the DC blocking capacitors C_s, is derived as

$$S_{21\_AMP}(\omega) = -K\frac{R_F}{Z_0}\frac{1+jQ(\omega/\omega_0-\omega_0/\omega)}{2R/Z_0+jQ(\omega/\omega_0-\omega_0/\omega)}e^{-j\beta\cdot l}, \tag{6.1}$$

where $Q=R(C/L)^{1/2}$ is the chosen quality factor of the *RLC* resonators, $\omega_0=1/(LC)^{1/2}$ is the resonance frequency, and the $exp(-j\beta l)$ term accounts for the phase delay due to finite physical dimensions. The design values are: f_0=310 MHz, Q=5.5, Z_0=50 Ω, L=4.7 nH, C=56 pF, C_s=130 pF, R=51 Ω, R_F=510 Ω and R_{OUT}=50 Ω. The simulated (expression (6.1), with K=0.44 and the addition of DC block capacitors C_s) and measured *S*-parameters of a single-branch circuit (A-A') are shown in Fig. 6-2.

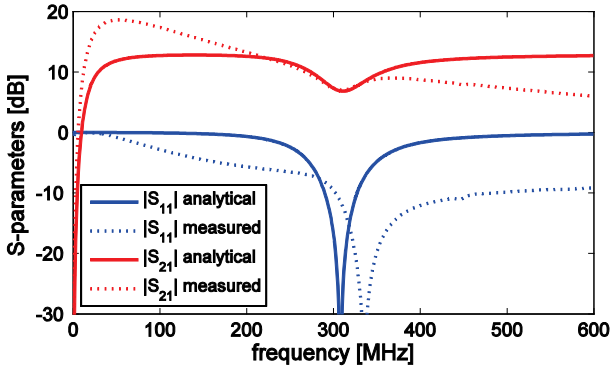

Figure 6-2: Measured and analytical (expression (6.1) with C_s) *S*-parameters of the single-branch (A-A') part of the circuit shown in Fig. 6-1.

The individual amplifiers are designed for a gain of 6 dB at the resonance frequency, in order to compensate for loss at the two splitters. The measured resonance frequency was 310 MHz while the amplifier gain at the resonance was 6.8 dB, which are in good agreement with the simulated values.

As discussed in Chapter 3, the transmission coefficient phase and the group delay can be expressed, respectively, as

$$\phi(\omega) = \arctan\left(\frac{\mathrm{Im}(S_{21})}{\mathrm{Re}(S_{21})}\right) \text{ and } \tau_g(\omega) = -\frac{d\phi(\omega)}{d\omega}. \tag{6.2}$$

The minimum group delay (largest NGD, if it becomes negative) occurs approximately at the resonance frequency, and can be evaluated from (6.2) as

$$GD_{\min} = \tau_g\big|_{\omega=\omega_0} = -\frac{2Q}{\omega_0}\left(1-\frac{Z_0}{2R}\right)+\tau_{pd}, \tag{6.3}$$

where τ_{pd} is the positive group delay associated with the physical delay of the circuit

(τ_{pd}=1.05 ns). Fig. 6-3 shows the measured and simulated group delay of the single-branch (A-A') circuit, which are in good agreement. Expression (6.3) predicts GD_{min}= -1.86 ns, while the measured value is -1.52 ns.

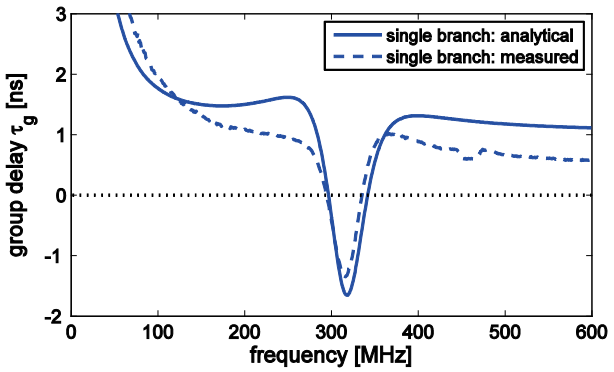

Figure 6-3: Measured and analytical (expression (6.1) with C_s) group delay of the single-branch (A-A') part of the circuit shown in Fig. 6-1.

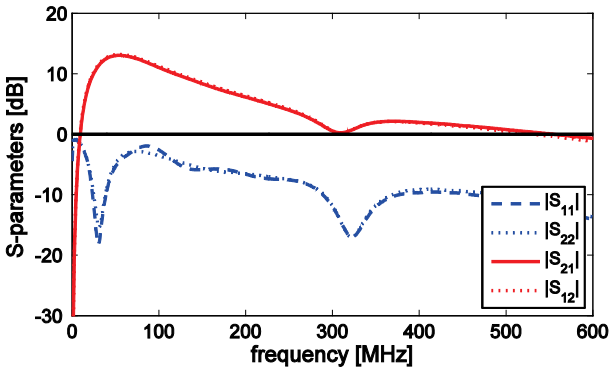

a)

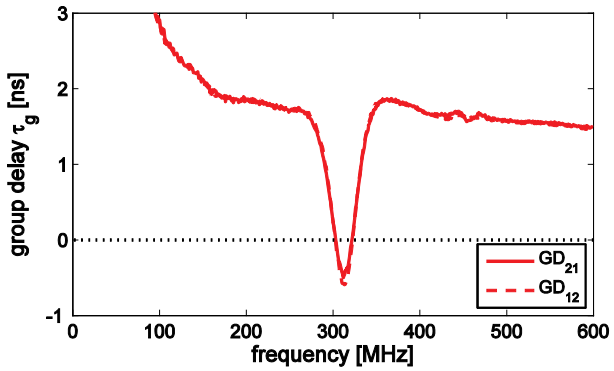

b)

Figure 6-4: Measured a) *S*-parameters and b) group delay of the overall bilateral gain-compensated circuit shown in Fig. 6-1.

The measured *S*-parameters and group delay of the overall reciprocal circuit from Fig. 6-1 are shown in Fig. 6-4. For matched terminations at both ports, the circuit is stable at all frequencies (both $|S_{11}|$ and $|S_{22}|$ are below 0 dB). The transmission coefficients in both directions at the resonance frequency are fully compensated for ($|S_{21}|$ and $|S_{12}|$ are both 0.29 dB). The circuit exhibits a negative group delay of -0.5 ns at the resonance, in both directions. This includes the delay of the amplifier, the splitter and the interconnecting transmission lines. For comparison, the speed-of-light delay across the circuit length is 0.34 ns, which demonstrates a complete group delay compensation.

6.1 Bilateral Gain-Compensated Circuit Stability

The measured input and output reflection coefficients are below 0 dB for all frequencies as shown in Fig. 6-4a, making the reciprocal circuit stable when matched terminations are applied. Since the power splitters/combiners used have a finite isolation between two of their ports, and the overall bilateral circuit terminations may not be perfectly matched at all frequencies, a conditional stability analysis was performed to identify the range of impedances for which the circuit remains stable. Based on the measured *S*-parameters and expressions for identifying the regions of instability [64], the maximum magnitude of the complex reflection coefficient for which the circuit is guaranteed to remain stable, $|\Gamma_{max}|$, is shown as a function of frequency in Fig. 6-5.

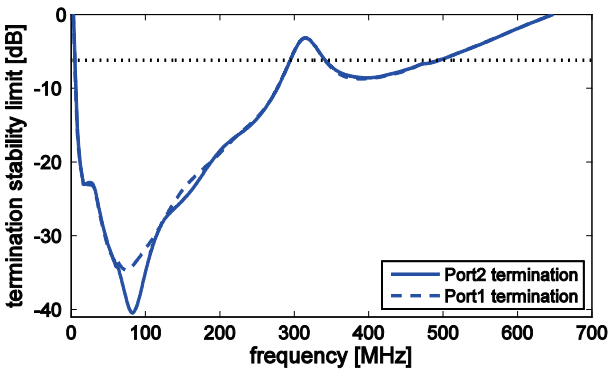

Figure 6-5: Lower limit of the maximum allowed termination reflection coefficient magnitude, $|\Gamma_{max}|$, for stability.

This is a lower stability limit since the circuit is stable even for reflection coefficient magnitudes larger than the ones shown in Fig. 6-5, but only for certain angles. The circuit is conditionally stable within the identified 296-320 MHz bandwidth, and the maximum magnitude of the complex reflection coefficient within bandwidth happens to be $|\Gamma_{max}|\leq 0.5$. The circuit is unconditionally stable ($|\Gamma_{max}|>1$) for frequencies beyond 650 MHz.

6.2 Reciprocal Constant Phase Shifter Application

The proposed reciprocal gain-compensated NGD circuit can be used in applications where a constant with frequency phase shift is needed within a bandwidth, in both propagating directions. For example, non-reciprocal gain-compensated constant phase shifters in series-fed phased array applications have been used for beam-squint minimization [49,50]. However, due to their non-reciprocal nature such circuits can only be used in either transmit or receive modes at a time. A reciprocal, gain-compensated 90° constant phase shifter operating at 310 MHz was fabricated by adding a delay line to the

design in Fig. 6-1. The S-parameter magnitude response is identical to that shown in Fig. 6-4a, while the phase response is shown in Fig. 6-6. A phase variation of ±1° is achieved over a 24 MHz bandwidth, with an insertion gain of 0.29 dB at the center frequency.

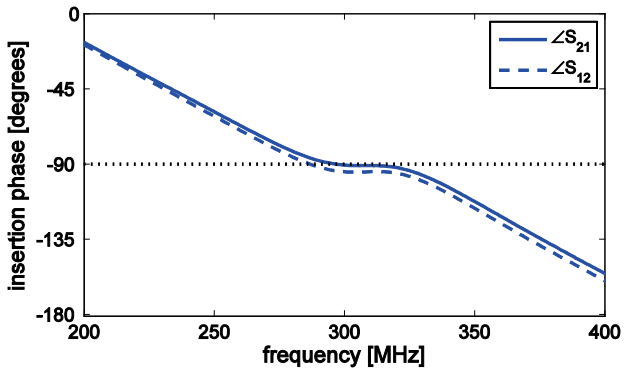

Figure 6-6: Measured insertion phase of a reciprocal gain-compensated 90° constant phase shifter.

The insertion phase responses of the single-branch (A-A') circuit, the overall bilateral circuit, and the bilateral circuit with the added delay line are shown in Fig. 6-7. The phase characteristic for the single-branch circuit exhibits an NGD within the bandwidth, which gets reduced in the bilateral configuration due to additional transmission lines, and finally gets reduced to about zero (flattened phase slope) when the external delay line is added.

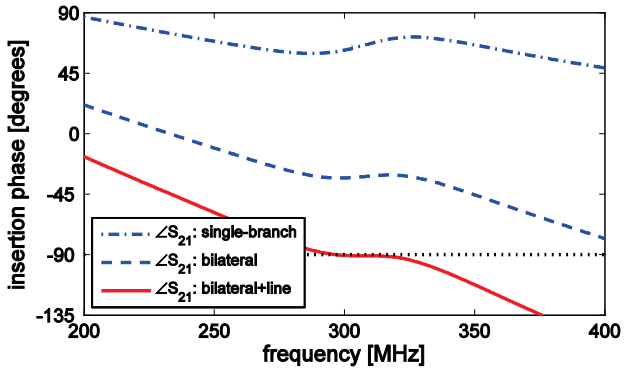

Figure 6-7: Measured insertion phase responses of the single-branch (A-A') part of the circuit shown in Fig. 6-1, the overall bilateral circuit, and the reciprocal gain-compensated 90° constant phase shifter.

6.3 Chapter Conclusion

A bilateral, conditionally stable gain-compensated circuit exhibiting NGD was presented. The design operates at 310 MHz, but it can be extended to higher frequency through choice of amplifiers and power splitters. The use of the circuit in a bidirectional, gain-compensated constant phase shifter was successfully demonstrated. Potential applications include bidirectional beam-squint minimization in linear phased arrays, bandwidth enhancement of hybrid couplers, bidirectional baluns, or reciprocal 90° feed for circular polarization of antennas. Furthermore, bilateral gain-compensated NGD circuits could possibly be used as a building block for 2-D gain-compensated NGD networks (which compensate for the positive delay), provided the stability constraints are met. Negative Refractive Index (NRI) 2-D circuits currently reported in the literature are narrow-band and stable. Bilateral gain-compensated NGD circuits could be used to improve their bandwidth performance by making the refractive angle at the NRI to Positive Refractive Index (PRI) interfaces more frequency independent.

7. Conclusion and Future Work

The work published in literature over the last decade or so presents different passive and gain-compensated circuit topologies which exhibit negative group delay. The objective set out for this thesis included formulating a generic representation for different NGD resonator-based topologies, identifying the trade-off quantities which accompany an increase in the achieved NGD, deriving asymptotic limits of NGD as a function of the trade-off quantities, time-domain transient analysis when finite duration signals are applied, and finally a contribution to the field involving the design and fabrication of a novel NGD application.

In Chapter 2, a fundamental background with NGD examples was presented, showing the NGD interpretation in both the frequency and the time domain and how it fits with fundamental physical laws, such as causality. It was demonstrated that, while certain parts of the signal (envelope peak) appear to be formed at the output even before the same signal part entered the input, this phenomenon does not violate causality since the earliest part of the signal (after the "turn on" point) still has to be positively delayed and can't propagate faster than the speed of light in vacuum. The rest of the applied pulse shape can be "estimated" by its early part, as long as the pulse and its derivatives are smooth following the "turn on" point. If the pulse undergoes another discontinuity at some later point the previously estimated pulse shape will not be valid beyond that point and a new "estimate" is needed. Therefore, genuine information lies in the signal discontinuities, while the signal values in between those points can be "estimated" and reshaped, without violating causality. An obvious example would be transmitting digital

signals, where each bit of the signal has one of two pre-determined pulse shapes, but the sequence of bits is random. The beginning of each bit pulse constitutes a discontinuity, and has to be positively delayed. The rest of that particular bit pulse can be reshaped to yield a time advancement of its peak.

In Chapter 3, different topologies of resonator-based NGD circuits were investigated and their performance compared in terms of achieved NGD as a desirable quantity on one hand and loss for passive circuits, or the out-of-band gain for gain-compensated ones as unwanted quantities, on the other hand. A generic formulation for resonator-based NGD circuits was presented as a function of the number of ideally-matched stages and out-of-band gain. The achieved maximum NGD as a function of these two quantities was derived and asymptotic limits established. A similar procedure was conducted for baseband signals, yielding the same NGD limits which were shown to have a square root dependency with both the number of stages and the out-of-band gain which is given in decibels. The derived limits can potentially be used as guidelines in some engineering application designs. For example, the maximum tolerable out-of-band gain can be specified based on the noise floor of the system, and then the derived limits will establish the maximum achievable NGD-bandwidth. Further, if a desired bandwidth is given, then the maximum achievable NGD can be obtained, in units of time. If a constant phase shifter is being designed for example, then the obtained NGD limit will uniquely determine the design frequency which yields that desired flat phase shift response over the specified bandwidth. Further, when inherent non-zero positive delays of NGD circuits are considered, the procedure described in Section 3.3.1 can be used to determine the optimum number of stages to be used in a design.

In Chapter 4, the NGD limits for physically realizable causal media were examined, regardless of its topology, using the known dependency between the frequency domain amplitude and phase characteristics of such media given by Kramers-Kronig relations. An optimally engineered dispersion characteristic which satisfies the causality requirement was derived. The medium's characteristic was optimized in terms of the maximized NGD to out-of-band gain ratio. The same square root relationship of the asymptotic NGD limit as a function of the decibel value of the out-of-band gain was obtained, with a slightly larger proportionality factor. Therefore, the limit presented in Chapter 3 for resonator-based circuits does not contradict the general limit from Chapter 4, derived for an optimally engineered causal medium. The motivation for the establishment of such a limit was to quantify how far the NGD-bandwidth product can be pushed in physically realizable media, and not to provide a guideline for synthesizing such a medium. However, since the analytical expression for the transfer function of the optimal medium is known, numerical methods can be employed to approximate it with a rational function of polynomials. The poles and zeros of the approximated transfer function can then be determined, which opens the possibility of synthesis via the use of cascaded electrical circuit elements.

In Chapter 5, transient responses of resonator-based and baseband NGD circuits were analyzed for various applied finite duration signals. Responses of single-stage and two-stage resonator-based NGD circuits to a step-modulated sinusoid signal were analytically obtained using the inverse Fourier integration. The same analysis was performed for single-stage baseband NGD circuits when a step-modulated signal (Heaviside function) was applied. More complicated instances (higher number of stages

or more complicated excitations such as Gaussian modulated signals) were handled by numerical simulation. A connection between the out-of-band gain discussed in Chapter 3 and the transient response amplitude of step-modulated signals was established. Therefore, the asymptotic NGD limits derived in Chapter 3 were also shown to be applicable, but as a function of the transient response amplitude in this case. The derived limits can potentially be used as guidelines in some engineering application designs. For example, the maximum tolerable transient amplitude can be specified for a particular transmitted finite duration waveform, and then the NGD limits will establish the maximum achievable NGD as a fraction of the waveform duration. It was demonstrated that the NGD-to-signal-duration ratio remains constant when finite duration Gaussian modulated signals are applied, and predetermined transient amplitude is specified. If the noise floor is taken into account as well, the maximum duration of a Gaussian modulated signal will be limited by the requirement that the signal magnitude at turn-on/off points remains above the noise level. This information can be used to specify the maximum Gaussian modulated signal duration for a given system, which then puts a limit on the NGD that can be achieved, when predetermined transient amplitude is given. An experiment with a fabricated NGD circuit presented in Chapter 3 was set up and transients were measured for a non-ideal step-modulated sinusoidal excitation. The results showed a good agreement when the circuit non-idealities were taken into account and the overall derived NGD limits were still applicable.

Finally, in Chapter 6 a novel NGD application was presented. A gain-compensated, conditionally stable bilateral NGD circuit was design and fabricated which can propagate signals in both directions. The circuit's stability limits were explored for unmatched

terminations, showing a smaller stability margin within a narrow frequency range which leaves room for future improvements. The circuit's application in a gain-compensated bilateral constant phase shifter was demonstrated over a finite bandwidth.

7.1 Future Work

As future work, a potential use of Non-Foster circuits in NGD applications can be investigated. The Foster reactance theorem states that both reactance and susceptance of a purely reactive network, without lossy resistive elements, are monotonically increasing functions of frequency. Alternatively, it can be said that a purely reactive (lossless) network has a monotonically decreasing phase characteristic and therefore exhibits positive group delay. Therefore, in order to achieve negative group delay, resistive (lossy) elements need to be combined with reactive elements, as it was the case with all NGD circuits presented in this thesis. Certain active circuits exhibit a Non-Foster reactance vs. frequency characteristic which can be interpreted as a "negative impedance" effect. These Non-Foster (or "negative impedance") circuits are mostly used for impedance matching [69], but they could potentially be used in NGD applications as well. The negative impedance behavior, however, can cause the transfer function poles to fall inside the lower-half of the complex frequency plane, which would violate causality. In practical terms, this translates into circuit instability. Therefore, circuit stability needs to be considered when investigating the use of negative impedance circuits in NGD applications.

Analytical transient analysis of distributed resonator-based circuits can be performed for step-modulated sinusoid excitation using the steepest descent method. This method is successfully used for media described by an exponential transfer function, such as Lorentzian dielectric medium [1,70]. Further, transient analysis for a wider variety of applied waveforms could be performed, which could potentially lead to formulating the preferred waveform shapes in terms of maximizing the NGD-to-transient-amplitude ratio.

Finally, the use of bilateral gain-compensated design in 2-D networks can be explored, but would require an improved conditional stability margin first. Negative Refractive Index (NRI) 2-D circuits currently reported in the literature are narrow-band and stable. Bilateral gain-compensated NGD circuits could be used to improve their bandwidth performance by making the refractive angle at the NRI to Positive Refractive Index (PRI) interfaces more frequency independent. Further, NRI media are used in electromagnetic "cloaking" applications, where an object is rendered "invisible" when placed inside an artificial NRI material. The characteristic impedance of the surrounding NRI material is designed to minimize the incident wave reflection. The transmitted wave is then guided around the cloaked object and the additional delay caused by the extra path is compensated for via negative phase delay of the NRI material within a narrow-band frequency interval. Bilateral gain-compensated circuits could potentially improve the bandwidth performance of electromagnetic "cloaking" artificial materials.

Appendix A

Any two-port passive network comprised only of resistive elements is also reciprocal and can be represented by three resistive elements connected in a T-network, as shown in Fig. A-1 [71]. Alternatively, a π-network of resistive elements can also be used. A two-port network is given by four parameters in general. However, a reciprocal network is specified by three parameters only, while the fourth parameter can be determined from the other three. For example, the three resistors shown in Fig. A-1 can be determined from the arbitrary network's transmission parameters, A_R, B_R, C_R and D_R, and the system characteristic impedance, Z_0, as $R_1=Z_0(A_R-1)/C_R$, $R_2=Z_0/C_R$, $R_3=Z_0(D_R-1)/C_R$, while the fourth parameter, B_R, does not play the part since it is uniquely defined by the reciprocity condition given by $A_RD_R-B_RC_R=1$.

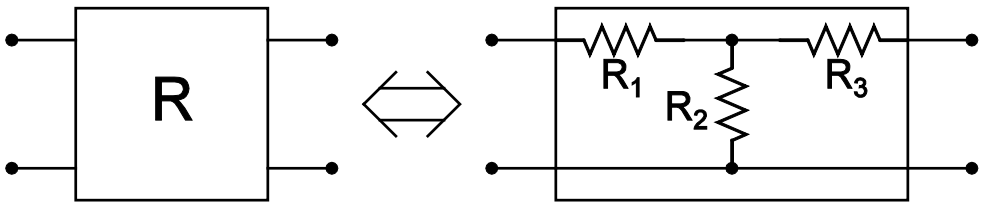

Figure A-1: Block diagram of a passive resistive two-port network and its T-network equivalent.

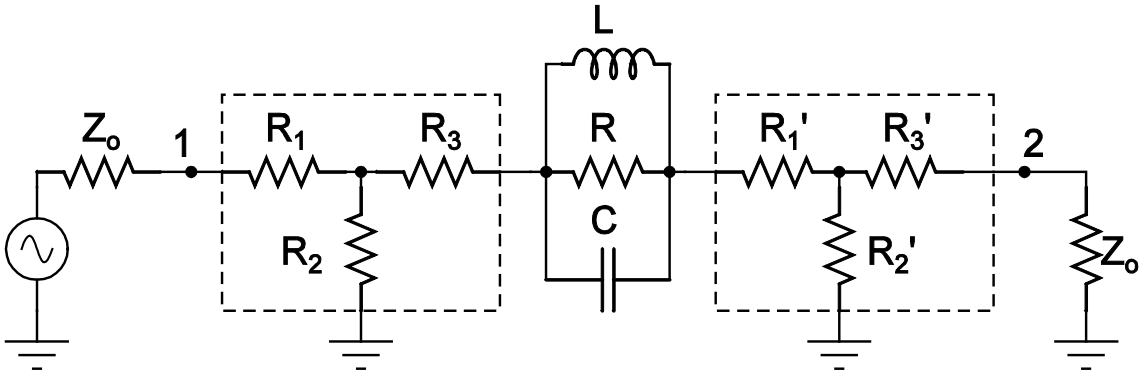

Figure A-2: A parallel-resonator based NGD circuit with matching T-networks at both ends.

Therefore, an NGD circuit comprised of a parallel resonator and arbitrary resistive networks at each end can be represented by an equivalent circuit shown in Fig. A-2.

The transmission coefficient of the passive circuit shown in Fig. A-2 is given by

$$S_{21}(\omega) = (A_0 A)\frac{\omega^2 - \omega_0^2 - j\frac{1}{Q}\omega_0\omega}{\omega^2 - \omega_0^2 - j\frac{1}{Q}A\omega_0\omega}, \tag{A.1}$$

where ω_0 and Q are the resonance frequency and the Q-factor of the resonator, respectively, and the other two parameters are given by

$$A_0 = \frac{2}{k_1 + k_2\, R/Z_0}\ , \qquad A = 1 + \frac{R}{Z_0}\frac{k_2}{k_1}, \tag{A.2}$$

$$k_1 = 2 + \frac{\left(R_2 + R_2^{'}\right)\left(R_1 + R_3 + R_1^{'} + R_3^{'} + Z_0\right) + \left(R_1^{'} + R_3\right)\left(R_1 + R_3^{'} + Z_0\right) + R_1 R_3\left(R_1^{'} + R_3^{'}\right)/Z_0}{R_2 R_2^{'}}$$

$$+ \frac{R_1\left(R_1^{'} + R_3 + R_3^{'}\right)}{R_2 Z_0} + \frac{R_3^{'}\left(R_1 + R_1^{'} + R_3\right)}{R_2^{'} Z_0} + \frac{R_1 + R_1^{'} + R_3 + R_3^{'}}{Z_0}, \tag{A.3}$$

$$k_2 = 1 + \frac{R_1 + Z_0}{R_2} + \frac{R_3^{'} + Z_0}{R_2^{'}} + \frac{Z_0 R_1 + Z_0^2 + R_3^{'}\left(R_1 + Z_0\right)}{R_2 R_2^{'}}. \tag{A.4}$$

An NGD circuit comprised of a series resonator and arbitrary resistive networks at each end can be represented by an equivalent circuit shown in Fig. A-3. The transmission coefficient of this circuit is given by the same expression as (A.1), while the other parameters are given by

$$A_0 = \frac{2}{m_1 + m_2\, Z_0 / R}, \qquad A = 1 + \frac{Z_0}{R}\frac{m_2}{m_1}, \tag{A.5}$$

$$m_1 = k_1, \tag{A.6}$$

$$m_2 = 1 + \frac{R_1 + R_3 + R_1^{'} + R_3^{'}}{Z_0} + \frac{\left(R_1 + R_3\right)\left(R_1^{'} + R_3^{'}\right)}{Z_0^2} + \frac{R_3\left(R_1 + R_1^{'} + R_3^{'}\right)}{R_2 Z_0} + \frac{R_1^{'}\left(R_1 + R_3 + R_3^{'}\right)}{R_2^{'} Z_0}$$

$$+ \frac{R_1 R_3\left(R_1^{'} + R_3^{'}\right)}{R_2 Z_0^2} + \frac{R_1^{'} R_3^{'}\left(R_1 + R_3\right)}{R_2^{'} Z_0^2} + \frac{R_1^{'} R_3\left(R_1 + R_3^{'}\right)}{R_2 R_2^{'} Z_0} + \frac{R_1 R_1^{'} R_3 R_3^{'}}{R_2 R_2^{'} Z_0^2} + \frac{R_3}{R_2} + \frac{R_1^{'}}{R_2^{'}} + \frac{R_1^{'} R_3}{R_2 R_2^{'}}. \tag{A.7}$$

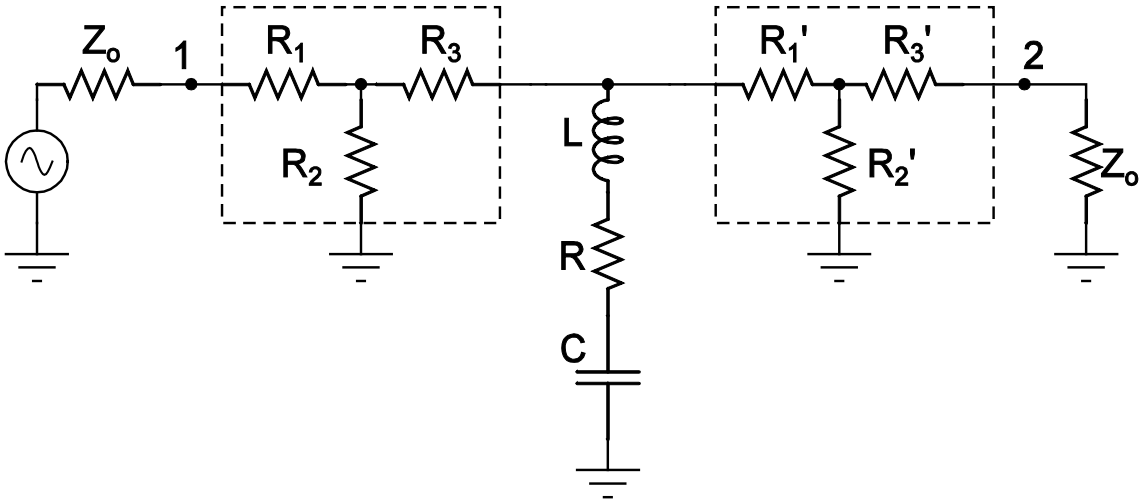

Figure A-3: A series-resonator based NGD circuit with matching T-networks at both ends.

In conclusion, the transmission coefficient of any passive network comprised of a single parallel or a series resonator and additional purely resistive elements, will have a 2nd order rational function form given by expression (A.1).

References

[1] L. Brillouin, “Wave Propagation and Group Velocity”, New York: Academic Press, 1960.

[2] C. G. B. Garrett and D. E. McCumber, “Propagation of a Gaussian light pulse through an anomalous dispersion medium”, *Phys. Rev. A, Gen. Phys.*, vol. 1, no. 12, pp. 305–313, Feb. 1970.

[3] S. Chu and S. Wong, “Linear pulse-propagation in an absorbing medium”, *Phys. Rev. Lett.*, vol. 48, pp. 738–741, 1982.

[4] T. Martin and R. Landauer, “Time delay of evanescent electromagnetic waves and the analogy to particle tunneling”, *Phys. Rev. A, Gen. Phys.*, vol. 45, no. 4, pp. 2611–2617, Feb. 1992.

[5] P. Balcou and L. Dutriaux, “Dual optical tunnelling times in frustrated total internal reflection”, *Phys. Rev. Lett.*, vol. 78, no. 5, pp. 851–854, Feb. 1997.

[6] E. L. Bolda, R. Y. Chiao, and J. C. Garrison, “Two theorems for the group velocity in dispersive media”, *Phys. Rev. A*, Gen. Phys., vol. 48, pp. 3890–3894, Nov. 1993.

[7] J.D. Jackson, “Classical electrodynamics”, John Wiley & Sons Inc., New York, 1998, 3rd edn.

[8] K. R. Waters, J. Mobley and J. G. Miller, “Causality-Imposed (Kramers-Kronig) Relationships Between Attenuation and Dispersion”, *IEEE transactions on ultrasonics, ferroelectrics, and frequency control*, vol. 52, no. 5, pp. 822-833, May 2005.

[9] M. Mojahedi, E. Schamiloglu, K. Agi, and K. J. Malloy, “Frequency domain detection of superluminal group velocity in a distributed Bragg reflector”, *IEEE J. Quantum Electron.*, vol. 36, pp. 418–424, Apr. 2000.

[10] M. Mojahedi, E. Schamiloglu, F. Hegeler, and K. J. Malloy, “Time-domain detection of superluminal group velocity for single microwave pulses”, *Phys.Rev. E*, vol. 62, no. 4, pp. 5758-5766, Oct. 2000.

[11] D. Stenner, D. J. Gauthier and M. A. Neifeld, “Fast Causal Information Transmission in a Medium With a Slow Group Velocity “, *Phys. Rev. Lett.* 94, 053902, Feb. 2005.

[12] P. Wyns, D.P. Foty and K.E. Oughstun, “Numerical analysis of the precursor fields in linear dispersive pulse propagation”, *Journal Of The Optical Society Of America A-Optics Image Science And Vision*, vol.6, No.9, pp.1421-1429, Sep. 1989.

[13] J.A. Solhaug, K.E. Oughstun, J.J. Stamnes, et al. “Uniform asymptotic description of the Brillouin precursor in a single-resonance Lorentz model dielectric”, *Pure And Applied Optics*, vol.7, No.3, pp. 575 602, May. 1998.

[14] K.E. Oughstun and X. Hong, “Influence of precursor fields on ultrashort pulse autocorrelation measurements and pulse width evolution”, *Optics Express*, vol.8, No.8, pp.481-491, Apr. 9 2001.

[15] K. E. Oughstun, “Dynamical evolution of the Brillouin precursor in Rocard-Powles-Debye model dielectrics”, *IEEE Trans. Antennas & Prop*., vol. 53, No. 5, pp. 1582–1590, 2005.

[16] R. Safian, C.D. Sarris and M. Mojahedi, “Joint time-frequency and finite-difference time-domain analysis of precursor fields in dispersive media”, *Phys. Rev. E*, vol.73, No.6, Part 2, Jun. 2006.

[17] Veselago, V.G., "The electrodynamics of substances with simultaneously negative values of 1 and m", *Soviet Phys. Uspekhi*, 10, (4), pp. 509–514, 1968.

[18] J. B. Pendry, "Negative Refraction Make a Perfect Lens", *Phys. Rev.Lett.* 85, 3966, 2000.

[19] D.R. Smith, W.J. Padilla, D.C. Vier, et al., "Composite medium with simultaneously negative permeability and permittivity", *Physical Review Letters*, Vol. 84, No.18, pp. 4184-4187, May 2000.

[20] R.A. Shelby, D.R. Smith, S. Schultz, "Experimental verification of a negative index of refraction", *Science*, Vol. 292, No. 5514, pp. 77-79, Apr. 6 2001.

[21] C. Caloz, and T. Itoh, "Application of the transmission line theory of left-handed (LH) materials to the realization of a microstrip 'LH line' ", *IEEE AP-S Int. Symp. Dig.*, pp. 412–415, 2002.

[22] G.V. Eleftheriades, A.K. Iyer, P.C. Kremer, "Planar negative refractive index media using periodically L-C loaded transmission lines", *IEEE Transactions On Microwave Theory And Techniques*, Vol. 50, No.12, pp. 2702-2712, Dec. 2002.

[23] M. A. Antoniades, and G. V. Eleftheriades, "A BroadBand Wilkinson Balun Using Microstrip Metamaterial Lines", *IEEE Antennas and Wireless Propagation Letters*, Vol. 4, 2005.

[24] M.A. Antoniades and G.V. Eleftheriades, "A broadband series power divider using zero-degree metamaterial phase-shifting lines", *IEEE Microwave And Wireless Components Letters*, Vol. 15, No.11, pp. 808-810, Nov. 2005.

[25] G.V. Eleftheriades and K.G. Balmain, "Negative-refraction metamaterials – fundamentals principles and applications", John Wiley & Sons Inc, Hoboken, New Jersey, 2005.

[26] Y. Wang, Y, Zhang, L. He, F. Liu, H. Li and H. Chen, "Direct observation of negative phase velocity and positive group velocity in time domain for composite right/left-handed transmission lines", *Journal of Applied Physics*, Vol. 100, 113503 (2006).

[27] S. Lucyszyn, I.D. Robertson and A.H. Aghvami, "Negative Group Delay Synthesizer", *Electronics Letters*, Vol. 29, No.9, pp. 798-800, Apr. 29 1993.

[28] S. Lucyszyn and I. D. Robertson, "Analog reflection topology building blocks for adaptive microwave signal processing applications", *IEEE Transactions on Microwave Theory Tech.,* vol. MTT-43, no. 3, pp. 601-611, Mar. 1995.

[29] H. Noto, K. Yamauchi, M. Nakayama and Y. Isota,, "Negative Group Delay Circuit for Feed-Forward Amplifier", *2007. IEEE/MTT-S International Microwave Symposium*, pp. 1103–1106, 3-8 Jun. 2007.

[30] O.F. Siddiqui, M. Mojahedi, and G.V. Eleftheriades, "Periodically loaded transmission line with effective negative refractive index and negative group velocity", *IEEE Trans. Antennas Propagat.*, 51, (10), pp. 2619–2625, 2003.

[31] O.F. Siddiqui, S.J. Erickson, G.V. Eleftheriades and M. Mojahedi, "Time-domain measurement of negative group delay in negative-refractive-index transmission-line metamaterials", *IEEE Trans. Microw. Theory Tech.*, 52, (5), pp. 1449–1454, 2004.

[32] A. Ibraheem, J. Schoebel and M. Koch, "Group delay characteristics in coplanar waveguide left-handed media", *Journal of Applied Physics*, Vol. 103, 024903 (2008).

[33] Mojahedi, K. J. Malloy, G. V. Eleftheriades, J. Woodley and R. Y. Chiao, "Abnormal wave propagation in passive media", *IEEE Journal Of Selected Topics In Quantum Electronics*, Vol. 9, No. 1, pp. 30-39, 2003.

[34] M.W. Mitchell and R.Y. Chiao, "Negative group delay and 'fronts' in a causal system: An experiment with very low frequency bandpass amplifiers", *Physics Letters A*, Vol. 230, No. 3-4, pp.133-138, Jun. 1997.

[35] M.W. Mitchell and R.Y. Chiao, "Causality and negative group delays in a simple bandpass amplifier", *American Journal Of Physics*, Vol. 66, No.1, pp.14-19, Jan. 1998.

[36] D. Solli, R. Y. Chiao and J. M. Hickmann, "Superluminal effects and negative group delays in electronics, and their applications ", *Phys. Rev. E*, 66, Nov. 2002.

[37] T. Nakanishi, K. Sugiyama and M. Kitano, "Demonstration of negative group delays in a simple electronic circuit", *Am. J. Phys.* 70 (11), pp. 1117-1121, Nov. 2002.

[38] M. Kitano, T. Nakanishi, and K. Sugiyama, "Negative Group Delay and Superluminal Propagation : An electronic circuit Approach", *IEEE Journal of selected Topics in Quantum electronics*, Vol. 9, no1, pp. 43-51, 2003.

[39] S.J. Erickson, M. Khaja, and M. Mojahedi, "Time and Frequency-Domain Measurements for an Active Negative Group Delay Circuit", *Antennas and Propagation Society International Symposium, 2005 IEEE Volume 3A,* 3-8 July 2005, pp. 790-793.

[40] B. Ravelo, A. Perennec, M. Le Roy et al., "Active microwave circuit with negative group delay", *IEEE Microwave And Wireless Components Letters*, Vol. 17, No. 12, pp. 861-863, Dec. 2007.

[41] B. Ravelo, A. Perennec and M. Le Roy, "Synthesis of Broadband Negative Group Delay Active Circuits", *2007. IEEE/MTT-S International Microwave Symposium*, pp. 2177–2180, 3-8 Jun. 2007.

[42] B. Ravelo, A. Perennec and M. Le Roy "Broadband balun using active negative group delay circuit", *2007. European Microwave Conference*, pp. 466–469, 9-12 Oct. 2007.

[43] B. Ravelo, M. Le Roy and A. Perennec, "Application of negative group delay active circuits to the design of broadband and constant phase shifters", *Microwave And Optical Technology Letters*, Vol. 50, No. 12, pp. 3078-3080, Dec. 2008.

[44] B. Ravelo, A. Perennec, and M. Le Roy, "Negative Group Delay Active Topologies Respectively Dedicated to Microwave Frequencies and Baseband Signals", *Journal of EuMA*, Vol. 4, pp. 124-130, Jun. 2008.

[45] B. Ravelo, A. Perennec and M. Le Roy, "Equalization of Interconnect Propagation Delay with Negative Group Delay Active Circuits", *11th IEEE Workshop on Signal Propagation On Interconnects*, pp. 15-18., Genova, Italy, May 2007.

[46] B. Ravelo et al., "New Technique of Inter-Chip Interconnect Effects Equalization with Negative Group Delay Active Circuits", *VLSI*, INTECH, Feb. 2010, Chap. 20, pp. 409-434.

[47] B. Ravelo, A. Perennec and M. Le Roy, "Application of negative group delay active circuits to reduce the 50% propagation Delay of RC-line model", *12th IEEE Workshop on Signal Propagation and Interconnects*, pp. 1-4, 12-15 May 2008.

[48] B. Ravelo et al., "Study and Application of Microwave Active Circuits with Negative Group Delay", *Microwave and Millimeter Wave Technologies Modern UWB antennas and equipment*, INTECH, Mar. 2010, Chap. 21, pp. 415- 439.

[49] S.S. Oh and L. Shafai, "Beam-squint minimization in microstrip series-fed array antenna using circuit of double negative materials", *IEEE Antennas and Propagation Society International Symposium*, Vol. 1A, pp. 688 – 691, 3-8 Jul. 2005.

[50] S.S. Oh and L. Shafai, "Compensated circuit with characteristics of lossless double negative materials and its application to array antennas", *IET Microwaves Antennas & Propagation*, Vol. 1, No.1, pp. 29-38, Feb. 2007.

[51] Y. C. Lim and Y. Lian, "The optimum design of one- and two-dimensional FIR filters using the frequency response masking technique", *IEEE Trans. Circuits Syst. II, Analog Digit. Signal Process*., vol. 40, no. 2, pp. 88–95, Feb. 1993.

[52] W.-S. Lu and T. Hinamoto, "Optimal design of frequency-response masking filters using semidefinite programming", *IEEE Trans. Circuits Syst. I, Fundam. Theory Appl*., vol. 50, no. 4, pp. 557–568, Apr. 2003.

[53] Y. Liu and Z. Lin, "Optimal Design of Frequency-Response Masking Filters With Reduced Group Delays", *IEEE Trans. Circuits Syst.*, vol. 55, no. 6, pp. 1560–1570, Jul. 2008.

[54] J. Piskorowski and M.A.G. de Anda, "A New Class of Continuous-Time Delay-Compensated Parameter-Varying Low-Pass Elliptic Filters With Improved Dynamic Behavior", *IEEE Trans. Circuits Syst.*, vol. 56, no. 1, pp. 179–189, Jan. 2009.

[55] J. Kim and J.F. Buckwalter, "Bandwidth Enhancement With Low Group-Delay Variation for a 40-Gb/s Transimpedance Amplifier", *IEEE Trans. Circuits Syst.*, vol. 57, no. 8, pp. 1964–1972, Aug. 2010.

[56] K. Murase, R. Ishikawa and K. Honjo, "Group delay equalised monolithic microwave integrated circuit amplifier for ultra-wideband based on right/left-handed transmission line design approach", *IET Microw. Antennas Propag.*, 2009, vol. 3, Iss. 6, pp. 967-973.

[57] A. Kyoung-Pyo, R. Ishikawa, and K. Honjo, "Low Noise Group Delay Equalization Technique for UWB InGaP/GaAs HBT LNA", *IEEE Microwave and Wireless Components Letters*, vol. 20, no. 7, pp. 405 - 407, Jul. 2010.

[58] H. Choi, Y. Jeong, C. D. Kim, and J. S. Kenney, "Efficiency enhancement of feedforward amplifiers by employing a negative group-delay circuit", *IEEE Trans. Microw. Theory Tech*., vol. 58, no. 5, pp. 1116-1125, May 2010.

[59] S. K. Podilchak, B.M. Frank, A. P. Freundorfer and Y.M.M. Antar, "High speed metamaterial-inspired negative group delay circuits in CMOS for delay equalization", *Microsystems and Nanoelectronics Research Conference*, pp. 9-12, 13-14 Oct. 2009.

[60] M. Kandic and G. Bridges, "Asymptotic Limits of Negative Group Delay in Active Resonator-Based Distributed Circuits", *IEEE Trans. Circuits Syst.*, vol. 58, no. 8, pp. 1727–1735, Aug. 2011.

[61] M. Kandic and G. Bridges, "Active Gain Compensated Negative Group Delay Circuit", *URSI General Assembly*, Chicago, IL., USA, Aug. 2008.

[62] M. Kandic and G. Bridges, "Transient-imposed limitations of negative group delay circuits", *14th International Symposium on Antenna Technology and Applied Electromagnetics & the American Electromagnetics Conference* (*ANTEM-AMEREM*), Jul. 2010.

[63] M. Kandic and G. Bridges, "Bilateral Gain-Compensated Negative Group Delay Circuit", *IEEE Microwave And Wireless Components Letters*, Vol. 21, No. 6, pp. 308-310, Jun. 2011.

[64] D.M. Pozar, "Microwave engineering", John Wiley & Sons, New York, 2nd edition, 1998.

[65] C.A. Balanis, "Antenna Theory", John Wiley & Sons, New York, 2nd edition, 1997.

[66] Ansoft Designer 1.0, Ansoft Corp., PA, USA, 2002.

[67] S.C. Dutta Roy, "On Q of cascaded identical resonators", *Proc. of IEEE*, vol. 61, pp. 790, Jun. 1973.

[68] H. W. Bode, "Network Analysis and Feedback Amplifier Design", Van Nostrand, New York, 1945.

[69] S.E. Sussman-Fort, "Matching network design using non-foster impedances", *International Journal Of RF and Microwave Computer-Aided Engineering* , Vol. 16, No. 2, pp. 135-142, Mar. 2006.

[70] R. Safian, M. Mojahedi and C.D. Sarris, "Asymptotic description of electromagnetic pulse propagation in active Lorentzian media", *IEEE Antennas and Propagation Society International Symposium 2006*, pp. 939-942, Jul. 2006.

[71] R. E. Thomas and A. J. Rosa, "The Analysis and Design of Linear Circuits", John Wiley & Sons, New York, 4th edition, 2003.